7-2015

Reducing Multiple Access Interference in Broadband Multi-User Wireless Networks

Ali Nayef Alqatawneh
University of Arkansas, Fayetteville

Reducing Multiple Access Interference in Broadband Multi-User Wireless Networks

Reducing Multiple Access Interference in Broadband Multi-User Wireless Networks

A dissertation submitted in partial fulfillment
of the requirements for the degree of
Doctor of Philosophy in Electrical Engineering

By

Ali Alqatawneh
Mu'tah University
Bachelor of Engineering, 1997
Mu'tah University
Master of Engineering, 2007

July 2015
University of Arkansas

This dissertation is approved for recommendation to the Graduate Council.

_____

Dr. Jingxian Wu

Dissertation Director

_____

Dr. Roy McCain

Committee Member

_____

Dr. Jing Yang

Committee Member

_____

Dr. Jia Di

Committee Member

Abstract

This dissertation is devoted to developing multiple access interference (MAI) reduction techniques for multi-carrier multi-user wireless communication networks. In multi-carrier code division multiple access (MC-CDMA) systems, a full multipath diversity can be achieved by transmitting one symbol over multiple orthogonal subcarriers by means of spreading codes. However, in frequency selective fading channels, orthogonality among users can be destroyed leading to MAI. MAI represents the main obstacle to support large number of users in multi-user wireless systems. Consequently, MAI reduction becomes a main challenge when designing multi-carrier multi-user wireless networks. In this dissertation, first, we study MC-CDMA systems with different existing MAI reduction techniques. The performance of the studied systems can be further improved by using a fractionally spaced receivers instead of using symbol spaced receivers. A fractionally spaced receiver is obtained by oversampling received signals in a time domain. Second, a novel circular-shift division multiple access (CSDMA) scheme for multi-carrier multi-user wireless systems is developed. In CSDMA, each symbol is first spread onto multiple orthogonal subcarriers in the frequency domain through repetition codes. The obtained frequency-domain signals are then converted to a time-domain representation. The time-domain signals of different users are then circularly shifted by different numbers of locations. The time-domain circular shifting enables the receiver to extract signals from different users with zero or a small amount of MAI. Our results show that the CSDMA scheme can achieve a full multipath diversity with a performance outperforms that of orthogonal frequency division multiple access (OFDMA). Moreover, multipath diversity of CSDMA can be further improved by employing the time-domain oversampling. Performance fluctuations due to a timing offset between transmitter and receiver clocks in MC-CDMA and CSDMA systems can be removed by employing the time-domain

oversampling. Third, we study the theoretical error performance of high mobility single-user wireless communication system with doubly selective (time-varying and frequency-selective) fading channel under impacts of imperfect channel state information (CSI). Throughout this dissertation, intensive computer simulations are performed under various system configurations to investigate the obtained theoretical results, excellent agreements between simulation and theoretical results were observed in this dissertation.

Acknowledgements

I would like to express my sincere and deepest appreciation and gratitude to those who made this dissertation possible. First, I would like to extend my thanks to my advisor, Dr. Jingxian Wu for his immeasurable support, motivation, and guidance over years. Without his continuous assistance and his guidance this dissertation will not be finished. Second, I would like to gratefully thank and appreciate dissertation committee members, Dr. Roy McCain, Dr. Jia Dai, and Dr. Jing Yang for their help. Third, I would like to thank my mom, my wife and my kids for their support.

Contents

List of Figures

Chapter 1

Introduction

1.1 Background and Motivation

Orthogonal frequency division multiplexing (OFDM) is a promising multi-carrier candidate for current and future multi-user multiple access broadband wireless communication systems [1]. The main advantage of OFDM is its immunity to inter-symbol interference (ISI) caused by multipath fading. OFDM is mainly designed to support a single-user transmission, but it can be adapted to support simultaneous transmission of multiple users. Orthogonal frequency division multiple access (OFDMA) is an OFDM-based multi-user wireless communication system. The majority of wideband wireless communication standards, including the fourth generation (4G) long-term evolution advanced (LTE-A) and IEEE 802.11ad Wireless Gigabit Alliance (WiGig) systems employ OFDMA to support the simultaneous access of multiple users. In OFDMA, multiple users simultaneous transmission is accomplished through assigning different orthogonal subcarriers to individual users, where the orthogonality among users allows simultaneous use of a same channel without multiple access interference (MAI). Even though the OFDMA system is a powerful multi-user system, it can not achieve the multipath diversity inherent in a frequency selective fading channel, because in OFDMA, uncorrelated signals are transmitted over orthogonal subcarriers.

Multi-carrier code division multiple access (MC-CDMA) is another example of OFDM-based multi-user multiple access wireless communication systems. The MC-CDMA system can be considered as a combination of the OFDM and the code division multiple access (CDMA) systems [2]. The MC-CDMA system can achieve multipath diversity, because the same data symbol is transmitted over

multiple orthogonal subcarriers.

Orthogonal spreading codes are used in the MC-CDMA system to differentiate between different users at the receiver, however, when the transmission channels undergo a frequency selective Rayleigh fading, orthogonality among different users might be destroyed leading to MAI. MAI has two major negative impacts on the MC-CDMA system: first, it causes a serious error performance degradation, second, it limits the number of supported users. Moreover, in most existing multi-user systems, MAI increases linearly with the number of users; therefore, MAI reduction arises as the biggest challenge facing multi-user networks, especially when the number of users is large [3].

Several detection techniques were proposed for multi-user systems including single-user based detection (SUBD) and multi-user based detection (MUBD) techniques. Most existing MUBD techniques require the knowledge of channel state information (CSI) for all users to make a decision about a specific user. Multi-user channel estimation errors can severely degrade the detection performance, in addition, the detection process becomes even more complicated as the number of users increases [4, 5]. On the other hand, in SUBD techniques, CSI of a desired user is enough to make a decision about that user, where signals from other users are considered undesirable MAI. Therefore, SUBD combined with MAI cancellation or reduction technique is likely to be more powerful and promising approach than MUBD, especially in networks with a large number of users. MC-CDMA systems with different MAI reduction schemes are proposed in [6]-[10]. In [6, 7], the proposed systems are approximately MAI-free, however, the systems can not achieve the multipath diversity and their computational complexity is high. Using appropriate spreading code selection priority can effectively remove MAI in partially loaded MC-CDMA systems [8]-[10]. The proposed systems in [8]-[10] can achieve multipath diversity. Symbol spaced receivers are considered for all MC-CDMA systems proposed in [6]-[10]. A fractionally spaced receiver can be obtained by employing a time-domain oversampling

at the receiver side. A considerable performance improvement in OFDM system with a fractionally spaced receiver over an equivalent system with a symbol spaced receiver was observed in [11]. The time-domain oversampling at the receiver side can enhance the collected multipath diversity gain leading to the performance improvement. Furthermore, employing the time-domain oversampling at the receiver side can tackle negative impacts of a timing offset between the transmitter and the receiver sampler clocks [11]. Oversampling in the time domain and a linear signal processing in the frequency domain can also be employed in multi-carrier multi-user systems to improve their overall performances.

1.2 Objectives

The main goal of this dissertation is to study and develop multi-carrier wireless systems with MAI cancellation or reduction capabilities to support multiple users simultaneous access over frequency-selective Rayleigh fading channels. The particular objectives that lead to accomplish this goal can be summarized as follows. The first objective is to modify an approximately MAI-free MC-CDMA system with a fractionally spaced receiver for uplink wireless communications. To achieve this objective, we consider the MC-CDMA system with a fractionally spaced receiver and a large number of subcarriers at the transmitter. When the number of subcarriers is sufficiently large, the frequency-domain of a frequency selective fading channel can be approximated by flat fading one leading to the approximately MAI-free MC-CDMA system as presented in [6] for a system with symbol spaced receiver. However, the modified system can not achieve a multipath diversity. The second objective is to modify an MAI-free MC-CDMA system with a fractionally spaced receiver and an ability of collecting a full multipath diversity. To accomplish this objective, we employ the code priority selection technique proposed in [8] along with the time-domain oversampling to obtain MC-CDMA system with a fractionally spaced receiver that can achieve the full multipath diversity. The optimum receivers of

the modified systems are derived; the statistical properties of channel coefficients and noise samples are employed to improve performance. Furthermore, error performance lower bounds are derived for systems with and without oversampling. Simulation and analytical results are obtained for systems with and without oversampling under various systems configurations. Our results show that the employment of the time-domain oversampling enhances system error performance and removes the performance fluctuations induced by the timing offset between transmitters and the receiver clocks.

The third objective is to propose a new MAI reduction scheme for multi-carrier multi-user wireless communication system in the uplink direction. The proposed system employs a novel MAI reduction technique that can completely remove or effectively reduce the MAI when channels experience a frequency selective Rayleigh fading. Furthermore, in all extended and new proposed systems, we focus on how to achieve a significant performance gain over conventional orthogonal frequency division multiple access (OFDMA) with the same spectral efficiency. Finally, we present the design of an optimum receiver for system with imperfect CSI. The impact of various system design parameters are identified. The optimum receiver is obtained for a single-user system, but it can be extended to include multi-user systems.

Throughout this dissertation, the above objectives are implemented using theoretical analysis, and then extensive computer simulations are carried out under various systems parameters and configurations to validate the derived analytical results. Also, during simulations, we consider practical configurations and parameters, such as power delay profiles, transmission energies, filters configurations, and modulation schemes. Therefore, the derived results can be used to anticipate the error performance of an equivalent actual systems. Additionally, some extended works are proposed in the future work chapter.

1.3 Dissertation Outline

The outline of the rest of this dissertation is summarized as follows.

Chapter 2: In this chapter, we develop approximately MAI-free MC-CDMA system, where oversampling in the time domain and a linear signal processing in the frequency domain are employed at the receiver side. Hadamard-Walsh codes are used to spread data symbols in the frequency domain before transmission over a frequency selective Rayleigh fading channel. When the number of subcarriers is sufficiently large, the frequency-domain of a frequency selective Rayleigh fading channel can be approximated by a flat fading channel leading to an approximately MAI-free system. The performance of the system with oversampling outperforms the original system without oversampling, both systems can support the same number of users with negligible MAI. In addition, the system with oversampling has immunity to impacts of the timing-offset between transmitter and receiver sampler clocks.

Chapter 3: In this chapter, we introduce an oversampled multi-carrier code division multiple access (OMC-CDMA) system, the system employs Hadamard-Walsh codes to spread symbols in the frequency domain and to establish orthogonality among different users. When channels experience frequency selective Rayleigh fading, orthogonality among users could be lost leading to MAI. To maintain orthogonality among users, Hadamard-Walsh codes can be partitioned into smaller subsets, then users select their respective spreading codes from the same subset [8]. The partitioning is done based on the ratio between the total number of subcarriers and the equivalent discrete-time channel length without oversampling. Our results show that the performance of the system with oversampling is much better than an equivalent system without oversampling for a typical urban (TU) power delay profile; both systems with and without oversampling can achieve multipath diversity. In addition, results show that the system with oversampling is protected against impacts of the timing offset between

transmitter and receiver clocks. Finally, the maximum number of supported users in this system does not exceed N/L, where N is the total number of available subcarriers at the transmitter, and L is the equivalent discrete-time channel length without oversampling.

Chapter 4: In this chapter, a novel circular-shift division multiple access (CSDMA) scheme is proposed for multi-carrier multi-user wireless communication systems. The system can be used in the uplink wireless communications. In CSDMA, a time-domain circular shift is employed at the transmitter to enable the receiver to differentiate signals from multiple users with MAI-free. The MAI-free system can be obtained when the number of users is equal to or less than M/L, where M is the number of repetitions in the frequency domain and L is the length of the equivalent discrete-time channel. In addition, when the number of users exceeds M/L the system will have MAI, the CSDMA system with MAI is presented in *chapter 5*. Finally, the CSDMA system can achieve the multipath diversity gain.

Chapter 5: In this chapter, we extend the CSDMA system presented in *Chapter 4* to support a number of users greater than M/L. To address the MAI problem in the CSDMA system when the number of users exceeds M/L, proper circular shifting values are proposed for users leading to at most L mutually interfering users at any given subcarrier. Consequently, the system can be considered as a multi-input multi-output (MIMO) system, where the optimum detection requires exhaustive searching. An iterative soft-input soft-output (SISO) block decision feedback equalization (BDFE) is proposed at the receiver, since it provides a balanced trade-off between performance and complexity [12]. Our results show that the performance of the CSDMA system with MAI and BDFE receiver is slightly worse than the CSDMA system without MAI.

Chapter 6: Inspired by results obtained in *Chapter 4* and *Chapter 5*, we further extend the CSDMA system by introducing oversampling in the time domain combined with a linear signal processing in the frequency domain at the receiver of the CSDMA system. The statistical properties of both the discrete-time channel and the correlated noise samples are considered in our analysis. An Optimum and sub-optimum receivers are designed for systems without and with MAI, respectively. The CSDMA system with oversampling shows a significant performance improvement over the CSDMA system without oversampling.

Chapter 7: In previous chapters, channel coefficients for all users are considered to be perfectly known at the receiver, which is not the case in practical wireless communication systems. Therefore, In this chapter, we study a theoretical error performance of high mobility wireless communication system with doubly selective (time-varying and frequency-selective) fading channel under the impacts of imperfect channel state information (CSI). The minimum mean squared error (MMSE) pilot-assisted channel estimation is employed to detect the channel fast time variations in high mobility wireless communications. With the help of the statistical properties of the discrete-time system model, we derive the average mean squared error (MSE) of the MMSE estimator. Also, the impacts of design parameters, such as Doppler frequency, pilot percentage, and energy allocation factor on the average MSE and on the system error performance are identified in this chapter. The study is done for a single-user system with Viterbi equalizer at the receiver. The generated results can be extended to cover multi-carrier multi-user systems.

Chapter 8: This chapter is dedicated to concluding our research and to present the main contributions of this dissertation.

Chapter 2

Repetitively Coded Multi-User Multiple Access (RC-MUMA) System

2.1 Introduction

Orthogonal frequency division multiple access (OFDMA) and multi-carrier code division multiple access (MC-CDMA) were proposed as a solutions to satisfy the huge demands on broadband multi-user wireless and mobile communications. In multi-user wireless networks, OFDMA is used to reach high data rates over multipath fading channels. The IEEE 802.16d and 802.16e standards which are commonly known as Worldwide Interoperability for Microwave Access (WiMAX) are the first multiple access standards that employ OFDMA [13]. High spectral efficiency and immunity to inter-symbol interference (ISI) in a multipath fading environment are the main advantages of the OFDMA system [3]. However, the OFDMA system can not achieve multipath diversity when the system is fully loaded, *i.e.*, the number of users equals the number of available subcarriers.

The MC-CDMA system was first proposed for multiple users indoor wireless radio networks [2]. The MC-CDMA system can be considered as an integration between the OFDM and the code division multiple access (CDMA) systems, consequently, the MC-CDMA system has the advantages of both systems. Multiple-access capability and robustness against ISI are the main advantages of the MC-CDMA system, these advantages are provided by CDMA and OFDM, respectively. Multi-carrier CDMA systems can be divided into two main types: the MC-CDMA system and the multi-carrier direct sequence CDMA (MC-DS-CDMA) system [3]. In the first type, data symbols are spread in the frequency domain into multiple chips by means of orthogonal spreading codes. Then these chips are used to modulate orthogonal subcarriers, where chips belonging to the same symbol modulate

different subcarriers. In the second type, the spreading is performed in the time domain, then chips corresponding to the same symbol modulate the same subcarrier [14, 15]. The MC-CDMA system has the advantage of collecting multipath diversity, because each modulated symbol is transmitted over multiple orthogonal subcarriers. Achieving multipath diversity is the main advantage of the MC-CDMA system over the OFDMA system [3]. Despite all advantages of the MC-CDMA system, the MC-CDMA system is not free of issues; the main issue in the MC-CDMA system is multiple access interference (MAI). In the MC-CDMA system, orthogonal codes are used to distinguish between different users at the receiver, however, in the frequency selective Rayleigh fading channels, orthogonality among different codes might be lost leading to MAI.

Various schemes are proposed in [6]-[9] to tackle the MAI problem in the MC-CDMA system. In [6, 7], a repetitively coded MC-CDMA (RCMC-CDMA) is proposed, the RCMC-CDMA system is approximately MAI-free. The number of subcarriers is considered to be large enough to approximate the frequency selective Rayleigh fading channel by flat fading channel [6]. The RCMC-CDMA system can achieve high spectral efficiency compared to the conventional MC-CDMA system, however, the computational complexity of the RCMC-CDMA is high compared to the conventional MC-CDMA system. Furthermore, The error performance of the RCMC-CDMA system is comparable to the MC-CDMA system with a linear minimum mean square error (LMMSE) multi-user detector, but it is better than the error performance of the MC-CDMA system with decorrelating multi-user detectors [7].

In [8], the Hadamard-Walsh matrix is first split into smaller equal-size submatrices based on the channel length. Then, the MC-CDMA system is MAI-free if two conditions are satisfied. First, the number of users is equal to or less than the number of codes per submatrix. Second, if all users select their unique spreading codes from the same submatrix. The MC-CDMA system in [8] can

achieve multipath diversity. A properly selected Hadamard-Walsh codewords or exponential codewords may lead to MAI-free MC-CDMA even in the presence of carrier frequency offset [9]. In [11], a time-domain oversampling is proposed for OFDM in doubly selective fading. The time-domain oversampling can significantly improve the diversity gain at the receive and can remove the impacts of timing offset between the transmitter and the receiver sampling clocks.

In this chapter, we investigate an MC-CDMA system with MAI-reduction technique which is based on approximation of frequency selective channels by flat fading channels. The system is designed for the uplink direction, where multiple users transmit to the same receiver at the same time. In our system, each user transmits N data symbols, the N data symbols are then spread into NM chips using spreading code of length M before transmission. At the receiver, the superposition of time-domain signals from all users are oversampled with oversampling factor q; the frequency-domain representation is then obtained for the sampled signals. When N is sufficiently large, the frequency domain of frequency selective fading channels can be approximated by flat fading channels leading to an approximately MAI-free system [6]. Finally, the system is called repetitively coded multi-user multiple access (RC-MUMA) system.

The rest of this chapter is organized as follows. Section 2.2 describes the RC-MUMA system model. In Section 2.3, we discuss the receiver design of the RC-MUMA system. Section 2.4 presents the error analysis of the MAI-free RC-MUMA system. Section 2.5 presents the simulation results. Finally, Section 2.6 concludes the chapter.

2.2 System Model

Consider a wireless communication system in the uplink direction, where K users utilize the same frequency band to communicate with the same receiver simultaneously, as shown in the block diagram in Fig. 2.1.

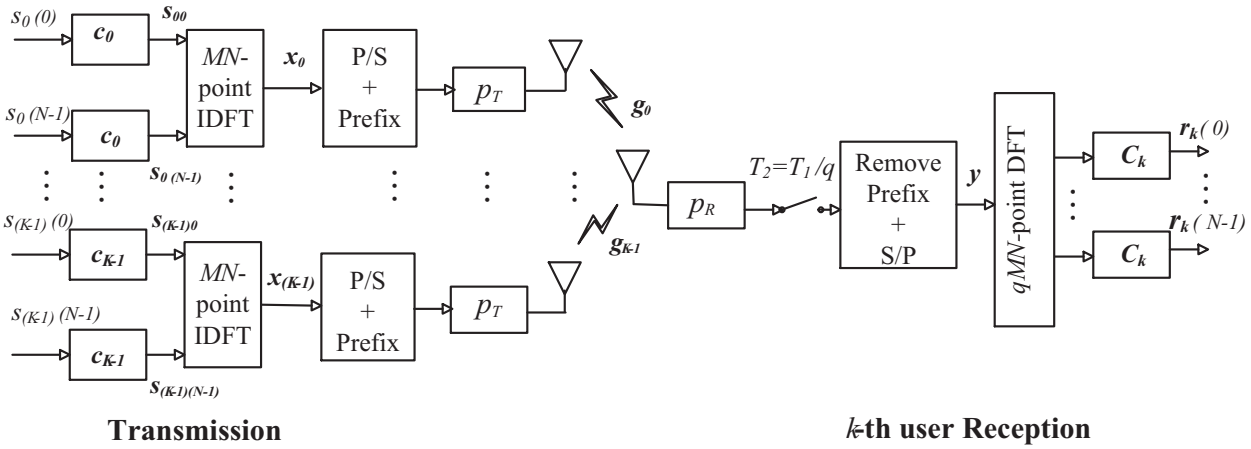

Figure 2.1: A block diagram of the RC-MUMA system with K users in the uplink direction.

Suppose that each user has N data symbols that need to be transmitted over a frequency selective Rayleigh fading channel. Each user spreads the N data symbols into NM chips using a unique spreading code selected from size M orthogonal Hadamard-Walsh matrix, $\mathbf{W}_h \in \pm 1$. The columns of $\mathbf{W}_h$ are orthogonal, *i.e.*, $\mathbf{W}_h^T \mathbf{W}_h = M\mathbf{I}_M$, where $\mathbf{I}_M$ is a size M identity matrix with M being an integer equal to or greater than K. Denote the N data symbols of the k-th user as $\mathbf{s}_k = [s_{k0}, \cdots, s_{k(N-1)}]^T \in \mathcal{S}^{N\times 1}$, where $\mathcal{S}$ is the modulation constellation set. Each data symbol in $\mathbf{s}_k$ is spread using the spreading vector $\mathbf{c}_k = [c_k(0), \cdots, c_k(M-1)]^T \in \mathbf{W}_h$ resulting in the frequency-domain vector $\bar{\mathbf{s}}_k = [s_{k0}\mathbf{c}_k^T, \cdots, s_{k(N-1)}\mathbf{c}_k^T]^T = [\mathbf{s}_{k0}^T, \cdots, \mathbf{s}_{k(N-1)}^T]^T \in S^{NM\times 1}$.

The time-domain signal is then obtained by applying the NM-point inverse discrete Fourier transform (IDFT) as

$$\mathbf{x}_k = \mathbf{F}_{NM}^H \bar{\mathbf{s}}_k, \tag{2.1}$$

where $\mathbf{F}_{NM}$ is the normalized size-NM discrete Fourier transform (DFT) matrix with the $(m+1, n+1)$-th element being $(\mathbf{F}_N)_{m+1,n+1} = \frac{1}{\sqrt{NM}} \exp\left(-j\frac{2\pi mn}{NM}\right)$. If the time duration of one OFDM symbol is T_0, then the time duration of a one time-domain sample will be $T_1 = \frac{T_0}{NM}$.

The output of IDFT is converted to serial samples, and a cyclic prefix (CP) of length $L-1$ is then

added to time-domain samples, $\mathbf{x}_k$, to remove ISI between OFDM symbols, where L is the length of the equivalent T_1-spaced discrete-time channel. The prefixed time-domain signals are then passed through a transmit filter $p_{_T}(t)$, and are then transmitted over a frequency selective Rayleigh fading channel where signals are corrupted by an additive white Gaussian noise (AWGN). The receiver observes the superposition of corrupted signals from K users. The time-domain signals observed at the receiver can be expressed as

$$y(t) = \sqrt{\frac{E_s}{M}} \sum_{n=-\infty}^{\infty} \sum_{k=0}^{K-1} x_{_k}(n) g_{_k}(t - nT_1) + w(t), \tag{2.2}$$

where E_s is the energy per symbol, $g_k(t) = p_{_T}(t) \odot \bar{g}_k(t) \odot p_{_R}(t)$ is the continuous time-domain composite channel impulse response (CIR) of the k-th user physical channel, $\bar{g}_k(t)$, $w(t) = p_{_R}(t) \odot u(t)$ is the noise with $u(t)$ being an AWGN with a variance N_0, and $\odot$ is the time-domain convolution operator. The output of the receiving filter is sampled at a time instant $T_2 + \tau_0$, where $T_2 = \frac{T_1}{q}$ with the oversampling factor, q, being an integer ≥ 1, and $\tau_0 \in [\frac{-T_2}{2}, \frac{T_2}{2}]$ is the timing offset. The output of the sampler can then be represented in the discrete-time domain as

$$y(n) = \sqrt{\frac{E_s}{M}} \sum_{k=0}^{K-1} \sum_{l=0}^{qL-1} \tilde{x}_{_k}(l - n) g_{_k}(l) + w(n), \text{for } n = 0, \cdots, qNM - 1, \tag{2.3}$$

where $y(n) = y(nT_2 + \tau_0), w(n) = w(n + \tau_0)$, and $\tilde{x}_k(n)$ is the oversampled version of $x_k(n)$ defined as

$$\tilde{x}_k(n) = \begin{cases} x_k(n/q), & n/q \text{ is integer} \\ 0, & \text{otherwise.} \end{cases} \tag{2.4}$$

It is assumed that the receiver has a perfect knowledge of the-discrete time CIR of all users. In addition, the channel length of the oversampled discrete-time CIR is assumed to be an integer multiple of the oversampling factor q, and this can be done by padding zeros to the CIR. To facilitate the analysis, equation (2.3) can be represented in a matrix format as

$$\mathbf{y} = \sqrt{\frac{E_s}{M}} \sum_{k=0}^{K-1} \mathbf{G}_k \mathbf{x}_k + \mathbf{w}, \tag{2.5}$$

where $\mathbf{y} = [y(0), \cdots, y(qNM-1)]^T \in \mathcal{C}^{qNM\times 1}$, $\mathbf{w} = [w(0), \cdots, w(qNM-1)]^T \in \mathcal{C}^{qNM\times 1}$is the noise vector, and $\mathbf{G}_k = [\mathbf{g}_{k_1}, \mathbf{g}_{k_{q+1}}, \mathbf{g}_{k_{2q+1}}, \cdots, \mathbf{g}_{k_{(NM-1)q+1}}] \in \mathcal{C}^{qNM\times NM}$ is the time-domain channel matrix with $\mathbf{g}_{k_i} \in \mathcal{C}^{qNM\times 1}$ being the i-th column of the matrix $\tilde{\mathbf{G}}_k$ given as

$$\tilde{\mathbf{G}}_k = \begin{pmatrix} g_k(0) & 0 & \dots & g_k(qL-1) & \dots & g_k(1) \\ g_k(1) & g_k(0) & \dots & 0 & g_k(qL-1) & \dots \\ \vdots & \ddots & \ddots & \vdots & \vdots & \vdots \\ 0 & \dots & g_k(qL-1) & \dots & \dots & g_k(0) \end{pmatrix} \in \mathcal{C}^{qNM\times qNM}, \tag{2.6}$$

When the transmission channels experience a wide sense stationary uncorrelated scattering (WSSUS) frequency selective Rayleigh fading, the discrete-time CIR, $g_k(l)$, is zero-mean Gaussian distributed with a time-domain covariance $\mathbb{E}[g_k(l_1)g_k^*(l_2)] = \rho(l_1, l_2)$ given as [16]

$$\rho(l_1, l_2) = \int_{-\infty}^{\infty} R_{TR}(l_1T_2 - \tau) R_{TR}^*(l_2T_2 - \tau) G(\tau - \tau_0) d\tau, \tag{2.7}$$

where $G(\tau)$ is a normalized channel power delay profile (PDP) with $\int_{-\infty}^{\infty} G(\tau)d\tau = 1$, $R_{TR}(\tau)$ is the convolution of the transmit and receive filters. The impacts of the timing offset on the system is included in the time-domain covariance of the discrete CIR, and it can be completely removed by using $q = 2$ for a system with transmit and receive filters at most 100% excessive bandwidth [17].

Sampling with oversampling factor $q > 1$ generates correlation among noise samples, hence, the noise becomes colored zero-mean Gaussian distributed with a time-domain covariance matrix given as $\mathbf{R}_w = \mathbb{E}(\mathbf{w}\mathbf{w}^H) = N_o\mathbf{R}_p$, where $\mathbf{R}_p \in \mathcal{C}^{qNM\times qNM}$, and the (m, n)-th element of the matrix $\mathbf{R}_p$ is $(\mathbf{R}_p)_{(m,n)} = \int_{-\infty}^{\infty} p_R((m-n)T_2 + \tau) p_R(\tau) d\tau$ [16].

At the receiver, the frequency-domain signal can be obtained by passing the time-domain signal through a discrete Fourier transform (DFT) of qNM-point; then we have

$$\mathbf{r} = \sqrt{\frac{E_s}{M}} \sum_{k=0}^{k-1} \mathbf{H}_k \bar{\mathbf{s}}_k + \mathbf{z}, \tag{2.8}$$

where $\mathbf{r} = [r(0), \cdots, r(qNM-1)]^T \in \mathcal{C}^{qNM\times 1}$, $\mathbf{z} = \mathbf{F}_{qNM}\mathbf{w} = [z(0), \cdots, z(qNM-1)]^T \in \mathcal{C}^{qNM\times 1}$, and $\mathbf{H}_k = \mathbf{F}_{qNM}\mathbf{G}_k\mathbf{F}_{NM}^H \in \mathcal{C}^{qNM\times NM}$ is the frequency-domain channel matrix of the k-th user. The channel matrix $\mathbf{H}_k$ can be partitioned into a stack of q diagonal submatrices as $\mathbf{H}_k = \left[\mathbf{H}_{k0}^T, \cdots, \mathbf{H}_{k_{q-1}}^T\right]^T$, where $\mathbf{H}_{k_p} \in \mathcal{C}^{NM\times NM}$ can be found as

$$\mathbf{H}_{k_p} = \mathbf{F}_{qNM}(p)\mathbf{G}_k\mathbf{F}_{NM}^H, \text{ for } p = 0, \cdots, q-1, \tag{2.9}$$

with $\mathbf{F}_{qNM}(p) \in \mathcal{C}^{NM\times qNM}$ being obtained by extracting the $pNM+1$ to $(p+1)NM$ rows of $\mathbf{F}_{qNM}$. The main diagonal of the p-th submatrix can be obtained as

$$\mathbf{d}_{k_p} = \sqrt{NM}\mathbf{F}_{qNM}(p)\mathbf{g}_{k1}, \text{ for } p = 0, \cdots, q-1, \tag{2.10}$$

where $\mathbf{g}_{k1}$ is the first column of matrix $\tilde{\mathbf{G}}_k$. We can stack the q diagonals of all submatrices into one column vector to form the frequency-domain channel coefficients vector, $\mathbf{h}_k \in \mathcal{C}^{NM\times 1}$, of the k-th user, which also can be obtained as

$$\mathbf{h}_k = \sqrt{NM}\mathbf{F}_{qNM}\mathbf{g}_{k1}, \text{ for } p = 0, \cdots, q-1, \tag{2.11}$$

2.3 Receiver Design of the RC-MUMA System

The frequency-domain signal that is only contributed by the $\{s_{kn}\}_{k=0}^{K-1}$ can be described as

$$\mathbf{r}(n) = \sqrt{\frac{E_s}{M}} \sum_{k=0}^{K-1} \mathbf{C}_k\mathbf{h}_k(n)s_{kn} + \mathbf{z}(n), \text{for } n = 0, \cdots, N-1, \tag{2.12}$$

where $\mathbf{r}(n) = [\mathbf{r}_0(n), \cdots, \mathbf{r}_{q-1}(n)]^T \in \mathcal{C}^{qM\times 1}$ with $\mathbf{r}_p(n) = [r(pN+n), \cdots, r(pN+M+n-1)]$, $\mathbf{h}_k(n) = [\mathbf{h}_{k0}(n), \cdots, \mathbf{h}_{k(q-1)}(n)]^T \in \mathcal{C}^{qM\times 1}$ with $\mathbf{h}_{kp}(n) = [h_k(pN+n), \cdots, h_k(pN+M+n-1)]$,

$\mathbf{z}(n) = [\mathbf{z}_0(n), \cdots, \mathbf{z}_{q-1}(n))]^T \in \mathcal{C}^{qM\times 1}$ with $\mathbf{z}_p(n) = [z(pN+n), \cdots, z(pN+M+n-1)]$, and $\mathbf{C}_k = \text{diag}\{\bar{\mathbf{c}}_k\}$ with $\bar{\mathbf{c}}_k = \mathbf{1}_q \otimes \mathbf{c}_k \in \pm 1$ and$\mathbf{1}_q$ being all ones vector of length q.

The received samples that are contributed exclusively by the s_{kn} can be obtained by multiplying (2.12) with the matrix $\mathbf{C}_k$, the result is then

$$\mathbf{r}_k(n) = \sqrt{\frac{E_s}{M}}\mathbf{h}_k(n)s_{kn} + \sqrt{\frac{E_s}{M}}\sum_{j=0,j\neq k}^{K-1}\mathbf{C}_k\mathbf{C}_j\mathbf{h}_j(n)s_{jn} + \mathbf{z}_k(n), \tag{2.13}$$

where $\mathbf{z}_k(n) = \mathbf{C}_k\mathbf{z}(n)$ is the frequency-domain noise vector.

The channel coefficients vector $\mathbf{h}_k(n)$, and the noise vector $\mathbf{z}_k(n)$ are zero-mean complex Gaussian distributed with covariance matrices given respectively as

$$\begin{aligned}\mathbf{R}_{hk}(n) &= \mathbb{E}[\mathbf{h}_k(n)\mathbf{h}_k(n)^H] \\ &= NM\bar{\mathbf{F}}_n\mathbf{R}_g\bar{\mathbf{F}}_n^H \in \mathcal{C}^{qM\times qM},\end{aligned} \tag{2.14}$$

$$\begin{aligned}\mathbf{R}_{zk}(n) &= \mathbb{E}[(\mathbf{z}_k(n))(\mathbf{z}_k(n))^H] \\ &= N_0\mathbf{C}_k\bar{\mathbf{F}}_n\mathbf{R}_p\bar{\mathbf{F}}_n^H\mathbf{C}_k^H \in \mathcal{C}^{qM\times qM},\end{aligned} \tag{2.15}$$

where $\bar{\mathbf{F}}_n \in \mathcal{C}^{qM\times qNM}$ is obtained by extracting a submatrix with rows indices set $\{1+nM, \cdots, M(n+1), 1+M(n+N), \cdots, M+M(1+n+N)\}$ from the DFT matrix, $\mathbf{F}_{qNM}$, and $\mathbf{R}_g \in \mathcal{C}^{qNM\times qNM}$ is the time-domain channel covariance matrix with its (m,n)-th element defined as $\mathbf{R}_g(m,n) = \rho(m-1,n-1)$, for $1 \leq m,n \leq qL-1$, and zero otherwise.

Since the noise vector $\mathbf{z}_k(n)$ contains correlated noise samples, the noise covariance matrix $\mathbf{R}_{zk}(n)$ could be rank deficient with rank u_k. Define the pseudo-inverse of $\frac{1}{N_0}\mathbf{R}_{zk}(n)$ as

$$\mathbf{\Phi}_k = \boldsymbol{V}_k\mathbf{\Omega}_k^{-1}\boldsymbol{V}_k^H \in \mathcal{C}^{qM\times qM}, \tag{2.16}$$

where $\mathbf{\Omega}_k = \text{diag}\big[\omega_1, \omega_2, \cdots, \omega_{u_k}\big] \in \mathcal{C}^{u_k\times u_k}$ is a diagonal matrix with diagonal components being the non-zero eigenvalues of $\frac{1}{N_0}\mathbf{R}_{zk}$ in a decreasing order, and $\boldsymbol{V}_k = [\mathbf{v}_1, \mathbf{v}_2, \cdots, \mathbf{v}_{u_k}] \in \mathcal{C}^{qM\times u_k}$ is the

matrix that includes the corresponding orthonormal eigenvectors. Now, define the noise whitening matrix as

$$\mathbf{D}_k = \mathbf{\Omega}_k^{-\frac{1}{2}} \mathbf{V}_k^H \in \mathcal{C}^{u_k \times qM}. \tag{2.17}$$

Multiplying (2.13) with the whitening matrix $\mathbf{D}_k$, we have

$$\bar{\mathbf{r}}_k(n) = \mathbf{D}_k \mathbf{r}_k(n) = \sqrt{\frac{E_s}{M}} \mathbf{D}_k \mathbf{h}_k(n) s_{kn} + \sqrt{\frac{E_s}{M}} \sum_{j=0, j\neq k}^{K-1} \mathbf{D}_k \mathbf{C}_k \mathbf{C}_j \mathbf{h}_j(n) s_{jn} + \mathbf{D}_k \mathbf{z}_k(n), \tag{2.18}$$

The noise vector in (2.18) is an AWGN with a covariance matrix $\bar{\mathbf{R}}_{zk}(n) = \mathbb{E}[(\mathbf{D}_k \mathbf{z}_k(n)) \cdot (\mathbf{D}_k \mathbf{z}_k(n))^H] = N_0 \mathbf{I}_{qM}$, where $\mathbf{I}_{qM}$ is size qM identity matrix. Performing maximum ratio combining (MRC) with respect to the k-th user as $b_{kn} = (\mathbf{D}_k \mathbf{h}_k(n))^H \mathbf{r}_k(n)$ we have

$$b_{kn} = \sqrt{\frac{E_s}{M}} \mathbf{h}_k^H(n) \mathbf{\Phi}_k \mathbf{h}_k(n) s_{kn} + \sqrt{\frac{E_s}{M}} \sum_{j=0, j\neq k}^{K-1} \mathbf{h}_k^H(n) \mathbf{\Phi}_k \mathbf{C}_k \mathbf{C}_j \mathbf{h}_j(n) s_{jn} + \mathbf{h}_k^H(n) \mathbf{\Phi}_k \mathbf{z}_k(n), \tag{2.19}$$

where $\sqrt{\frac{E_s}{M}} \sum_{j=0, j\neq k}^{K-1} \mathbf{h}_k^H(n) \mathbf{\Phi}_k \mathbf{C}_k \mathbf{C}_j \mathbf{h}_j(n) s_{jn}$ is the MAI.

When the number of subcarriers N is sufficiently large, the frequency-domain channel coefficients vector $\mathbf{h}_k(n)$ can be approximated by $\tilde{\mathbf{h}}_k(n) = [\tilde{\mathbf{h}}_{k0}(n), \cdots, \tilde{\mathbf{h}}_{k(q-1)}(n)]^T \in \mathcal{C}^{qM \times 1}$ with $\tilde{\mathbf{h}}_{kp}(n) = \mathbf{1}_M \otimes h_k(pN + n)$. If we consider the above approximation, the MAI will be very small, *i.e.*, $\tilde{\mathbf{h}}_k^H(n) \mathbf{\Phi}_k \mathbf{C}_k \mathbf{C}_j \tilde{\mathbf{h}}_j(n) \approx 0$ for $k \neq j$. Thus, (2.19) can be approximated by

$$\tilde{b}_{kn} = \sqrt{\frac{E_s}{M}} \tilde{\mathbf{h}}_k(n) \mathbf{\Phi}_k \tilde{\mathbf{h}}_k^H(n) s_{kn} + \tilde{\mathbf{h}}_k^H(n) \mathbf{\Phi}_k \mathbf{z}_k(n). \tag{2.20}$$

Based on (2.20), the decision rule can then be described as

$$\hat{s}_{kn} = \underset{s_m \in S}{\operatorname{argmin}} |\tilde{b}_{kn} - s_m \tilde{\beta}_{kn}|^2, \tag{2.21}$$

where, $\tilde{\beta}_{kn} = \sqrt{\frac{E_s}{M}} \tilde{\mathbf{h}}_k(n)^H \mathbf{\Phi}_k \tilde{\mathbf{h}}_k(n)$.

2.4 Error Analysis of MAI-free RC-MUMA System

In this section, we derive the theoretical error performance of the MAI-free RC-MUMA system. The MAI-free RC-MUMA system can be obtained by setting $K = 1$. The derived error performance can serve as a lower bound for the RC-MUMA system with MAI. For the MAI-free system, (2.19) is reduced to

$$(b_{kn})_{MAI-free} = \sqrt{\frac{E_s}{M}}\mathbf{h}_k^H(n)\mathbf{\Phi}_k\mathbf{h}_k(n)s_{kn} + \mathbf{h}_k^H(n)\mathbf{\Phi}_k\mathbf{z}_k(n), \tag{2.22}$$

Based on (2.22), the signal-to-noise ratio (SNR) observed at the receiver output for the n-th data symbol can be written as

$$\gamma_{kn} = \frac{|\mathbf{h}_k^H(n)\mathbf{\Phi}_k\mathbf{h}_k(n)|^2 E_s}{M\mathbf{h}_k^H(n)\mathbf{\Phi}_k\mathbf{R}_{zk}\mathbf{\Phi}_k^H\mathbf{h}_k(n)} = \frac{1}{M}\mathbf{h}_k^H(n)\mathbf{\Phi}_k\mathbf{h}_k(n)\gamma_0, \tag{2.23}$$

where, $\gamma_0 = \frac{E_s}{N_o}$ is the SNR without fading, and N_0 is the noise variance. Since the matrix $\mathbf{\Phi}_k$ is a Hermitian matrix the scalar value $\eta_{kn} = \mathbf{h}_k^H(n)\mathbf{\Phi}_k\mathbf{h}_k(n)$ is a quadratic form of the zero-mean complex Gaussian random variable (CGRV) vector $\mathbf{h}_k^H(n)$, and the characteristic function (CHF) of η_{kn} is given as

$$\phi_{\eta_{kn}}(w) = \mathbb{E}[e^{jw\eta_{kn}}] = \left[\det\left(\mathbf{I}_{qM} - jw\mathbf{R}_{hk}(n)\mathbf{\Phi}_k\right)\right]^{-1}. \tag{2.24}$$

The conditional SER performance of the n-th data symbol of the M-ary phase shift keying (MPSK), M-ary amplitude shift keying (MASK), and M-ary quadrature amplitude modulation (MQAM), can be written as [18]

$$P(E|\gamma_{kn}) \;=\; \sum_{i=1}^{2}\frac{\sigma_i}{\pi}\int_0^{\theta_i}\exp\left(-\zeta\cdot\frac{\gamma_{kn}}{\sin^2(\theta)}\right)d\theta. \tag{2.25}$$

The unconditional SER can be obtained as $P_n(E) = \mathbb{E}[P(E|\gamma_{kn})]$

Based on the CHF in (2.24), the SER for systems with the MPSK or MQAM can be given as [19]

$$\begin{aligned} P_n(E) &= \sum_{i=1}^{2} \frac{\sigma_i}{\pi} \int_0^{\theta_i} \left[\det \left(\mathbf{I}_{qM} + \frac{\zeta \gamma_0}{M \sin^2 \theta} \mathbf{R}_{hk}(n) \mathbf{\Phi}_k \right) \right]^{-1} d\theta, \\ &= \sum_{i=1}^{2} \frac{\sigma_i}{\pi} \int_0^{\theta_i} \left[\det \left(\mathbf{I}_{qM} + \frac{\zeta \gamma_0}{M \sin^2 \theta} \mathbf{R}_{n} \right) \right]^{-1} d\theta, \end{aligned} \tag{2.26}$$

where the parameters σ_i, θ_i, and ζ are related to different modulation schemes as listed in [19, Table 1]; $\mathbf{R}_n = \mathbf{\Phi}_k^{\frac{1}{2}} \mathbf{R}_{hk}(n) (\mathbf{\Phi}_k^{\frac{1}{2}})^H$ with $\mathbf{\Phi}_k = (\mathbf{\Phi}_k^{\frac{1}{2}})^H \mathbf{\Phi}_k^{\frac{1}{2}}$. The identity $\det(\mathbf{I} + \mathbf{XY})) = \det(\mathbf{I} + \mathbf{YX}))$ is used to find the final result in (2.26). Performing eigenvalue decomposition on $\mathbf{R}_n$ yields

$$P_n(E) = \sum_{i=1}^{2} \frac{\sigma_i}{\pi} \int_0^{\theta_i} \prod_{l=1}^{\tilde{L}_n} \left[1 + \gamma_0 \cdot \frac{\zeta \lambda_{nl}}{M \sin^2 \theta} \right]^{-1} d\theta, \tag{2.27}$$

where $\tilde{L}_n$ is the rank of $\mathbf{R}_n$, and λ_{nl} is a non-zero eigenvalue of $\mathbf{R}_n$. The average SER of the single user RC-MUMA system can then be obtained as, $\bar{P}(E) = \frac{1}{N} \sum_{u=0}^{N-1} P_n(E)$.

2.5 Simulation Results

In this chapter, simulation results are given for the RC-MUMA system with a frequency selective Rayleigh fading channels. Indeed, analytical results are provided to validate the obtained simulation results. For simulations we use, $T_1 = 3.69\mu s$, quadrature phase shift keying (QPSK), typical urban (TU) power delay profile (PDP), and a root-raised cosine (RRC) filter with 100% excessive bandwidth is considered to be both a transmit and a receive filters. In Fig. 2.2, we plot the imaginary and real parts of the channel vector $\mathbf{h}_k(n)$ for $n = 0$, $k = 1$, $M = 4$, and oversampling factor, q=2. Each data symbol is transmitted over qM parallel subcarriers. In addition, when N is sufficiently large such as $N = 64$, the first M channel coefficients of the vector $\mathbf{h}_k(n)$ become approximately the same, similarly, the second M coefficients of the vector $\mathbf{h}_k(n)$ have approximately same values. The second M coefficients represent the expansion of the frequency-domain support due to oversampling. However, channel coefficients become different from each other when $N = 8$. Thus, for a

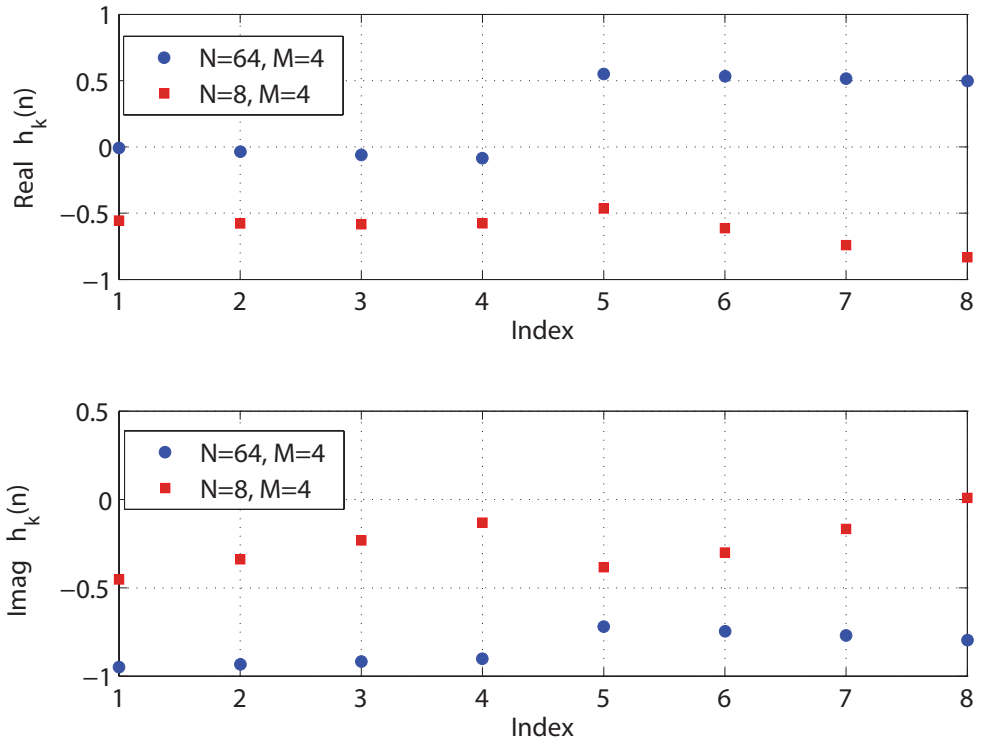

Figure 2.2: The imaginary and real parts of channel coefficient, $\mathbf{h}_k(n)$. A typical urban delay profile and $q = 2$ are used to obtain the figure.

large N the frequency-domain channel coefficients of the frequency selective Rayleigh fading can be approximated by flat fading channel coefficients as we illustrated in section 2.3.

In Fig. 2.3, the SER performance of the RC-MUMA system with and without oversampling is shown for different values of N. In simulations, the number of users is set as $K = 4$, and each data symbol is transmitted over M orthogonal subcarriers. In addition, the analytical results for the MAI-free single-user RC-MUMA system are provided for performance comparison. Two observations can be made from Fig. 2.3. First, systems with oversampling show better performance over systems without oversampling. Second, MAI reduction can be achieved by having sufficiently large N, when N is sufficiently large the system is approximately MAI-free for systems with and without oversampling. In Fig. 2.3, $N = 64$ is sufficiently large to approximate the channel coefficients by a flat fading leading to a system with very small MAI. The analytical and simulation results have

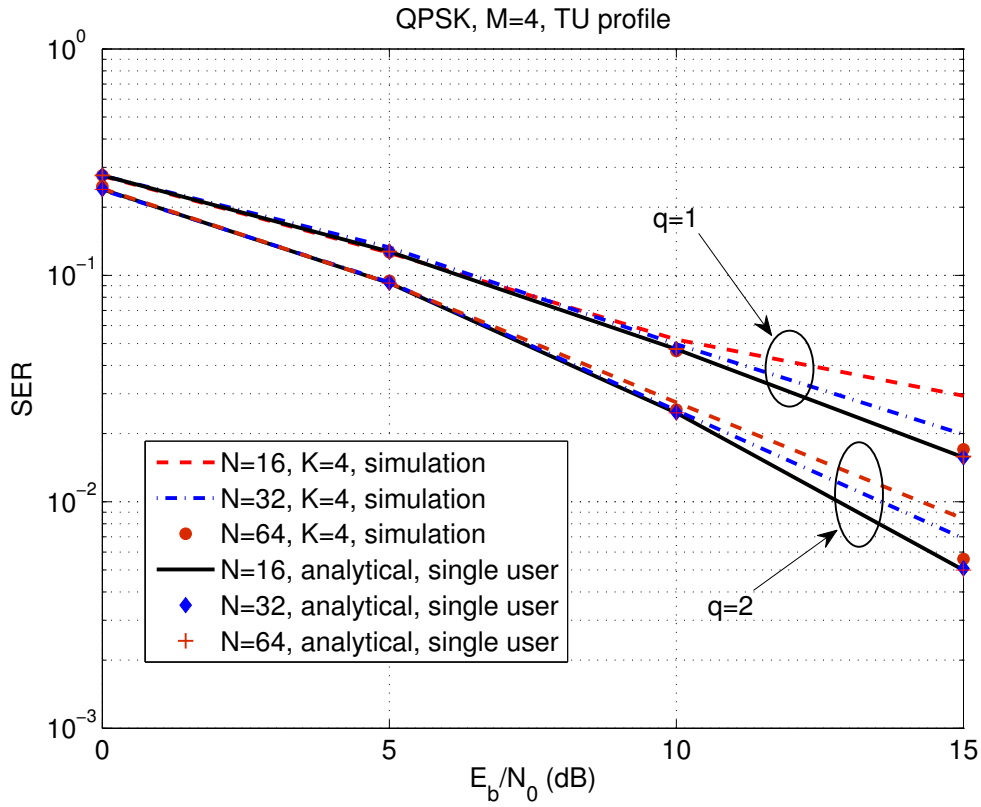

Figure 2.3: The SER performance of the RC-MUMA system over a frequency selective Rayleigh fading channels for different N values.The number of users is $K = 4$, and the spreading code length is $M = 4$. QPSK is used in all systems.

excellent matching when $N = 64$ for both systems with and without oversampling, which means that systems with $N = 64$ have a negligible MAI.

In Fig. 2.4, the performance of the RC-MUMA system with oversampling is compared with the equivalent system without oversampling in the presence of sampler timing offset, τ_o, between transmitter and the receiver sampler clocks. The timing offset ,τ_0, can produce spectrum aliasing between sampled signals at the receiver, and the overlapped samples could be combined either positively or negatively depending on their phase differences leading to performance fluctuations. However, the spectrum aliasing can be completely removed for systems with at most 100% excessive bandwidth by setting the oversampling factor as $q = 2$ [17]. Thus, in Fig. 2.4, systems with $q = 2$ are robust against sampler timing offset variations, while SER fluctuations can be observed in systems without

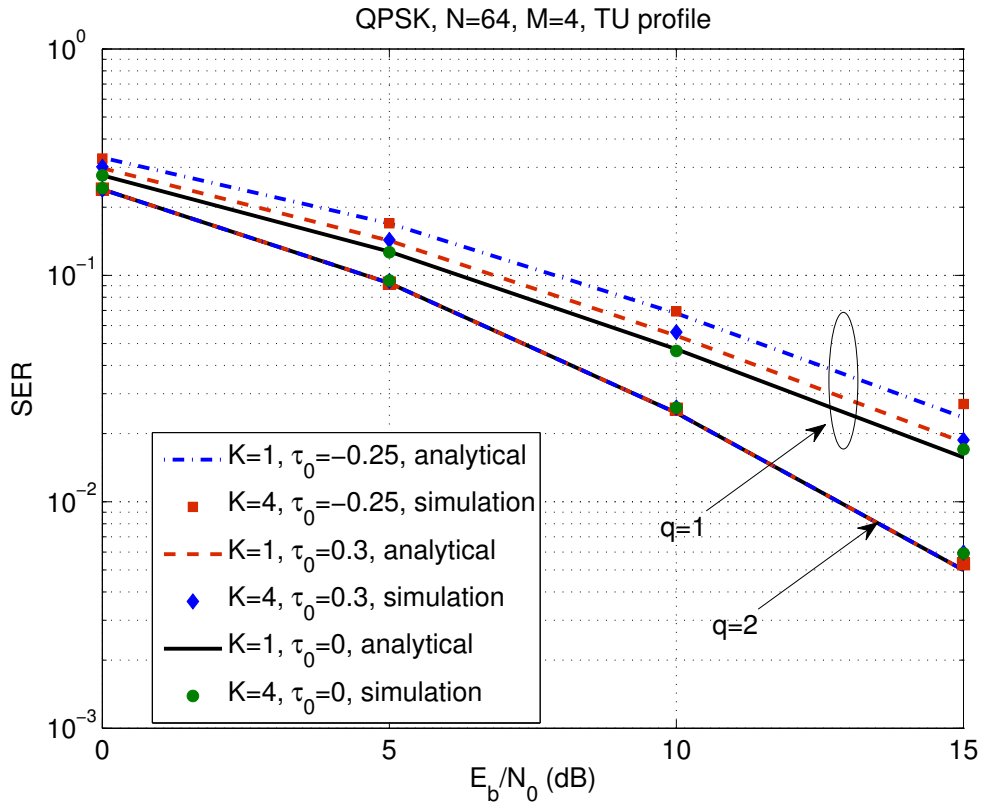

Figure 2.4: The Performance of the RC-MUMA system with and without oversampling in the presence of timing offset. $N = 64$, and $M = 4$.

oversampling where $q = 1$.

2.6 Conclusions

Based on theoretical analysis and simulation results presented in this chapter we can conclude this chapter with the following points. First, when N is sufficiently large, the frequency-domain channel coefficients of a frequency selective fading can be approximated by flat fading channel coefficients, accordingly, the system is approximately MAI-free. Second, the SER performance of the RC-MUMA system with oversampling outperforms that of an equivalent system without oversampling. Third, the performance variations that are introduced by the timing offset in the RC-MUMA system can be mitigated by employing the time-domain oversampling at the receiver side, *i.e.*, when $q = 2$. Finally, the maximum system capacity can be achieved by spreading each data symbol of N symbols into N

chips, thus the number of supported users can be up to $K = N$ users. However, the lack of multipath diversity gain and the high computational complexity are the main drawbacks of the RC-MUMA system.

Chapter 3

Oversampled Multi-Carrier Code Division Multiple Access (OMC-CDMA) System

3.1 Introduction

Multi-carrier code division multiple access (MC-CDMA) has recently received a great deal of attention as a promising multi-user technique in wireless networks. The main advantages of MC-CDMA are: First, multiple users can access the same channel at the same time leading to high bandwidth efficiency. Second, MC-CDMA can achieve high data rate transmission over multipath fading channels. Third, MC-CDMA can collect the diversity gain from multipath fading components. However, the main problem in the MC-CDMA system is the multiple access interference (MAI). In the MC-CDMA system, multiple orthogonal users transmit simultaneously over the same frequency, so when transmission channels undergo a frequency selective Rayleigh fading, orthogonality among users might be destroyed leading to MAI. MAI degrades the overall performance of the MC-CDMA system, therefore, several techniques have been proposed to reduce MAI in the MC-CDMA system. In [8], Hadamard-Walsh codes are used to spread data symbols in the frequency domain and to create orthogonality among different users. MAI-free communications can be reached by splitting the Hadamard-Walsh matrix into smaller subsets, then all users are assigned codes from the same subset. The number of supported users without MAI in [8] does not exceed the ratio between the total number of subcarriers and the channel length. The MAI reduction technique proposed in [8] is developed in [9] to support MC-CDMA with carrier frequency offsets (CFO). Another scheme to reduce MAI in the MC-CDMA system is proposed in [10], where exponential orthogonal codes are used. Furthermore, the MAI-reduction scheme in [8] is designed based on the orthogonality of the spreading codes in

the frequency domain, while, in [10], the MAI reduction scheme design is based on the time-domain structure of the spreading codes.

To collect diversity gain, different diversity combining techniques can be employed in the MC-CDMA system [20]-[27]. The maximum ratio combing (MRC) technique is used in the MC-CDMA system to achieve the full diversity gain [22]. MRC and equal gain combining (EGC) techniques are used in [25] for the MC-CDMA system with Rayleigh channel and additive white Gaussian noise (AWGN). Analysis of MRC receivers for asynchronous MC-CDMA with imperfect channel estimation are presented in [5]. A complexity reduction scheme for MC-CDMA with a minimum mean squared error (MMSE) receiver is proposed in [27].

In *Chapter 2*, we found that a trade-off between performance and computational complexity should be considered in the RC-MUMA system. Also, we observed that the diversity gain in the RC-MUMA system is only the diversity gain offered by oversampling. In this chapter, we propose MC-CDMA system with a fractionally spaced receiver by employing the time domain oversampling at the receiver side. Furthermore, we employ the code selection technique proposed in [8] to reduce the MAI in the proposed system. The proposed system is named oversampled multi-carrier code division multiple access (OMC-CDMA). The statistical properties of the discrete time model are considered in our analysis. The OMC-CDMA system can achieve a full multipath diversity where a part of this diversity is gained through oversampling. The complexity of OMC-CDMA is low compared to that of RC-MUMA.

The rest of this chapter is organized as follows. Section 3.2 demonstrates OMC-CDMA system model. In Section 3.3, the receiver design of OMC-CDMA is presented. In Section 3.4, we derive the error probability of the MAI-free OMC-CDMA system. Simulations and analytical results are given in section 3.5. Finally, we present our conclusions in section 3.6.

3.2 System Model

Consider a wireless communication system in the uplink direction where U users transmit simultaneously to the same receiver. At the transmitter, each symbol is transmitted over N orthogonal subcarriers by means of Hadamard-Walsh spreading codes. Different users are assigned different codes to generate orthogonality among users, where a loss of orthogonality among users leads to MAI.

Let the transmitted data symbol of the u-th user be represented by $s_u \in \mathcal{S}$, where $\mathcal{S}$ is the modulation alphabet set with cardinality S, then s_u is first spread into N chips in the frequency domain using the Hadamard-Walsh codes as $\mathbf{s}_u = \mathbf{c}_u \otimes s_u \in \mathcal{S}^{N\times 1}$, where $\mathbf{c}_u = [c_{u_0}, \cdots, c_{u_{(N-1)}}]^T \in \pm 1$ is the spreading code assigned to the u-th user. The spreading codes satisfy orthogonality condition, *i.e.*, $\mathbf{c}_u^T \cdot \mathbf{c}_v = N\delta_{uv}$, where δ_{uv} is the Kronecker delta function.

After spreading, the time-domain signal is obtained by passing the N chips through N-point normalized inverse discrete Fourier transform (IDFT), the time-domain signal is then

$$\mathbf{x}_u = \mathbf{F}_N^H \mathbf{s}_u, \tag{3.1}$$

where $\mathbf{F}_N$ is the normalized size-N discrete Fourier transform (DFT) matrix with the $(m+1, n+1)$-th element being $(\mathbf{F}_N)_{m+1,n+1} = \frac{1}{\sqrt{N}} \exp\left(-j\frac{2\pi mn}{N}\right)$. The output of the IDFT is passed through a parallel-to-serial converter, and then a cyclic prefix is added to the time-domain sequence to mitigate the problem of inter-symbol interference (ISI). The resultant time-domain sequence is then passed through a root raised cosine transmit filter, $p_{_T}(t)$, which satisfies $\int_{-\infty}^{\infty} p_{_T}(t)p_{_T}^*(t) = 1$ [11]. The multicarrier signal is then transmitted over a frequency selective fading channel. The receiver observes the superposition of signals from U users corrupted by an additive white Gaussian noise (AWGN).

At the receiver, the observed time-domain signals from U users are first passed through a root raised cosine receive filter, $p_{_R}(t)$, which satisfies $\int_{-\infty}^{\infty} p_{_R}(t)p_{_R}^*(t) = 1$. The superposition of the continuous

time-domain signals from all users is then presented as

$$y_{_R}(t) = \sqrt{\frac{E_s}{N}} \sum_{n=-\infty}^{\infty} \sum_{u=0}^{U-1} x_u(n) g_{_u}(t - nT_1) + w_{_R}(t), \tag{3.2}$$

where E_s is the average transmission energy per symbol, $w_{_R}(t) = p_{_R}(t) \odot \nu(t)$ is the noise part of the received signal, with $\nu(t)$ being AWGN with a variance N_0, and $g_u(t) = p_{_T}(t) \odot \tilde{g}_u(t) \odot p_{_R}(t)$ is the continuous time composite channel impulse response (CIR), which involves the effects of the transmit filter, the receive filter and the physical channel, $\tilde{g}_u(t)$ [11]. If we consider the timing offset, τ_0, between the transmitter and the receiver sampler clocks, then the output of the receiver filter is sampled at a time instant $T_s + \tau_0$, where, $\tau_0 \in [\frac{-T_s}{2}, \frac{T_s}{2}]$, and $T_s = \frac{T_1}{\eta}$ with the oversampling factor, η, being a non-negative integer. The discrete time-domain received signal can then be represented as

$$y(n) = \sqrt{\frac{E_s}{N}} \sum_{u=0}^{U-1} \sum_{l=0}^{\eta L-1} \tilde{x}_u(l - n) g_u(l) + w(n), \text{for } n = 0, \cdots, \eta N - 1, \tag{3.3}$$

where, $y(n) = y_{_R}(nT_s + \tau_0)$, $w(n) = w_{_R}(nT_s + \tau_0)$, and $\tilde{x}_u$ is the oversampled version of x_u which can be obtained as

$$\tilde{x}_u(n) = \begin{cases} x_u(n/\eta), & n/\eta \text{ is integer}, \\ 0, & \text{otherwise}, \end{cases} \tag{3.4}$$

with ηL being the channel length of the oversampled discrete-time CIR. The channel length of the oversampled discrete-time CIR is assumed to be an integer multiple of the oversampling factor η, and that can be accomplished by padding zeros to the discrete-time CIR. To simplify our analysis, we represent system equations in (3.3) in matrix format as

$$\mathbf{y} = \sqrt{\frac{E_s}{N}} \sum_{u=0}^{U-1} \mathbf{G}_u \mathbf{F}_N^H \mathbf{s}_u + \mathbf{w}, \tag{3.5}$$

where $\mathbf{y} = \big[y(0), \cdots, y(\eta N - 1)\big]^T \in \mathcal{C}^{\eta N \times 1}$, $\mathbf{w} = \big[w(0), \cdots, w(\eta N - 1]\big)^T \in \mathcal{C}^{\eta N \times 1}$ is the noise samples vector, and $\mathbf{G}_u = \big[\mathbf{g}_{u1}, \mathbf{g}_{u(\eta+1)}, \mathbf{g}_{u(2\eta+1)}, \cdots, \mathbf{g}_{u(N-1)\eta+1}\big] \in \mathcal{C}^{\eta N \times N}$ is the time-domain

channel matrix related to the u-th user with $\mathbf{g}_{uk}$ being the k-th column of the channel matrix, $\tilde{\mathbf{G}}_u$, which is given as

$$\tilde{\mathbf{G}}_u = \begin{pmatrix} g_u(0) & 0 & \dots & g_u(\eta L-1) & \dots & g_u(1) \\ g_u(1) & g_u(0) & \dots & 0 & g_u(\eta L-1) & \dots \\ \vdots & \ddots & \ddots & \vdots & \vdots & \vdots \\ 0 & \dots & g_u(qL-1) & \dots & \dots & g_u(0) \end{pmatrix} \in \mathcal{C}^{\eta N \times \eta N}. \quad (3.6)$$

The first column of matrix $\tilde{\mathbf{G}}_u$ is $\mathbf{g}_{u1} = [g_u(0), g_u(1), \cdots, g_u(\eta L-1), \mathbf{0}_{\eta(N-L)}]^T \in \mathcal{C}^{\eta N \times 1}$, with $g_u(l)$ being the equivalent discrete-time CIR of the u-th user, while the rest columns are circularly shifted versions of the first column, $\mathbf{g}_{u1}$.

For channels experience a wide sense stationary uncorrelated scattering (WSSUS) frequency selective Rayleigh fading, the discrete time-domain CIR, $g_u(l)$, is zero-mean complex Gaussian distributed with covariance given as [11]

$$\rho(l_1, l_2) = \int_{-\infty}^{\infty} R_{TR}(l_1 T_s - \eta + \tau_0) R^*_{TR}(l_2 T_s - \eta + \tau_0) G(\tau) d\tau, \quad (3.7)$$

where $G(\tau)$ is the normalized channel power delay profile (PDP) with $\int_{-\infty}^{\infty} G(\tau)d\tau = 1$, and $R_{TR}(t)$ is the convolution of the transmit and receive filters. It should be noted that the effect of the timing offset, τ_0 is included in the channel covariance. It is shown in [17] that the impacts of timing offset can be removed by using $\eta = 2$ for a system with at most 100% excessive bandwidth. Furthermore, if the signal is corrupted by AWGN, the vector $\mathbf{w}$ is zero-mean complex Gaussian distributed with a covariance matrix $\mathbf{R}_w$ given as $\mathbf{R}_w = \mathbb{E}[\mathbf{w}\mathbf{w}^H] = \frac{1}{N_0}\mathbf{R}_p$ where $\mathbf{R}_p \in \mathcal{C}^{qN \times qN}$, and the (m,n)-th element of matrix $\mathbf{R}_p$ is $(\mathbf{R}_p)_{(m,n)} = \int_{-\infty}^{\infty} p_R((m-n)T_s + \tau) p_R(\tau) d\tau$ [11].

3.3 Receiver Structure of the OMC-CDMA System

The frequency-domain representation of the discrete-time observed signal is obtained by performing the ηN-point DFT over $\mathbf{y}$ in (3.5) as $\mathbf{r} = \mathbf{F}_{\eta N}\mathbf{y}$, where $\mathbf{F}_{\eta N}$ is the normalized ηN-point DFT matrix with the $(m+1, n+1)$-th element being $(\mathbf{F}_{\eta N})_{m+1,n+1} = \frac{1}{\sqrt{\eta N}} \exp\left(-j\frac{2\pi mn}{\eta N}\right)$; the frequency-domain system representation can then be represented as

$$\mathbf{r} = \sqrt{\frac{E_s}{N}} \sum_{u=0}^{U-1} \mathbf{H}_u \mathbf{s}_u + \mathbf{z}, \tag{3.8}$$

where $\mathbf{H}_u = \mathbf{F}_{\eta N}(\mathbf{G}_u)\mathbf{F}_N^H \in \mathcal{C}^{\eta N \times N}$, is the frequency-domain channel coefficient matrix, and $\mathbf{z} = \mathbf{F}_{\eta N}\mathbf{w} \in \mathcal{C}^{\eta N \times 1}$ is the frequency domain noise samples vector. The frequency domain channel coefficient matrix, $\mathbf{H}_u$ can be partitioned into a stack of size-ηN diagonal submatrices as $\mathbf{H}_u = \left[\mathbf{H}_{u_0}^T, \cdots, \mathbf{H}_{u_{\eta-1}}^T\right]^T$. Now, let $\mathbf{h}_u \in \mathcal{C}^{\eta N \times 1}$ be a column vector that contains the frequency-domain subcarriers over which a single modulated data symbol is transmitted from the u-th user. The channel vector, $\mathbf{h}_u$, can be expressed as

$$\mathbf{h}_u = \sqrt{N}\mathbf{F}_{\eta N}\mathbf{g}_{u1}, \tag{3.9}$$

where $\mathbf{g}_{u1}$ is the first column of the matrix $\tilde{\mathbf{G}}_u$. Furthermore, the vector $\mathbf{h}_u$ can be obtained by stacking all diagonals of submatrices into one column vector. With the help of the frequency-domain channel vector, $\mathbf{h}_u$, (3.8) can be rewritten as

$$\mathbf{r} = \sqrt{\frac{E_s}{N}} \sum_{u=0}^{U-1} \mathbf{C}_u \mathbf{h}_u s_u + \mathbf{z}, \tag{3.10}$$

where, $\mathbf{C}_u \in \mathcal{C}^{\eta N \times \eta N}$ is a size ηN diagonal matrix with $\mathbf{d}_{c_u} = \mathbf{1}_\eta \otimes \mathbf{c}_u \in \mathcal{C}^{\eta N \times 1}$ being the main diagonal. We have the following lemma about both the frequency-domain channel and the frequency-domain noise vectors in (3.10).

Lemma 3.1: For the OMC-CDMA system with a frequency selective Raleigh fading channel and AWGN, both $\mathbf{h}_u$ and $\mathbf{z}$ are zero-mean complex Gaussian distributed with their respective covariance matrices given as

$$\mathbf{R}_h = N \cdot \mathbf{F}_{uN}\mathbf{R}_g\mathbf{F}_{uN}^H \tag{3.11}$$

$$\mathbf{R}_z = N_0 \cdot \mathbf{F}_{uN}\mathbf{R}_p\mathbf{F}_{uN}^H \tag{3.12}$$

where, $\mathbf{R}_g = \mathbb{E}[\mathbf{g}_{u1}\mathbf{g}_{u1}^H] \in \mathcal{C}^{\eta N \times \eta N}$ is the time-domain channel covariance matrix with its (m,n)-th element defined as $\mathbf{R}_g(m,n) = \sigma(m-1, n-1)$, for $1 \leq m, n \leq \eta L - 1$, and zero otherwise [11].

Proof: $\mathbf{R}_h = \mathbb{E}[\mathbf{h}_u.\mathbf{h}_u^H] = \mathbf{F}_{\eta N}\mathbb{E}[\mathbf{g}_{u1}\mathbf{g}_{u1}^H]\mathbf{F}_{\eta N}^H$, the first ηL of $\mathbf{g}_{u1}$ are the discrete-time CIR with a covariance given in (3.7). For the noise covariance, $\mathbf{R}_z = \mathbf{F}_{\eta N}\mathbb{E}[\mathbf{w}\mathbf{w}^H]\mathbf{F}_{\eta N}^H$, where $\mathbb{E}[\mathbf{w}\mathbf{w}^H] = N_0\mathbf{R}_p$ and that completes the proof. ■

At the receiver, the received signal of the u-th user can be obtained by multiplying (3.10) with the despreading matrix, $\mathbf{C}_u$, as

$$\mathbf{r}_u = \sqrt{\frac{E_s}{N}}\mathbf{h}_u s_u + \sqrt{\frac{E_s}{N}}\mathbf{C}_u \sum_{v=0, v\neq u}^{U-1} \mathbf{C}_v\mathbf{h}_v \cdot s_v + \mathbf{C}_u\mathbf{z}, \tag{3.13}$$

where $\mathbf{C}_u\mathbf{C}_u = \mathbf{I}_{\eta M}$ is used in the above equation. Next we consider the OMC-CDMA system without and with oversampling, respectively.

3.3.1 System Without Oversampling

If $T_s = T_1$, *i.e.*, the oversampling factor $\eta = 1$, the noise in (3.13) is zero-mean white Gaussian noise with a covariance matrix $\mathbb{E}[\mathbf{C}_u\mathbf{z}\mathbf{z}^H\mathbf{C}_u] = N_0\mathbf{I}_N$, thus, we can directly apply the MRC to the system by multiplying (3.13) with $\mathbf{h}_u^H$ as

$$b_u = \mathbf{h}_u^H\mathbf{r}_u = \sqrt{\frac{E_s}{N}}\mathbf{h}_u^H\mathbf{h}_u s_u + \sqrt{\frac{E_s}{N}}\mathbf{h}_u^H\mathbf{C}_u \sum_{v=0, v\neq u}^{U-1} \mathbf{C}_v\mathbf{h}_v \cdot s_v + \mathbf{h}_u^H\mathbf{C}_u\mathbf{z}, \tag{3.14}$$

The first part in (3.14) is the desired signal, the second part is the MAI, and the third part is the noise. The mutual interference between user u and user v can be described as

$$\begin{aligned} I_{uv} &= \sqrt{\frac{E_s}{N}}\mathbf{h}_u^H \mathbf{C}_u \mathbf{C}_v \mathbf{h}_v \cdot s_v, \\ &= \sqrt{\frac{E_s}{N}}\mathbf{g}_u^H \mathbf{A}_{uv} \mathbf{g}_v \cdot s_v, \end{aligned} \tag{3.15}$$

where $\mathbf{A}_{uv} = \mathbf{F}_N^H \mathbf{C}_u \mathbf{C}_v \mathbf{F}_N \in \mathcal{C}^{N\times N}$, $\mathbf{g}_u = [g_u(0), \cdots, g_u(L-1), \mathbf{0}_{(N-L)}]^T \in \mathcal{C}^{N\times 1}$, and $\mathbf{g}_v = [g_v(0), \cdots, g_v(L-1), \mathbf{0}_{(N-L)}]^T \in \mathcal{C}^{N\times 1}$. Since the first L elements of $\mathbf{g}_u$ and $\mathbf{g}_v$ are non-zero elements and the rest $N-L$ elements are zeros, it can be easily shown that $I_{uv} = 0$ if the first $L \times L$ elements of the matrix $\mathbf{A}_{uv}$ are zeros for any $u \neq v$. In [8], a spreading code selection technique was proposed to obtain the matrix $\mathbf{A}_{uv}$ with zero elements, the code selection technique can be summarized in the following lemma.

Lemma 3.2: Let the Hadamard-Walsh codes matrix of size N be partitioned into L submatrices with N/L codewords in each submatrix, then the first $L \times L$ elements of matrix $\mathbf{A}_{uv}$ are zeros for any $u \neq v$ if user u and user v select their respective spreading codes from the same submatrix [8].

Proof: The proof of lemma 3.2 is omitted here for brevity, but it can be found in [8]. ■

If spreading codes are selected for all users according to lemma 3.2, the system in (3.14) can support a number of users not greater than N/L without MAI. Thus, for MAI-free system, equation (3.14) is reduced to

$$\begin{aligned} b_u &= \sqrt{\frac{E_s}{N}}\mathbf{h}_u^H \mathbf{h}_u s_u + \mathbf{h}_u^H \mathbf{C}_u \mathbf{z}, \\ &= \sqrt{\frac{E_s}{N}} \sum_{l=0}^{L-1} |h_u(l)|^2 s_u + \mathbf{h}_u^H \mathbf{C}_u \mathbf{z}, \end{aligned} \tag{3.16}$$

The conventional MRC receiver is the optimum receiver for MAI-free system. Based on (3.16),

the decision rule can be expressed as

$$\hat{s}_u = \underset{s_m \in S}{\operatorname{argmin}} |b_u - s_m \alpha_u|^2, \tag{3.17}$$

where, $\alpha_u = \sqrt{\frac{E_s}{N}} \mathbf{h}_u^H \mathbf{h}_u$. In the next subsection we will study the OMC-CDMA when $\eta > 1$.

3.3.2 System With Oversampling

For system with oversampling, *i.e.*, $\eta > 1$, the noise part in (3.13) contains correlated zero-mean Gaussian distributed samples, so the noise is colored with a covariance matrix $\mathbf{R}_{zu} = \mathbf{C}_u \mathbf{R}_z \mathbf{C}_u$. Since the noise is not white, a noise whitening is required before applying the maximum ratio combining to (3.13). Indeed, the covariance matrix, $\mathbf{R}_{zu}$ might be rank deficient with rank $p \leq \eta N$, so let the pseudo-inverse of $\frac{1}{N_0}\mathbf{R}_{zu}$ be defined as

$$\mathbf{\Phi}_u = \boldsymbol{V}_p \mathbf{\Omega}_p^{-1} \boldsymbol{V}_p^H \in \mathcal{C}^{\eta N \times \eta N}, \tag{3.18}$$

where $\mathbf{\Omega}_p = \operatorname{diag}\big[\omega_1, \omega_2, \cdots, \omega_p\big] \in \mathcal{C}^{p \times p}$ is a diagonal matrix with diagonal elements being the non-zero eigenvalues of $\frac{1}{N_0}\mathbf{R}_{zu}$ in a decreasing order, and $\boldsymbol{V}_p = [\mathbf{v}_1, \mathbf{v}_2, \cdots, \mathbf{v}_p] \in \mathcal{C}^{\eta N \times p}$ is the orthonormal eigenvectors matrix of $\frac{1}{N_0}\mathbf{R}_{zu}$.

Define the whitening matrix as $\mathbf{D}_u = \mathbf{\Omega}_p^{-\frac{1}{2}} \boldsymbol{V}_p^H \in \mathcal{C}^{p \times \eta N}$, then the noise whitening of the colored noise in (3.13) can be obtained by multiplying (3.13) by the whitening matrix $\mathbf{D}_u$, the result can then be written as

$$\begin{aligned} \bar{\mathbf{r}}_u &= \mathbf{D}_u \mathbf{r}_u \\ &= \sqrt{\frac{E_s}{N}} \mathbf{D}_u \mathbf{h}_u s_u + \sqrt{\frac{E_s}{N}} \mathbf{D}_k \sum_{v=0, v \neq u}^{U-1} \mathbf{C}_u \mathbf{C}_v \mathbf{h}_v \cdot s_v + \boldsymbol{\zeta}_u, \end{aligned} \tag{3.19}$$

where $\boldsymbol{\zeta}_u = \mathbf{D}_u \mathbf{C}_u \mathbf{z}_u$ is AWGN with a covariance matrix $N_0 \mathbf{I}_{\eta N}$. Applying MRC by multiplying

(3.19) with $(\mathbf{D}_u\mathbf{h}_u)^H$ we have

$$\begin{aligned}\varphi_u &= \sqrt{\frac{E_s}{N}}\mathbf{h}_u^H\mathbf{\Phi}_u\mathbf{r}_u, \\ &= \sqrt{\frac{E_s}{N}}\sigma_u s_u + \sqrt{\frac{E_s}{N}}\mathbf{h}_u^H\mathbf{\Phi}_u \sum_{v=0,v\neq u}^{U-1} \mathbf{C}_u\mathbf{C}_v\mathbf{h}_v \cdot s_{v_k} + \bar{\zeta}_u, \end{aligned} \tag{3.20}$$

where $\sigma_u = \mathbf{h}_u^H\mathbf{\Phi}_u\mathbf{h}_u$, and $\bar{\zeta}_u = \mathbf{h}_u^H\mathbf{\Phi}_u\mathbf{C}_u\mathbf{z}_u$, is the noise. The mutual interference between user u and user v can be expressed as

$$I_{uv} = \sqrt{\frac{E_s}{N}}\mathbf{h}_u^H\mathbf{\Phi}_u\mathbf{C}_u\mathbf{C}_v\mathbf{h}_v \cdot s_v. \tag{3.21}$$

If all users select their spreading codes according to *Lemma 1.2*, the mutual interference among them will be small and can be neglected, *i.e.*, $I_{uv} \approx 0$ for $u \neq v$. Thus, (3.20) can be approximated as

$$\varphi_u \approx \sqrt{\frac{E_s}{N}}\sigma_u s_u + \bar{\zeta}_u. \tag{3.22}$$

It should be noted that the above approximation was investigated and validated for TU PDP by comparing the analytical error performance of a system when $U = 1$ with the simulated one for a system with multiple users. The decision rule can then be described as

$$\hat{s}_u = \underset{s_m \in S}{\text{argmin}} |\varphi_u - s_m\sigma_u|^2. \tag{3.23}$$

3.4 Performance Analysis of an MAI-free OMC-CDMA System

In this section, we derive the error performance of MAI-free OMC-CDMA system in frequency selective Rayleigh fading channels. The OMC-CDMA system with $\eta = 1$ and $U \leq N/L$ is MAI-free if all users select their spreading codes from the same subset. Also, the MAI-free OMC-CDMA system can be obtained by setting $U = 1$ for $\eta \geq 1$. The derived error performance can be considered as the lower bound of the OMC-CDMA system with MAI. For the MAI-free OMC-CDMA system the

decision variable in (3.20) is reduced to

$$\begin{aligned}\varphi_u &= \sqrt{\frac{E_s}{N}}\mathbf{h}_u^H\mathbf{\Phi}_u\mathbf{h}_u + \mathbf{h}_u^H\mathbf{\Phi}_u\mathbf{C}_u\mathbf{z}_u, \\ &= \sqrt{\frac{E_s}{N}}\sigma_u s_u + \bar{\zeta}_u \end{aligned} \tag{3.24}$$

The instantaneous signal-to-noise ratio (SNR) γ_u at the receiver output can be described by

$$\gamma_u = \frac{E_s\sigma_u\sigma_u^*}{NN_0\mathbf{h}_u^H\mathbf{\Phi}_u\mathbf{R}_{zu}\mathbf{\Phi}_u^H\mathbf{h}_u} = \frac{1}{N}\gamma_s\sigma_u, \tag{3.25}$$

where $\gamma_s = \frac{E_s}{N_0}$ is the SNR without fading, E_s is the average transmission energy per transmitted data symbol, and N_0 is the noise variance. In terms of the instantaneous SNR, γ_u, the conditional error probability of the MAI-free OMC-CDMA system with *m*-ary Phase-shift keying (MPSK) modulation can be expressed as [28]

$$P(E_u|\gamma_u) = \sum_{i=1}^{2}\frac{\beta_i}{\pi}\int_0^{\frac{(M-1)\pi}{M}}\exp\bigg(-\frac{\gamma_s\sigma_u\sin^2(\pi/M)}{N\sin^2(\theta)}\bigg)d\theta, \tag{3.26}$$

The unconditional error probability $P(E_u)$ is then found by averaging $P(E|\gamma_u)$ over the instantaneous SNR γ_u, *i.e.*, $P(E_u) = \mathbb{E}[P(E_u|\gamma_u)]$. The pseudo-inverse matrix ,$\mathbf{\Phi}_u$, is a Hermitian matrix, thus, the scalar $\sigma_u = \mathbf{h}_u^H\mathbf{\Phi}_u\mathbf{h}_u$ is a real quadratic form of the complex Gaussian random variable (CGRV) vector $\mathbf{h}_u$ with characteristic function (CHF) given as [28]

$$\mathbb{E}(e^{jw\beta_u}) = [\det(\mathbf{I}_{\eta N} - jw\mathbf{R}_h\mathbf{\Phi}_u)]^{-1}, \tag{3.27}$$

Substituting (3.27) in (3.26) and using the identity $\det[\mathbf{I}_{\eta N}+\mathbf{AB}] = \det[\mathbf{I}_{\eta N}+\mathbf{BA}]$, the unconditional error probability $P(E_u)$ can be written as

$$\begin{aligned}P(E_u) &= \sum_{i=1}^{2}\frac{\beta_i}{\pi}\int_0^{\psi_i}\bigg[\det\bigg(\mathbf{I}_{\eta N} + \frac{\gamma_s\xi}{N\sin^2(\theta)}\mathbf{R}_h\mathbf{\Phi}_u\bigg)\bigg]^{-1}d\theta, \\ &= \sum_{i=1}^{2}\frac{\beta_i}{\pi}\int_0^{\psi_i}\bigg[\det\bigg(\mathbf{I}_{\eta N} + \frac{\gamma_s\xi}{N\sin^2(\theta)}\mathbf{\Phi}_u^{\frac{1}{2}}\mathbf{R}_h(\mathbf{\Phi}_u^{\frac{1}{2}})^H\bigg)\bigg]^{-1}d\theta, \end{aligned} \tag{3.28}$$

where, $\mathbf{\Phi}^{\frac{1}{2}}$ is the square root of matrix $\mathbf{\Phi}$ such that $\mathbf{\Phi} = (\mathbf{\Phi}^{\frac{1}{2}})(\mathbf{\Phi}^{\frac{1}{2}})^H$. Performing an eigenvalues decomposition of the product $\mathbf{R}_u = \mathbf{\Phi}_u^{\frac{1}{2}}\mathbf{R}_h(\mathbf{\Phi}_u^{\frac{1}{2}})^H$ as

$$\mathbf{R}_u = \mathbf{\Omega}_u\mathbf{\Lambda}_u^{-1}\mathbf{\Omega}_u^H \in \mathcal{C}^{\eta N\times\eta N}, \tag{3.29}$$

where $\mathbf{\Lambda}_u = \text{diag}\big[\lambda_1, \lambda_2, \cdots, \lambda_\upsilon\big] \in \mathcal{C}^{\upsilon\times\upsilon}$ is a diagonal matrix that contains the non-zero eigenvalues of $\mathbf{R}_u$ in a decreasing order, with υ being the number of non-zero eigenvalues, and $\mathbf{\Omega}_u = [\omega_1, \omega_2, \cdots, \omega_\upsilon] \in \mathcal{C}^{\eta N\times\upsilon}$ is the orthonormal eigenvectors matrix of $\mathbf{R}_u$. Employing (3.29) in (3.28) we get

$$P(E_u) = \sum_{i=1}^{2}\frac{\beta_i}{\pi}\int_0^{\psi_i}\prod_{j=1}^{\upsilon}\left[1+\gamma_0\cdot\frac{\xi\lambda_p}{\sin^2\theta}\right]^{-1}d\theta. \tag{3.30}$$

The parameters β_i, ψ_i, and ξ are found in [19, Table 1], these parameters are corresponding to various modulation schemes. To investigate our analytical results, simulation results are presented next.

3.5 Numerical and simulation Results

Computer simulations were generated to examine the performance of the OMC-CDMA system and to verify the analytical results obtained in the previous sections. In all simulations and analytical results, we consider a frequency selective Rayleigh fading channel with a typical urban (TU) power delay profile (PDP), unless otherwise mentioned. A root raised cosine filter with 100% excessive band width is used as a transmit and receive filters. The transmitter sampling period was set as $T1 = 3.69\mu s$.

In Fig. 3.1, the absolute value of MAI between two users is plotted for the OMC-CDMA system without oversampling. The equivalent length of the discrete-time CIR is $L = 4$. QPSK-modulation with a total number of orthogonal subcarriers at transmitter being $N = 64$ is employed for all users. The spreading Hadamard-Walsh matrix of size N is divided into four groups with 16 different codes

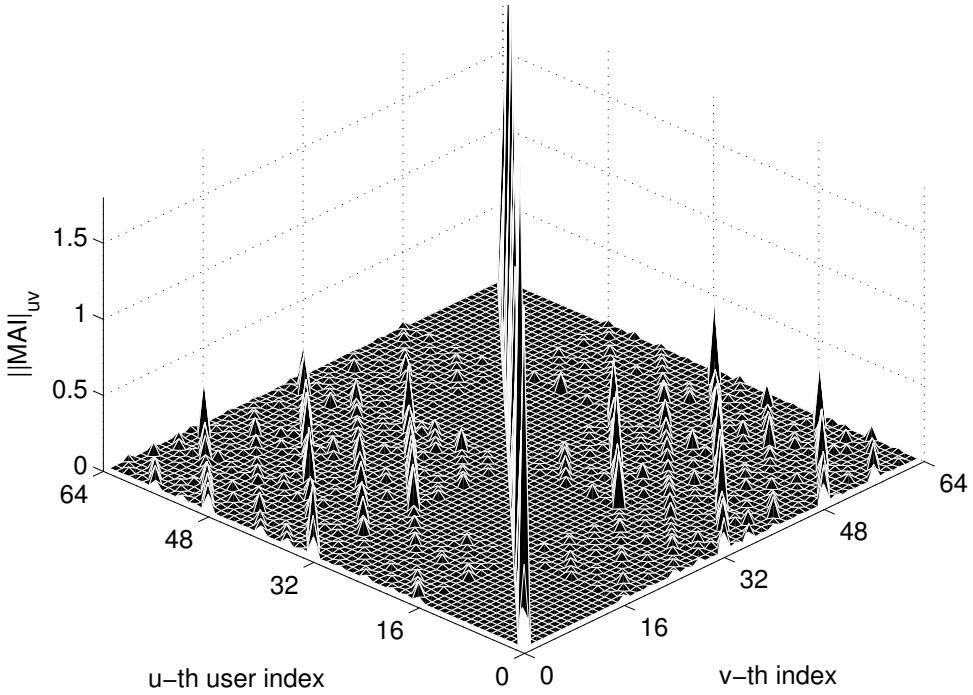

Figure 3.1: The absolute value of MAI between the u-th user and the v-th user as a function of the user index. Typical urban profile, $\eta = 1$, and $N = 64$ are used in this figure.

in each group, consequently, the system can have 16 users transmit simultaneously without MAI if all users select their respective codes from the same group. The diagonal protrusions in Fig. 3.1 represent the desired signals, while the off diagonal ones are the unwanted MAI.

Fig. 3.2, and Fig. 3.3 show the absolute value of MAI between two users in the OMC-CDMA system for the TU and the equal gain (EG) power delay profiles, respectively. In both figures, all users select their respective spreading codes from the same group. The oversampling factor was set as $\eta = 2$ for the two figures. When users select their spreading codes from the same set, MAI can be neglected for the OMC-CDMA system with $\eta = 2$ and TU PDP. However, MAI is considerable and can not be neglected for the OMC-CDMA system with EG PDP and $\eta = 2$, even when all users select their codes from the same subset.

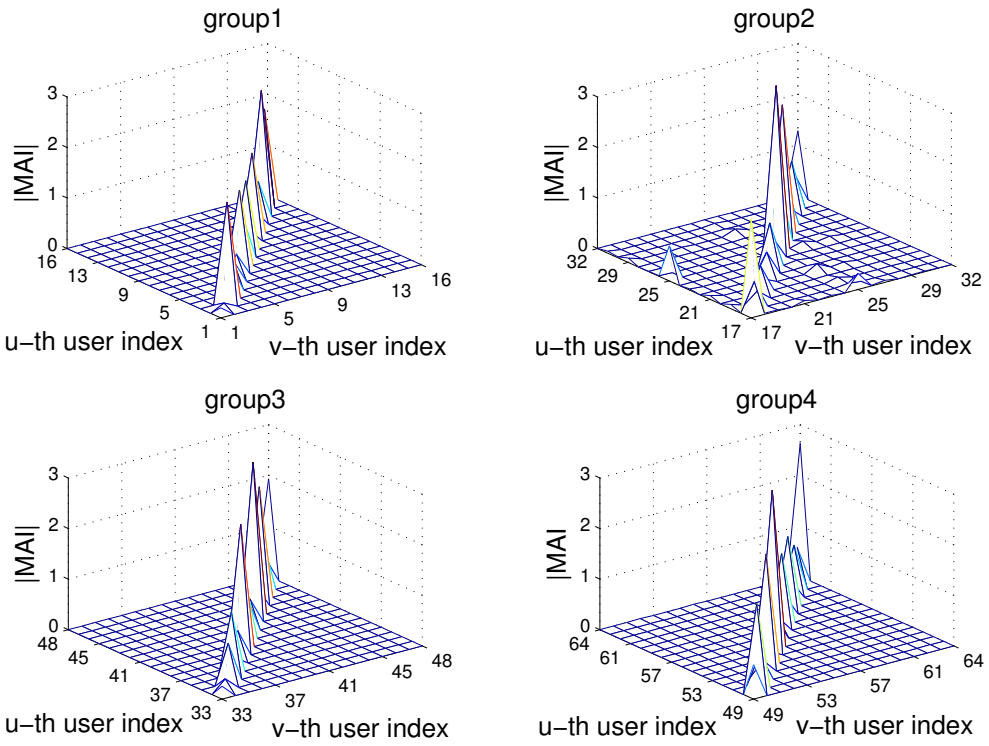

Figure 3.2: The absolute value of MAI for users located in the same group. The channel has a Typical Urban PDP.

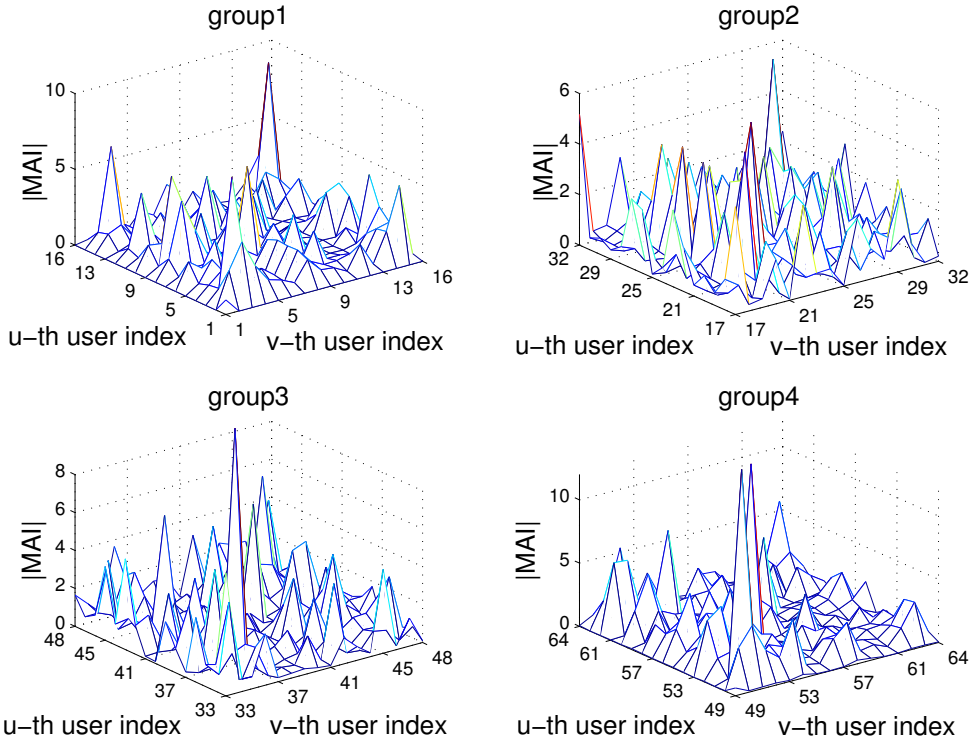

Figure 3.3: The absolute value of MAI for users located in the same group. The channel has an Equal Gain PDP.

In Fig. 3.4, the symbol error rate (SER) performance is plotted for the OMC-CDMA system with and without oversampling.

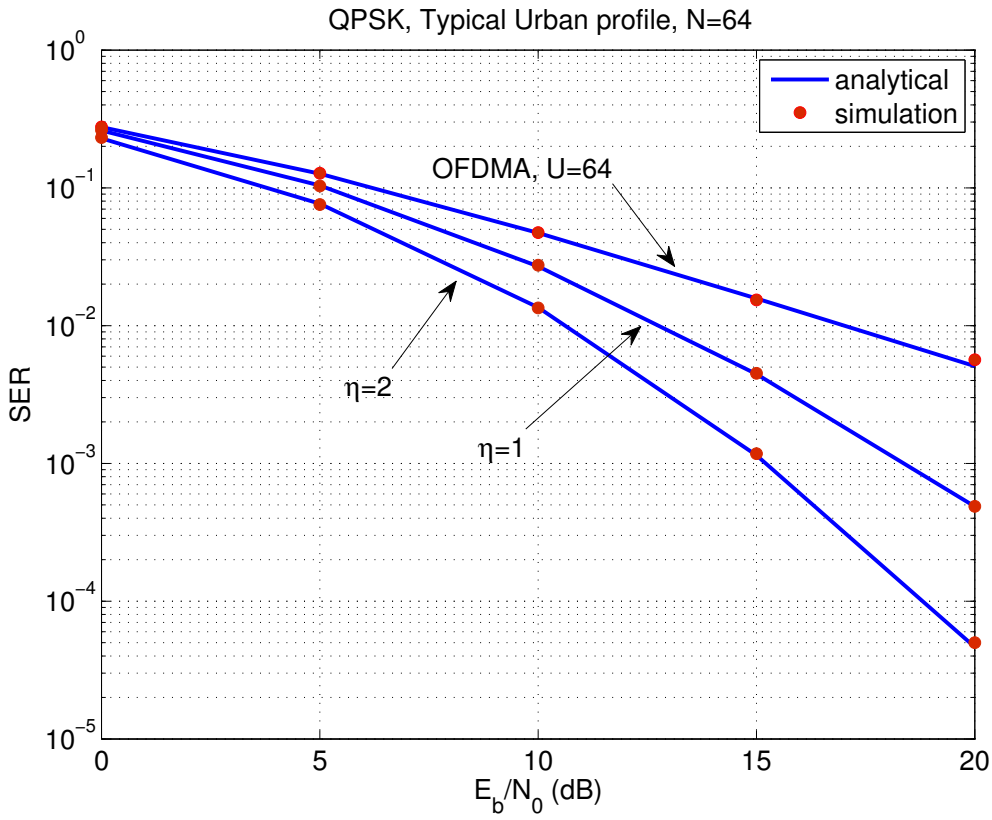

Figure 3.4: The SER performance of the OMC-CDMA and OFDMA systems in a frequency selective Rayleigh fading channel. In the OMC-CDMA system, $U = 16$ was used in the simulations. In the OFDMA system, the number of users was the same as the number of subcarriers, *i.e.* $U = N = 64$. The QPSK modulation was used in all systems.

For comparison purposes, the SER of the OFDMA system was also plotted. The QPSK modulation was used in all systems. Three observations can be made about the figure, first, there are excellent agreements between simulation and analytical results for all systems. Second, the simulation result of the OMC-CDMA system with $U = 16$ matches very well with the analytical result of an equivalent system with $U = 1$, that means the system with $U = 16$ has a negligible MAI. Third, due to the diversity gain, the SER performance of the OMC-CDMA system without oversampling outperforms OFDMA system. Finally, employing oversampling in the time domain at the receiver enhances

the collected diversity, as a result, the SER performance of the OMC-CDMA system becomes much better with oversampling.

The impact of the timing offset, τ_0, between the transmitter and the receiver sampler clocks on the SER performance of the OMC-CDMA system is illustrated in Fig. 3.5 for systems with and without oversampling. Fig. 3.5 clarifies that systems with time-domain oversampling are robust against

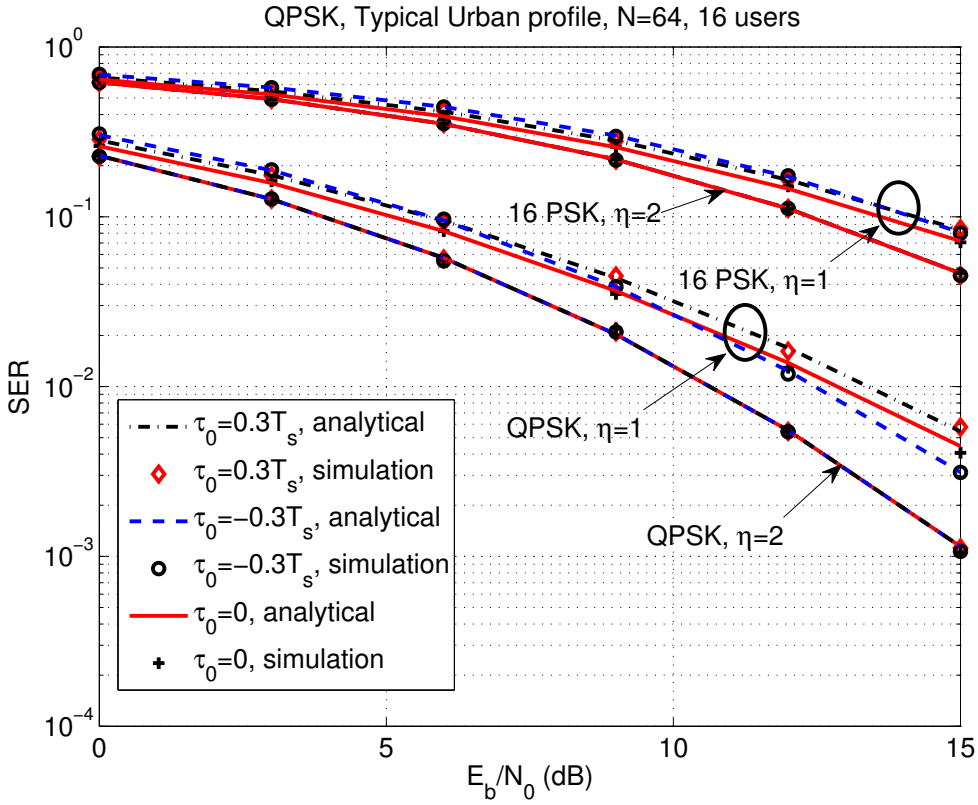

Figure 3.5: The SER performance of the OMC-CDMA system with and without oversampling in the presence of the timing offset. All systems employ $N = 64$ subcarriers; the results were obtained for both OPSK and 16-PSK modulations.

performance fluctuations induced by τ_0, on the other hand, performance variations in systems without oversampling can be observed due to the timing offset. Furthermore, oversampling with a factor $\eta = 2$ is sufficient to cancel the spectrum aliasing between sampled signals at the receiver leading to performance fluctuations avoidance [17].

3.6 Conclusions

In this section, we summarize and conclude this chapter based on obtained results. In this chapter, we presented the oversampled-multi-carrier code division multiple access (OMC-CDMA) system. Hadamard-Walsh codes were employed in the OMC-CDMA system to spread symbols in the frequency domain and to generate orthogonality among different users. Orthogonality among users can be kept by assigning different users orthogonal codes selected from the same Hadamard-Walsh submatrix [8]. Excellent matching between simulation and analytical results were observed. Indeed, a significant performance improvement was achieved by using oversampling in the time domain at the receiver. The OMC-CDMA system can achieve multipath diversity where a part of this diversity was provided by the time-domain oversampling. Oversampling also can remove the impacts of the time-offset between the transmitter and the receiver sampler clocks.

Chapter 4

MAI-Free Circular-shift Division Multiple Access (CSDMA)

4.1 Introduction

Multi-carrier communications, such as orthogonal frequency division multiplexing (OFDM), have been adopted as the primary physical layer transmission schemes by a wide range of current and future broadband communication standards, including the fourth generation (4G) long term evolution advanced (LTE-A) and IEEE 802.11ad Wireless Gigabit Alliance (WiGig) systems. OFDM can be extended to orthogonal frequency division multiple access (OFDMA) to support the simultaneous access of multiple users. Neither uncoded OFDM nor OFDMA system can achieve multipath diversity because uncorrelated data streams are transmitted over orthogonal sub-carriers.

Multi-carrier code division multiple access (MC-CDMA) system can achieve full multipath diversity by spreading one symbol across all the sub-carriers with orthogonal or quasi-orthogonal spreading codes. The multipath diversity gains can be collected by using maximal ratio combining (MRC) [3, 5], equal gain combining (EGC) [25] or minimum mean squared error (MMSE) [27] receivers. MC-CDMA system can achieve the full multipath diversity gain while supporting the same number of simultaneous users as OFDMA systems. However, MC-CDMA suffers from multiple access interference (MAI), because the frequency selectivity of the fading channel will destroy the orthogonality among users. The negative impacts of MAI can be reduced by employing multi-user detection (MUD), the complexity of which grows significantly as the number of users increases [29]. MAI-free MC-CDMA system are proposed in [6]–[8] by employing a subset of Hadamard-Walsh codes. The MAI-free operation is achieved at the cost of a lower spectral efficiency, because such systems can

support no more than N/L simultaneous users, with N being the number of sub-carriers and L the length of the discrete-time channel.

In this chapter we propose a circular-shift division multiple access (CSDMA) scheme for multi-carrier multi-user wireless systems, where multiple users access the same spectrum at the same time [30]. The proposed scheme can be used for the uplinks of wireless systems, such as cellular systems, satellite systems, or wireless sensor networks. In the CSDMA scheme, each modulated symbol is spread over M sub-carriers through simple repetition codes. The obtained time domain signals are then circularly shifted by different number of samples at different users. The receiver observes the superposition of the circularly shifted time domain signals distorted by frequency selective fading and noise. The time domain circular shifting operation can remove or reduce MAI at the receiver. Furthermore, if the number of users is no more than M/L, then MAI-free communication can be achieved. Analytical and simulation results demonstrate that full multipath diversity gains can be achieved by the proposed CSDMA system regardless of the presence of MAI [30]. We will focus in this chapter on CSDMA system without MAI, CSDMA system with MAI where number of users exceeds M/L will be presented in the next chapter.

Throughout this chapter we use the following common notations.The superscripts $(\cdot)^T$ and $(\cdot)^H$ represent matrix transpose and Hermitian transpose, respectively; $\mathbb{E}(\cdot)$ is the mathematical expectation operator; $\mathcal{C}^{M\times N}$ denotes the $(M\times N)$-dimensional complex space; $\mathcal{C}^M$ is the space of M-dimensional complex column vectors; $\lfloor a \rfloor$ is the largest integer smaller than a; $\mathbf{1}_K$ is a size K all-one vector; $\mathbf{I}_N$ is a size-N identity matrix; diag $\{\mathbf{a}\}$ is a diagonal matrix with the vector $\mathbf{a}$ on its main diagonal; and $(\mathbf{a})_u = [a_{N-u}, \cdots, a_{N-1}, a_0, \cdots, a_{N-u-1}]^T$ is obtained by circularly shifting the length-N vector $\mathbf{a} = [a_0, \cdots, a_{N-1}]^T$ downwards by u locations.

4.2 System Structure of CSDMA

Consider the uplink of a cellular system or a wireless network, where U users transmit to the same receiver. Multi-carrier modulation is employed at the users, and each user uses N sub-carriers, indexed from 0 to $N-1$. The data stream at each user is divided into slots and each slot contains $K \leq N$ modulated symbols. Both K and N are assumed to be powers of two. Each data symbol is transmitted over $M = \frac{N}{K}$ subcarriers through repetition coding. Denote $s_{uk} \in \mathcal{S}$ as the k-th modulated symbol at the u-th user, for $k = 0, \cdots, K-1$, where $\mathcal{S}$ is the modulation constellation set with cardinality S, then s_{uk} is transmitted over subcarriers with indices $mK + k$, for $m = 0, \cdots, M-1$. The frequency domain data vector at the u-th user can be represented by $\bar{\mathbf{s}}_u = \mathbf{1}_M \otimes [s_{u0}, \cdots, s_{u(K-1)}]^T \in \mathcal{S}^{N\times 1}$, where $\otimes$ is the Kronecker product operator, $\mathbf{1}_M$ is a size M all-one vector, and $\mathbf{s}_u = [s_{u0}, \cdots, s_{u(K-1)}]^T \in \mathcal{S}^{K\times 1}$ contains the K modulated symbols from user u. The frequency domain data vector is converted to the time domain by means of inverse discrete Fourier transform (IDFT) as

$$\mathbf{x}_u = \mathbf{F}_N^H \bar{\mathbf{s}}_u \tag{4.1}$$

where $\mathbf{F}_N$ is the size-N discrete Fourier transform (DFT) matrix with the $(m+1, n+1)$-th element being $(\mathbf{F}_N)_{m+1,n+1} = \exp\left(-j\frac{2\pi mn}{N}\right)$.

At the u-th user, the time domain vector $\mathbf{x}_u$ is circularly shifted downwards by c_u samples, where c_u satisfies $\max\{c_u\} \leq M$. The circularly shifted data vector is denoted as $(\mathbf{x}_u)_{c_u}$. The circular shift operations in the time domain renders a signal structure that can remove or reduce MAI. Details will be given in the next section.

A cyclic prefix (CP) of length $L-1$ is then added to $(\mathbf{x}_u)_{c_u}$, where L is the length of the equivalent discrete-time channel. Denote the time domain sequence with CP as $\tilde{\mathbf{x}}_u \in \mathcal{C}^{N+L-1}$. The time domain samples pass through a transmit filter $p_{_T}(t)$, and are then transmitted through the frequency-selective

fading channel.

The receiver observes the superposition of signals from all U users plus the additive white Gaussian noise (AWGN). The received signal passes through a receive filter $p_{_R}(t)$. The output of the receive filter is sampled. After the removal of the cyclic prefix, the equivalent discrete-time representation of the system in the time domain can be represented by

$$\mathbf{r} = \sqrt{\frac{E_s}{M}} \sum_{u=0}^{U-1} \mathbf{H}_u \cdot (\mathbf{x}_u)_{c_u} + \mathbf{w}, \tag{4.2}$$

where E_s is the average energy of one modulated symbol, $\mathbf{r} = [r_0, \cdots, r_{N-1}]^T \in \mathcal{C}^{N\times 1}$ is the discrete-time received signal vector in the time domain, $\mathbf{w} = [w_0, \cdots, w_{N-1}]^T \in \mathcal{C}^{N\times 1}$ is the zero-mean AWGN vector with the covariance matrix being $\mathbb{E}(\mathbf{w}\mathbf{w}^H) = N_0\mathbf{I}_N$, and $\mathbf{H}_u \in \mathcal{C}^{N\times N}$ is a circulant matrix contains the equivalent discrete-time channel impulse response (CIR) of the u-th user. The matrix $\mathbf{H}_u$ can be expressed as

$$\mathbf{H}_u = [\tilde{\mathbf{h}}_u, (\tilde{\mathbf{h}}_u)_1, \cdots, (\tilde{\mathbf{h}}_u)_{N-1}], \tag{4.3}$$

where $\tilde{\mathbf{h}}_u = [h_u(0), h_u(1), \cdots, h_u(L-1), \mathbf{0}_{N-L}]^T \in \mathcal{C}^{N\times 1}$, with $h_u(l)$ being the equivalent discrete-time CIR that contains the effects of the transmit filter, receive filter, and the physical fading channel. In the proposed CSDMA scheme, the parameter M is chosen such that $M \geq L$.

The time domain system equation can be alternatively expressed as

$$\mathbf{r} = \sqrt{\frac{E_s}{M}} \sum_{u=0}^{U-1} (\mathbf{H}_u)_{-c_u} \cdot \mathbf{x}_u + \mathbf{w}, \tag{4.4}$$

where $(\mathbf{H}_u)_{-k} = [(\tilde{\mathbf{h}}_u)_k, \cdots, (\tilde{\mathbf{h}}_u)_{N-1}, \tilde{\mathbf{h}}_u, \cdots, (\tilde{\mathbf{h}}_u)_{k-1}] \in \mathcal{C}^{N\times N}$ is obtained by circularly shifting the columns of $\mathbf{H}_u$ to the left by k positions. Thus a downward circular shift of the transmitted signals results in an equivalent left circulant shift of the time domain channel matrix.

Performing N-point DFT over $\mathbf{r}$ as $\mathbf{y} = \mathbf{F}_N\mathbf{r}$, and we have the frequency domain system representation as

$$\begin{aligned}\mathbf{y} &= \sqrt{\frac{E_s}{M}}\sum_{u=0}^{U-1}\mathbf{F}_N(\mathbf{H}_u)_{-c_u}\mathbf{F}_N^H\bar{\mathbf{s}}_u + \mathbf{z} \\ &= \sqrt{\frac{E_s}{M}}\sum_{u=0}^{U-1}\mathbf{G}_u\bar{\mathbf{s}}_u + \mathbf{z}, \end{aligned} \tag{4.5}$$

where $\mathbf{G}_u = \mathbf{F}_N(\mathbf{H}_u)_{-c_u}\mathbf{F}_N^H = \text{diag}\{\mathbf{g}_u\}$ is a diagonal matrix containing the frequency domain channel coefficients, with the main diagonal being the DFT of the first column of $(\mathbf{H}_u)_{-c_u}$

$$\mathbf{g}_u = \sqrt{N}\mathbf{F}_N(\tilde{\mathbf{h}}_u)_{c_u}. \tag{4.6}$$

The k-th element of $\mathbf{g}_u$ can be written as

$$g_u(k) = \sum_{n=0}^{N-1} h_u(n-c_u)\exp\left(-j\frac{2\pi nk}{N}\right). \tag{4.7}$$

It is assumed that $h_u(-n) = h_u(N-n)$ for $n > 0$ because of the cyclic shift operation, and $h_u(n) = 0$ for $n \geq L$.

4.3 Receiver Design of CSDMA

This section studies the optimum receiver design for MAI-free CSDMA system.

For the frequency domain system equation given in (4.5), each user transmits K symbols over N subcarriers, and each symbol is spread over M sub-carriers. Define the set of subcarrier indices that are used to transmit the k-th modulated symbol as $\mathcal{I}_k = \{i_{km} | i_{km} = mK + k, m = 0, \cdots, M-1\}$, for $k = 0, \cdots, K-1$.

Define $\mathbf{y}_k = [y_k, \cdots, y_{(M-1)K+k}]^T \in \mathcal{C}^{M\times 1}$, which are the received frequency domain symbols contributed by $\{s_{uk}\}_{u=0}^{U-1}$, then from (4.5)

$$\mathbf{y}_k = \sqrt{\frac{E_s}{M}}\sum_{u=0}^{U-1}\mathbf{g}_{uk}s_{uk} + \mathbf{z}_k, \tag{4.8}$$

where $\mathbf{z}_k = [z_k, \cdots, z_{(M-1)K+k}]^T \in \mathcal{C}^{M\times 1}$ and $\mathbf{g}_{uk} = [g_u(k), \cdots, g_u((M-1)K+k)]^T \in \mathcal{C}^{M\times 1}$ are sub-vectors extracted from $\mathbf{z}$ and $\mathbf{g}_u$, respectively.

We have the following lemma regarding the frequency domain channel coefficient vector $\mathbf{g}_{uk}$.

Lemma 4.1: The frequency domain channel coefficient vector $\mathbf{g}_{uk}$ can be expressed as [30]

$$\mathbf{g}_{uk} = \sqrt{M} \cdot \mathbf{F}_M \cdot \mathbf{\Lambda}_{kc_u} \cdot (\mathbf{h}_u)_{c_u}, \text{ for } u = 0, \cdots, U-1, \text{ and } k = 0, \cdots, K-1 \quad (4.9)$$

where $(\mathbf{h}_u)_{c_u} \in \mathcal{C}^{M\times 1}$ is obtained by shifting $\mathbf{h}_u = [h_u(0), \cdots, h_u(L-1), \mathbf{0}_{M-L}]^T \in \mathcal{C}^{M\times 1}$ downwards by c_u locations, and $\mathbf{\Lambda}_{kc_u} = \text{diag}\left\{e^{-j\frac{2\pi c_u k}{N}}(\boldsymbol{\lambda}_k)_{c_u}\right\}$, with $\boldsymbol{\lambda}_k = [e^{-j\frac{2\pi 0k}{N}}, \cdots, e^{-j\frac{2\pi(M-1)k}{N}}]^T \in \mathcal{C}^{M\times 1}$.

Proof: If $K = 1$, then (4.9) can be directly obtained from (4.7). Next we consider the case $K > 1$.

When $K > 1$, we will always have $h(-n) = 0$ for $n > 0$ in (4.7) because only the zero elements of $\tilde{\mathbf{h}}_u$ will wrap around after shifting downwards by $c_u \leq M$ positions with $L \leq M$. The m-th element of $\mathbf{g}_{uk}$ is $g(mK+k)$, which can be calculated as [30]

$$g(mK+k) = \sum_{n=c_u}^{c_u+M-1} h_u(n-c_u)e^{-j\frac{2\pi n(mK+k)}{N}}. \quad (4.10)$$

Equation (4.10) can be alternatively expressed as

$$g(mK+k) = \sum_{n=c_u}^{M-1} h_u(n-c_u)e^{-j\frac{2\pi nm}{M}}e^{-j\frac{2\pi nk}{N}} + \sum_{n=M}^{c_u+M-1} h_u(n-c_u)e^{-j\frac{2\pi nm}{M}}e^{-j\frac{2\pi nk}{N}}. \quad (4.11)$$

Setting $n' = n - M$ in the second summation term in (4.11) and simplifying yields [30]

$$g(mK+k) = \sum_{n=c_u}^{M-1} h_u(n-c_u)e^{-j\frac{2\pi nk}{N}}e^{-j\frac{2\pi nm}{M}} + \sum_{n=0}^{c_u-1} h_u(n-c_u+M)e^{-j\frac{2\pi(n+M)k}{N}}e^{-j\frac{2\pi nm}{M}} \quad (4.12)$$

The above equation can be written in matrix format as

$$g(mK+k) = \sqrt{M}\mathbf{f}_M(m) \cdot \mathbf{\Lambda}_{kc_u} \cdot (\mathbf{h}_u)_{c_u}, \tag{4.13}$$

where $\mathbf{f}_M(m) = \frac{1}{\sqrt{M}}[e^{-j\frac{2\pi 0m}{M}}, \cdots, e^{-j\frac{2\pi(N-1)m}{M}}]$ is the $(m+1)$-th row of $\mathbf{F}_M$.

Stacking $\{g(mK+k)\}_{m=0}^{M-1}$ in (4.13) into a vector yields (4.9). ■

The result in Lemma 4.1 states that the frequency domain channel vector $\mathbf{g}_{uk}$ of the k-th subsystem can be considered as the M-point DFT of $\mathbf{\Lambda}_{kc_u} \cdot (\mathbf{h}_u)_{c_u}$, which is a circularly shifted version of the time domain channel vector with some phase shifts.

Combining (4.8) and (4.9) yields a frequency domain system equation

$$\mathbf{y}_k = \sqrt{E_s}\sum_{u=0}^{U-1} \mathbf{F}_M \cdot \mathbf{\Lambda}_{kc_u} \cdot (\mathbf{h}_u)_{c_u} \cdot s_{uk} + \mathbf{z}_k. \tag{4.14}$$

Performing M-point IDFT on $\mathbf{y}_k$ as $\mathbf{r}_k = \mathbf{F}_M^H \mathbf{y}_k$, we have

$$\mathbf{r}_k = \sqrt{E_s}\sum_{u=0}^{U-1} \mathbf{\Lambda}_{kc_u} \cdot (\mathbf{h}_u)_{c_u} \cdot s_{uk} + \mathbf{w}_k, \tag{4.15}$$

where $\mathbf{w}_k = \mathbf{F}_M^H \mathbf{z}_k$.

In (4.15), the system is equivalently represented as the superposition of U single-input multiple-output (SIMO) systems, each with up to M outputs. Performing MRC with respect to the u-th user as $b_{uk} = (\mathbf{h}_u)_{c_u}^H \mathbf{\Lambda}_{kc_u}^H \mathbf{r}_k$, we have

$$b_{uk} = \sqrt{E_s}\sum_{l=0}^{L-1} |h_u(l)|^2 s_{uk} + \sqrt{E_s}\sum_{v\neq u} (\mathbf{h}_u)_{c_u}^H \mathbf{\Lambda}_{kc_u}^H \mathbf{\Lambda}_{kc_v} (\mathbf{h}_v)_{c_v} \cdot s_{vk} + \xi_{uk} \tag{4.16}$$

where $\xi_{uk} = (\mathbf{h}_u)_{c_u}^H \mathbf{\Lambda}_{kc_u}^H \mathbf{w}_k$ is the noise component.

From (4.16), it can be seen that the desired signal s_{uk} can achieve the full multipath diversity order, even though s_{uk} is transmitted over only $M \leq \frac{N}{K}$ subcarriers, where K could be any positive integer.

The interference from the v-th user to the u-th user is

$$I_{uv} = \sqrt{E_s}(\mathbf{h}_u)_{c_u}^H \mathbf{\Lambda}_{kc_u}^H \mathbf{\Lambda}_{kc_v} (\mathbf{h}_v)_{c_v} \cdot s_{vk} \tag{4.17}$$

The interference term can be removed or reduced by carefully selecting the shifting values c_u and c_v. Next we will consider the receiver design of MAI-free systems, systems with MAI will be presented in the next chapter.

4.3.1 MAI-free Systems

If $\mathbf{\Lambda}_{kc_u} \cdot (\mathbf{h}_u)_{c_u}$ and $\mathbf{\Lambda}_{kc_v} \cdot (\mathbf{h}_v)_{c_v}$ are mutually orthogonal, then $I_{uv} = 0$ and there will be no mutual interference between users u and v. We have the following results regarding a set of users that are mutually orthogonal [30].

Proposition 4.1: Define a subset of $\lfloor \frac{M}{L} \rfloor$ users $\mathcal{U}_l$, such that if $u \in \mathcal{U}_l$, then the time shift employed by the u-th user is $c_u = uL + l$, for $u = 0, \cdots, \lfloor \frac{M}{L} \rfloor - 1$, and l is an integer between 0 and $L - 1$. The users belong to the same subset $\mathcal{U}_l$ are mutually orthogonal, that is, $I_{uv} = 0$ for any $u \neq v$ and $u, v \in \mathcal{U}_l$

Proof: We first consider the case $l = 0$. Since the maximum shift of the length M vector $\mathbf{h}_u$ is $(\lfloor \frac{M}{L} \rfloor - 1)L \leq M - L$, there will be no wrapping around during the shifting operation, and all the shifts are linear shifts when $l = 0$. For the u-th user, the vector $(\mathbf{h}_u)_{c_u}$ has L non-zero elements with indices $uL, uL + 1, \cdots, (u + 1)L - 1$, and all other elements are 0. It can be easily shown that $(\mathbf{h}_u)_{c_u}^H (\mathbf{h}_u)_{c_v} = 0$ for $u \neq v$ and $u, v \in \mathcal{U}_0$. Since $\mathbf{\Lambda}_{kc_u}$ is diagonal, it can be shown that $I_{uv} = 0$ for $u \neq v$ and $u, v \in \mathcal{U}_0$. When $l > 1$, all the $\mathbf{h}_u$ vectors for users in $\mathcal{U}_l$ can be obtained by circularly shifting all the CIR vectors in $\mathcal{U}_0$ downwards by l locations, and the circular shifting operation does not affect the orthogonality among the channel vectors in the same subset [30]. ■

The results in Lemma 4.1 state that $L\lfloor\frac{M}{L}\rfloor$ users can be divided into L subsets, with $\lfloor\frac{M}{L}\rfloor$ users in each subset. There is no mutual interference for users belonging to the same subset. For the special case $K = 1$, that is, one symbol is transmitted over all the subcarriers, the maximum number of orthogonal users is $\lfloor\frac{N}{L}\rfloor$. This is similar to the results in [8], which states that MAI-free communications can be achieved in a MC-CDMA system with at most $\lfloor\frac{N}{L}\rfloor$ users by using a subset of the Hadamard-Walsh codes.

MAI-free system can be used for cellular systems. Assume the cells are grouped into clusters with $R \geq L$ cells in each cluster. Users in the same cell belong to the same orthogonal subset, such that there is no MAI inside a cell. Users in different cells of the same cluster can use shifting patterns from the same or different orthogonal subsets based on the relative value between the cluster size R and the channel length L. Thus there might be co-channel interference (CCI) among neighboring cells. With such a structure, each cell can support up to $\lfloor\frac{M}{L}\rfloor$ simultaneous users. For a given channel length, more simultaneous users can be supported in each cell by increasing M, at the cost of a wider bandwidth or a longer delay.

From (4.16), the MAI-free system can be represented by

$$b_{uk} = \sqrt{E_s}\sum_{l=0}^{L-1}|h_u(l)|^2 s_{uk} + \xi_{uk}. \tag{4.18}$$

This is a SIMO system with L branches, and full multipath diversity order can be achieved by this system. For MAI-free systems, the MRC receiver is optimum.

4.4 Performance Analysis

The theoretical error probability of the MAI-free CSDMA system is derived in this section by considering the statistical properties of the equivalent discrete-time CIR. The MAI-free error probability can also be considered as a lower bound for systems with MAI.

From (4.18), the signal-to-noise ratio (SNR) of the MAI-free system can be expressed by [30]

$$\gamma_u = \gamma_0 \sum_{l=0}^{L-1} |h_u(l)|^2, \tag{4.19}$$

where $\gamma_0 = \frac{E_s}{N_0}$ is the SNR without fading.

The performance of the MAI-free system depends on the statistical properties of the discrete-time CIR $h_u(l)$. The discrete-time CIR incorporates the effects of the transmit filter $p_{_T}(t)$, the receive filter $p_{_R}(t)$, and the physical fading channel. Due to the time span of the transmit and receive filters, the discrete-time channel coefficients are correlated in the delay domain l, even though the underlying physical channel might experience uncorrelated scattering. For system experiences wide sense stationary uncorrelated scattering (WSSUS) Rayleigh fading, the channel coefficient $h_u(l)$ is zero-mean Gaussian distributed with covariance $\rho_u(l_1, l_2) = \mathbb{E}[h_u(l_1)h_u^*(l_2)]$ given by [31, eqn. (17)].

$$\rho_u(l_1, l_2) = \int_{-\infty}^{+\infty} R_p(l_1 T_2 - \tau) R_p^*(l_2 T_2 - \tau) G(\tau) d\tau, \tag{4.20}$$

where $G(\tau)$ is the power delay profile of the physical channel, and $R_p(t)$ is the convolution of the transmit and receive filters.

The SNR in (4.19) can be expressed as $\gamma = \gamma_0 \mathbf{h}_u^H \mathbf{h}_u$, which is the quadratic form of the complex Gaussian random vector (CGRV) $\mathbf{h}_u = [h_u(0), \cdots, h_u(L-1)]^T \in \mathcal{C}^{L\times 1}$. The characteristic function (CHF) of γ_u is [19]

$$\Phi_u(j\omega) = [\det(\mathbf{I}_L - j\omega \mathbf{R}_{hu})]^{-1} \tag{4.21}$$

where $\mathbf{R}_{hu} = \mathbb{E}(\mathbf{h}_u \mathbf{h}_u^H)$ is the covariance matrix of $\mathbf{h}_u$, with the elements given in (4.20).

Based on the CHF given in (4.21), the SER for systems with phase shift keying (PSK) and square quadrature amplitude modulation (QAM) can be expressed by [19, eqn. (24)]

$$P_u(E) = \sum_{i=1}^{2} \frac{\beta_i}{\pi} \int_0^{\psi_i} \prod_{l=1}^{\tilde{L}_u} \left[1 + \gamma_0 \cdot \frac{\zeta \lambda_{ul}}{\sin^2 \theta}\right]^{-1} d\theta. \tag{4.22}$$

where $\tilde{L}_u$ is the rank of $\mathbf{R}_{hu}$, and λ_{ul} are the non-zero eigenvalues of $\mathbf{R}_{hu}$. The parameters β_i, ψ_i, and ζ are related to different modulation schemes, and they can be found in [19, Table 1]. The average symbol error rate (SER) can then be evaluated as SER $= \frac{1}{U}\sum_{u=0}^{U-1} P_u(E)$. For modulations with Gray mapping, the bit error rate (BER) can be approximated by BER $\approx \frac{1}{\log_2(S)}$SER.

It should be noted that the error probability result is independent of N, M, K, or U, as long as the condition $U \leq M/L$ is satisfied.

4.5 Simulation Results

Simulation results are presented in this section to demonstrate the performance of the proposed MAI-free CSDMA scheme.

Fig. 4.1 shows the MAI-free BER performance of the proposed CSDMA system with different values of channel length L. The power delay profiles of the channels are sample-spaced equal gain profiles as $G(\tau) = \sum_{l=0}^{L-1} \frac{1}{\sqrt{L}}\delta(\tau - lT_s)$, where T_s is the sampling period of the system, and $\delta(t)$ is the Kronecker delta function. QPSK modulations and $M = 16$ are employed in all systems. Each user transmits $K = 4$ symbols, so the total number of subcarrier is $N = 64$. The number of users in each system is $U = \lfloor \frac{M}{L} \rfloor$ to achieve MAI-free communications, and this results in 8, 4, and 2 users for systems with $L = 2, 4$, and 6, respectively. For comparison purpose, the BER performance of conventional OFDMA system with $U = N = 64$ are also shown in the figure when $L = 6$. The analytical BERs of the proposed CSDMA systems are obtained by using the expression in (4.22). The analytical BER of the OFDMA system is obtained by using the result in [11]. Both simulation and analytical results are obtained for MAI-free systems. Excellent agreement is observed between the simulation and analytical results for all system configurations. When the channel length L increases, the BER performances of CSDMA increase because of the higher multipath diversity order. On the other hand, the performance of the conventional OFDMA system with $L = 6$ is worse than that of

the CSDMA system with $L = 2$, because OFDMA system cannot achieve multipath diversity gains. At BER = 2×10^{-3}, the BER performance of CSDMA system with $L = 6$ outperforms the OFDMA system by 12 dB [30].

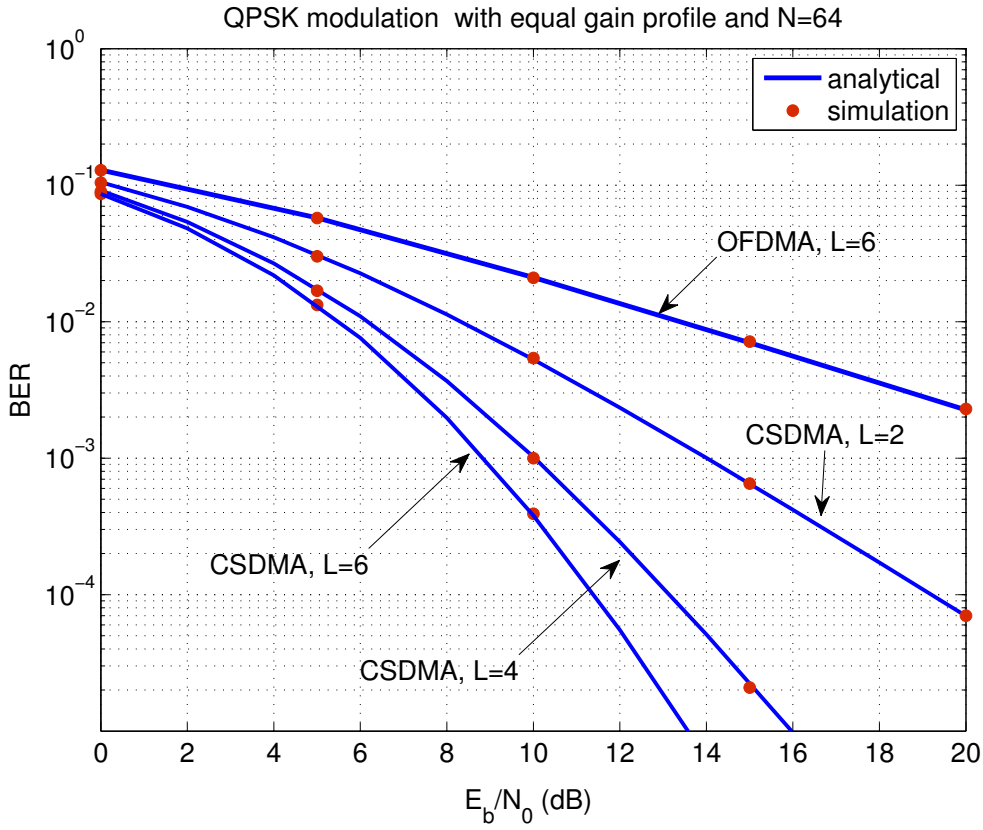

Figure 4.1: BER performance of systems in equal gain power delay profiles. QPSK modulations and $M = 16$ are used for all systems.

Fig. 4.2 shows the BER performance of the proposed MAI-free CSDMA system with QPSK modulations and $M = 16$ are employed in all systems. Each user transmits $K = 4$ symbols, so the total number of subcarriers is $N = 64$. Two different system configurations are considered. For the first system, the sampling period at the input of the receive filter is $T_1 = 3.69$ μs, which results in an equivalent channel length of $L = 4$ for the reduced TU profile. The value of T_1 for the second system is $T_1 = 1.85$ μs, half of that of the first system, and the equivalent channel length is $L = 8$ with the reduced TU profile. For the CSDMA systems, MAI-free communications can be achieved

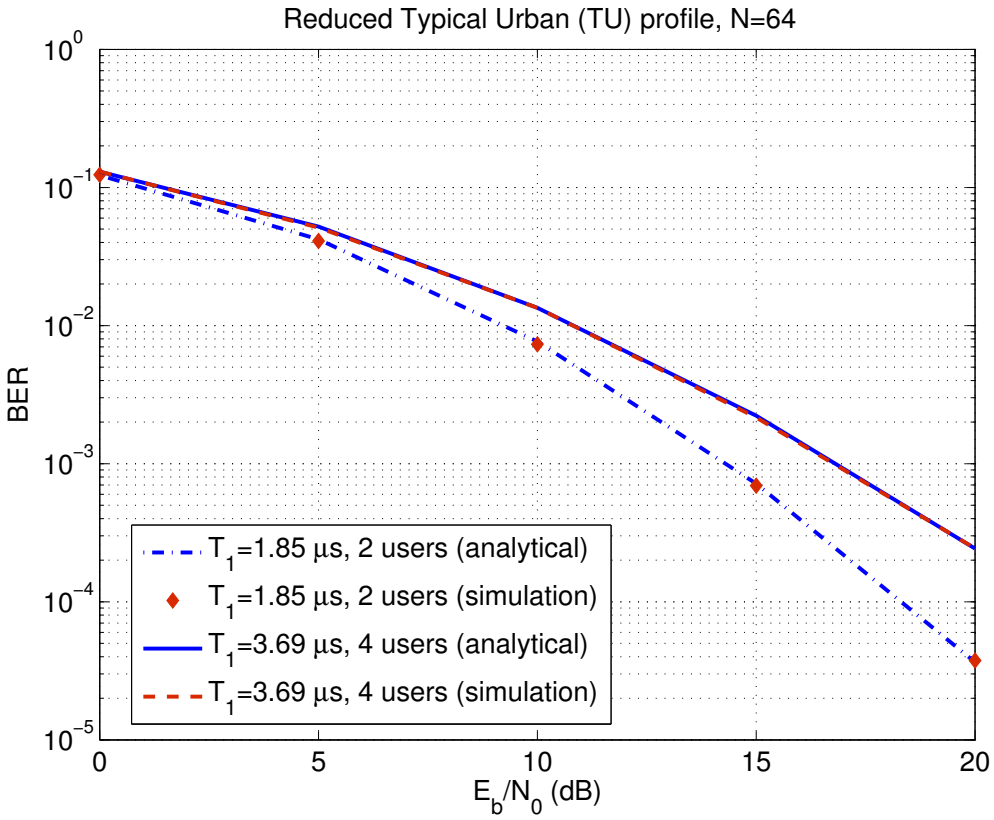

Figure 4.2: BER performance of systems in reduced typical urban power delay profiles. QPSK modulations and N = 64 are used for all systems

with $U = 4$ or $U = 2$ for systems with $T_1 = 3.69$ μs or $T_1 = 1.85$ μs, respectively. The analytical results have excellent matching with the simulation results of the MAI-free systems. Changing the receiver sampling rates has an impact on the length of the discrete-time channel CIR. Sampling at rates $T_1 = 3.69$ and $T_1 = 1.85$ yields channels with lengths $L = 4$, and $L = 8$, respectively. Therefore, the performance of the CSDMA system improves by reducing T_1, because a smaller T_1 means a larger channel length, thus a higher multipath diversity.

Fig. 4.3 shows the MAI-free CSDMA for various modulations schemes in a typical urban power delay profiles. In each system, we have 4 users transmit simultaneously to the same receiver. Each user transmits 4 symbols over $N = 64$ orthogonal subcarriers. Simulation results show excellent matching with analytical results.

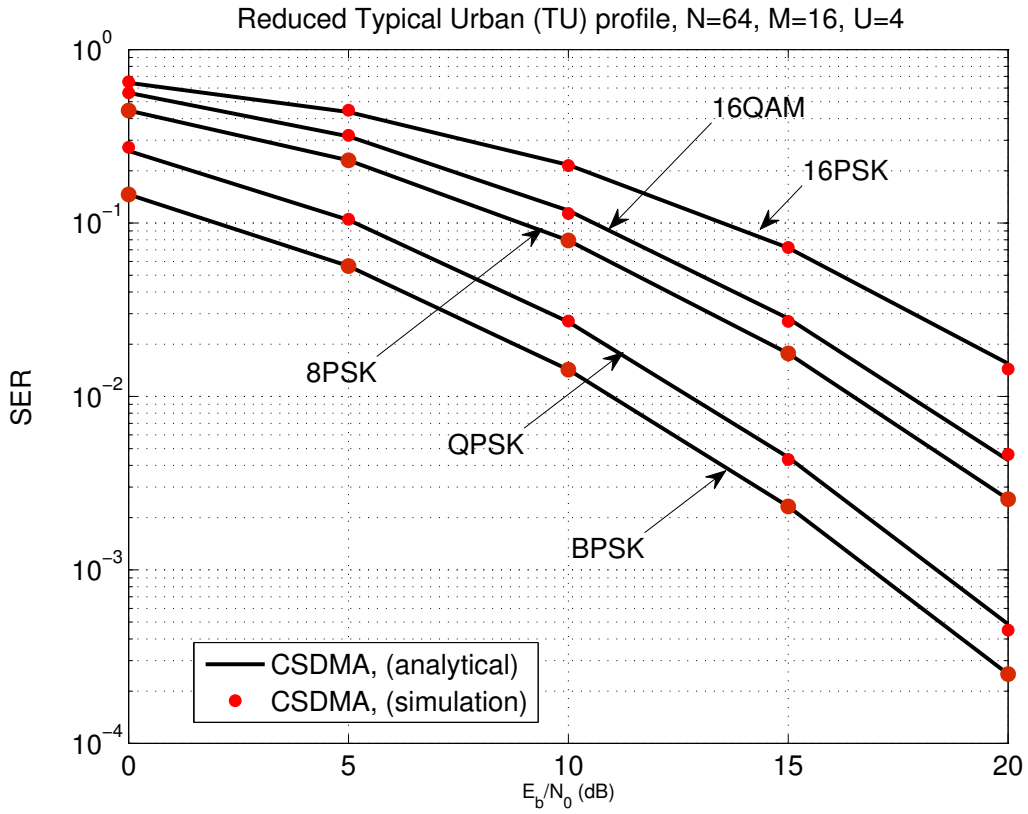

Figure 4.3: SER performance of MAI-free CSDMA systems in reduced typical urban power delay profiles. $N = 64$, $M = 16$, and $U = 4$ are used for all systems

4.6 Conclusions

This chapter presented a multi-carrier circular-shift division multiple access scheme that can be used for the uplink of wireless communication systems, such as cellular system, satellite systems, or wireless sensor networks. The modulated signals are evenly spread out in a subset of subcarriers through simple repetition codes, and the obtained signals are then circularly shifted in the time domain. The circular shifting operation in the time domain renders a special signal structure that allows the receiver to differentiate the signals from different users. MAI-free communication was achieved when the number of users is less than M/L, where M is the number of repetitions in the frequency domain and L is the length of the equivalent discrete-time channel. Both analytical and simulation results demonstrated that the proposed CSDMA system can achieve the full multipath diversity order.

Chapter 5

CSDMA with Multiple Access Interference (MAI)

5.1 Introduction

For multi-carrier multi-user systems, the main obstacle to support a large number of users is multiple access interference (MAI). Orthogonality among users is necessary to achieve multiple access with MAI-free. However, in frequency Rayleigh fading channels, orthogonality among different users might be destroyed resulting an interference among users.

The MAI in multi-user wireless communications can be reduced by employing on-off accumulative transmission (OOAT) [32], where each symbol is divided into many sub-symbols, and each data symbol is transmitted over a small subset of sub-symbols to reduce the interference among users. The OOAT scheme is originally proposed for systems with frequency flat fading [32]. A frequency domain OOAT is proposed in [33] for systems with frequency selective fading by means of multi-carrier communications, where each data symbol is transmitted over a small subset of sub-carriers. In [32] and [33], the receiver differentiates the users by using their respective on-off transmission patterns.

In the previous chapter, we presented the MAI-free CSDMA system where the number of users does not exceed M/L. Indeed, a full multipath diversity was achieved by using the maximum ratio combining (MRC) receiver, MRC is the optimum receiver in the MAI-free CSDMA system. In this chapter, and inspired by results obtained in the previous chapter, we extend the CSDMA system to support a number of users greater than M/L. When the number of users of the CSDMA system exceeds M/L the system will have MAI [30]. However, by choosing appropriate circular shifting values, there are at most L mutually interfering users at any given subcarrier, as long as the number

of users is less than M, which is the number of subcarriers bearing the same modulated symbol. This is different from most existing multi-carrier multiple access schemes where the number of interfering sources increases linearly with the number of users. Such a property also enables the design of low complexity MUD receivers. Sub-optimum soft-input soft-output (SISO) block decision feedback equalization (BDFE) receivers are used to perform MUD for systems with MAI [12]. The complexity of the SISO-BDFE receiver is mainly determined by the number of interfering sources, which is upper bounded by L. In addition, with the SISO-BDFE receiver, the performance of system with MAI is less than 1 dB away from that of MAI-free systems for various modulation schemes [30].

The rest of this chapter is organized as follows. In Section 5.2, CSDMA systems with MAI are presented. In Section 5.3, we study the BDFE equalizer. Finally, in Section 3.4 and Section 3.5, we present the simulation results and the conclusions, respectively.

5.2 System Model for CSDMA with MAI

In this section, and based on the analysis and discussions conducted in *chapter 4* we extend our analysis to include CSDMA systems with MAI. When there are more than $\lfloor \frac{M}{L} \rfloor$ users, there will be MAI in the system. Since each vector $(\mathbf{h}_u)_{c_u}$ has at most L non-zero elements, the interference between two users can be reduced by misaligning the non-zero elements in their respective channel vectors. We propose to circularly shift the time domain signals of the u-th user by [30]

$$c_u = u\lfloor \frac{M}{U} \rfloor \tag{5.1}$$

where $U \leq M$ is the total number of users in the system. Such a shifting amount will create the maximum mis-alignments between the non-zero elements of any pair of discrete-time CIR vectors.

From (4.15), the system equation in the presence of MAI can be alternatively expressed as [30]

$$\mathbf{r}_k = \sqrt{E_s}\mathbf{Q}_k\boldsymbol{\theta}_k + \mathbf{w}_k \tag{5.2}$$

where $\mathbf{Q}_k \in \mathcal{C}^{M\times U}$ is the equivalent channel matrix with the u-th column being $\mathbf{\Lambda}_{kc_u} \cdot (\mathbf{h}_u)_{c_u}$, and $\boldsymbol{\theta}_k = [s_{0k}, \cdots, s_{(U-1)k}]^T \in \mathcal{S}^{U\times 1}$. The MAI among the users is determined by the structure of $\mathbf{Q}_k$.

When there are $U = M$ users, we have $c_u = u$. In this case, each row of $\mathbf{Q}_k$ has exactly L non-zero elements. This can be easily shown by considering the $(m+1)$-th row of $\mathbf{Q}_k$, which is $[\lambda_{kc_0}(m)h_0(m), \cdots \lambda_{kc_m}(m)h_m(0), \lambda_{kc_{m+1}}(m)h_{m+1}(M-1), \cdots, \lambda_{kc_{M-1}}(m)h_{M-1}(m+1)]$, where $\lambda_{kc_u}(m)$ is the $(m+1)$-th diagonal element of $\mathbf{\Lambda}_{kc_u}$. Since $h_u(n) = 0$ for $n \geq L$ and for all u, there are exactly L non-zero elements on the m-th row of $\mathbf{Q}_k$. When there are $U < M$ users, the number of non-zero elements on each row is no more than L.

Based on the above analysis, each element of $\mathbf{r}_k$ is contributed by no more than L users. Consequently, there will be no more than L mutually interfering users at a given subcarrier. Thus the number of MAI sources is upper bounded by $L-1$ on each subcarrier.

In (5.2), the system is equivalently converted to a multiple-input multiple-output (MIMO) system. At any given subcarrier, there are at most L simultaneous inputs, even though the length of the input vector $\boldsymbol{\theta}_k$ is U. Due to the special structure of $\mathbf{Q}_k$, the system can be considered as an L-input M-output system.

The optimum detection of (5.2) requires the exhaustive search of $\mathbf{s}_k$, which might become prohibitively complex as L and S become large. We propose to solve the problem by using an iterative soft-input soft-output (SISO) block decision feedback equalization (BDFE) [12], which provides a balanced trade off between performance and complexity. Our simulation results indicate that the suboptimum BDFE can achieve the performance that is very close to that of an MAI-free system, which means that the BDFE can effectively remove the MAI among the users [30].

When the CSDMA system is operating at its maximum capacity, that is, there are $U = M$ simultaneous users, then the spectral efficiency of the system is the same as OFDM or OFDMA, because

the proposed system can simultaneously transmit $K \times U = N$ unique symbols over N subcarriers.

Next we will study the iterative soft-input soft-output (SISO) block decision feedback equalization (BDFE).

5.3 Block Decision Feedback Equalization (BDFE)

In this section, we present the design of the BDFE receiver based on the CSDMA system model presented in (5.2). Using BDFE receiver can significantly reduce the negative impacts of the MAI on the CSDMA system.

The BDFE receiver consists of two filters, a feedforward filter represented by the matrix $\mathbf{A}_k \in \mathcal{C}^{U \times U}$ and a feedback filter represented by a unitary-upper triangular matrix, $\mathbf{B}_k \in \mathcal{C}^{U \times U}$. The feedforward filter is used to suppress the ISI, and the feedback filter is used to cancel the ISI [12]. The matrices ,$\mathbf{A}_k$ and $\mathbf{B}_k$, are obtained by employing the minimum mean square error (MMSE) criterion. If we assume a correct past symbol detection, the error vector, $\mathbf{e}_k$ of the BDFE equalizer can be written as

$$\mathbf{e}_k = \mathbf{A}_k \mathbf{r}_k - \mathbf{B}_k \boldsymbol{\theta}_k. \tag{5.3}$$

The orthogonality principle $\mathbb{E}[\mathbf{e}_k \mathbf{r}_k^H] = 0$ is then used to minimize the mean-squared error $||\mathbf{e}_k^2|| = \mathbb{E}[\mathbf{e}_k \mathbf{e}_k^H]$, with $||\mathbf{a}||$ being the mean-squared error of vector $\mathbf{a}$. The received signals vector ,$\mathbf{r}_k$, is zero-mean Gaussian distributed with covariance matrix $\mathbf{R}_{r_k r_k}$ given as

$$\mathbf{R}_{r_k r_k} = \mathbb{E}[\mathbf{r}_k \mathbf{r}_k^H] = E_s \mathbf{Q}_k{}^H \mathbf{Q}_k + N_0 \mathbf{I}_U, \tag{5.4}$$

where we use $\mathbb{E}[\boldsymbol{\theta}_k \boldsymbol{\theta}_k^H] = \mathbf{I}_U$, and $\mathbb{E}[\mathbf{w}_k \mathbf{w}_k^H] = N_0 \mathbf{I}_U$ to obtain (5.4).

Using the orthogonality principle $\mathbb{E}[\mathbf{e}_k \mathbf{r}_k^H] = 0$ along with (5.4) the feedforward matrix, $\mathbf{A}_k$, can be obtained as [34]

$$\mathbf{A}_k = \mathbf{B}_k \mathbf{Q}_k^H \left[\frac{1}{\gamma_0} \mathbf{I}_{p_k} + \mathbf{Q}_k{}^H \mathbf{Q}_k \right]^{-1}, \tag{5.5}$$

where $\gamma_0 = \frac{E_s}{N_0}$ is the SNR without fading. The feedback filter, $\mathbf{B}_k$, is derived from the Cholesky decomposition as

$$\frac{1}{E_s} \mathbf{I}_U + \frac{1}{N_0} \mathbf{Q}_k{}^H \mathbf{Q}_k = \mathbf{B}_k^H \mathbf{\Psi}_k \mathbf{B}_k, \tag{5.6}$$

where $\mathbf{\Psi}_k$ is a diagonal matrix.

The (u, v)-th element of $\mathbf{B}_k$ matrix satisfies $b_{uv} = 0, \forall u < v$. Hence, the transmitted symbols in vector θ_k are detected in the reverse order, which means that the $s_{(U-1)k}$ is detected first, and s_{0k} is detected last. The output of the BDFE receiver can then be expressed by

$$\hat{s}_{(U-1)k} = \underset{s_{(U-1)k} \in \mathcal{S}}{\arg\min} \left| \mathbf{r}_k(U-1) - b(U,U) s_{(U-1)k} \right|^2 \tag{5.7}$$

$$\hat{s}_{uk} = \underset{s_{uk} \in \mathcal{S}}{\arg\min} \left| \mathbf{r}_k(u) - b(u,u) s_{uk} - \sum_{v=u+1}^{U-1} b(u,v) \hat{s}_{vk} \right|^2$$

$$\text{for } u = 0, 1, \cdots, U-2. \tag{5.8}$$

5.4 Simulation Results

In this section, we present the simulation results of CSDMA systems with MAI, the obtained results are then compared with that of MAI-free CSDMA systems.

Fig. 5.1 shows the SER performance of systems with and without MAI, for systems with QPSK, 8PSK, and 16QAM modulations, respectively. The power delay profile of the frequency selective fading is the typical urban reduced profile. For all systems we have $N = M = 64$ and $K = 1$. The value of K has no impact on the SER performance. Results of systems with $U = 1$ and $U = 64$ users are presented in the figure for the different modulation schemes. When $U = 1$, the SER performance matches perfectly with the analytical result for all system configurations. When $U = 64$,

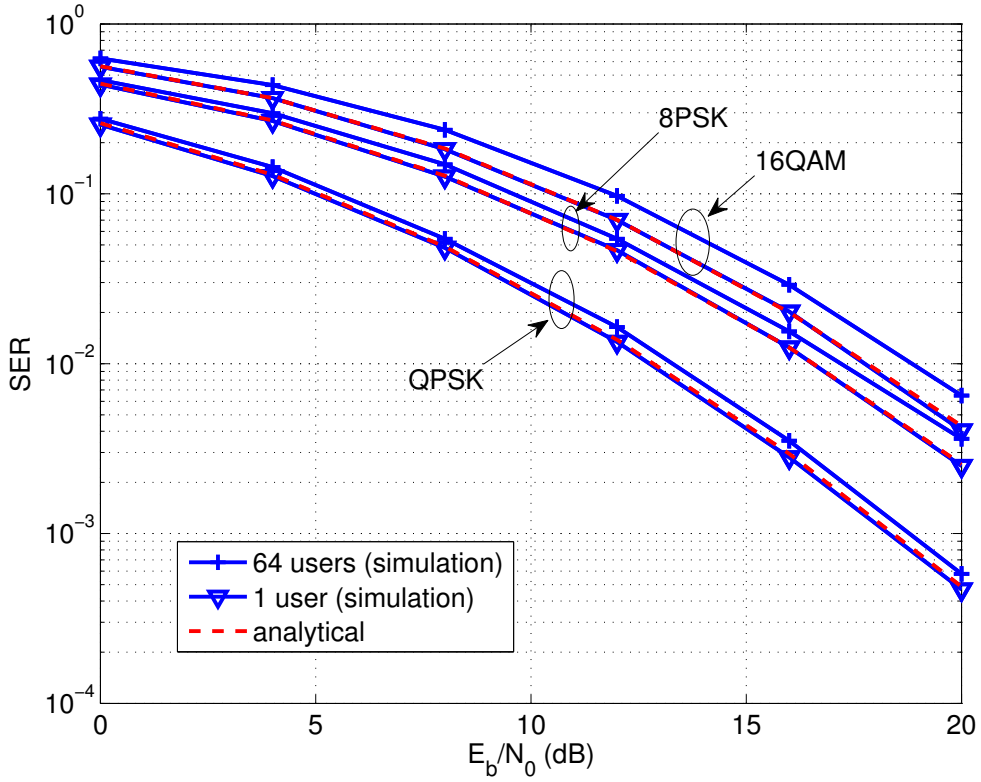

Figure 5.1: SER performance of systems with different number of users and various modulations.

the simulation results obtained in the presence of MAI are slightly worse than the analytical results derived for the MAI-free cases. When $N = 64$, the differences between the simulation and analytical results are 0.2 dB, 0.3 dB, and 0.9 dB for QPSK, 8PSK, and 16QAM systems, respectively. The results indicate that the sub-optimum interactive BDFE receiver can effectively remove the MAI.

Fig. 5.2 shows the BER performance of CSDMA systems with and without MAI. QPSK modulations and $N = 16$ are used in all systems. For MAI-free CSDMA systems, each user transmits $K = 4$ symbols where each symbol is transmitted over M subcarriers, so the total number of subcarriers is $N = 64$. Two different system sampling rates are considered, in the first system, the sampling period at the input of the receive filter is $T_1 = 3.69$ μs, which results in an equivalent channel length of $L = 4$ for the reduced TU profile. The value of T_1 for the second system is $T_1 = 1.85$ μs, half of that of the first system, and the equivalent channel length is $L = 8$ with the reduced TU profile. For

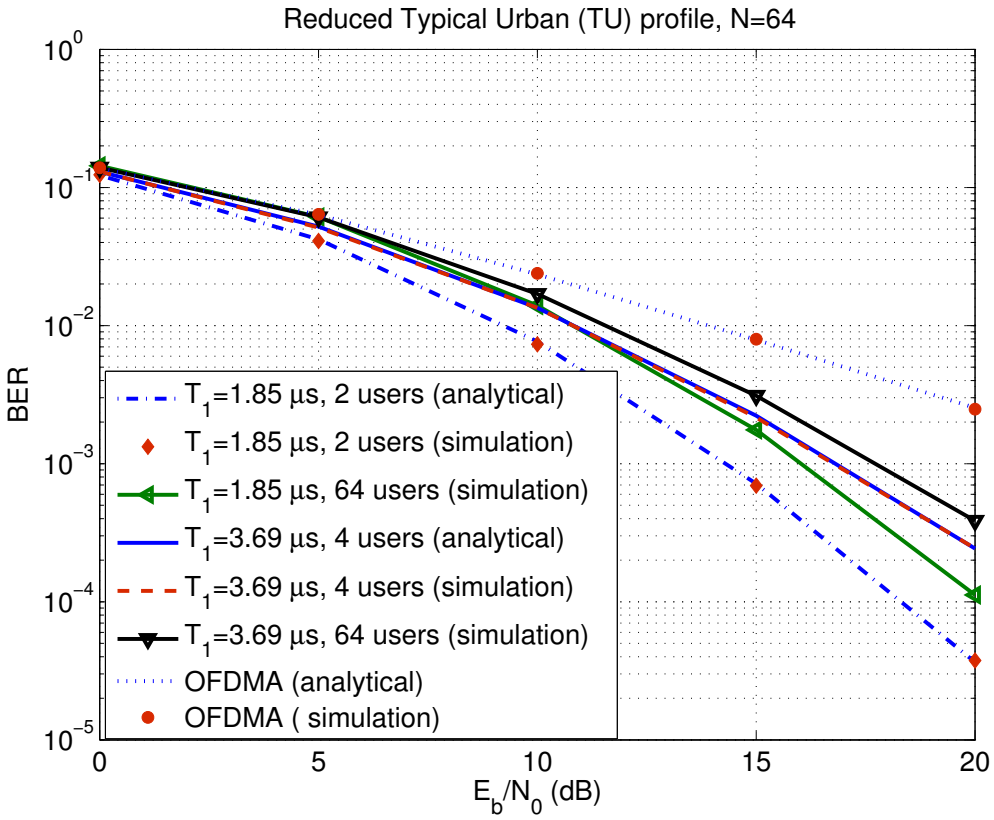

Figure 5.2: BER performance of systems in reduced typical urban power delay profiles. QPSK modulations and N = 64 are used for all systems

comparison purpose, the BER performance of conventional OFDMA system with $U = N = 64$ and $T_1 = 3.69$ μs is also shown in the figure. For the CSDMA systems, MAI-free communications can be achieved with $U = 4$ or $U = 2$ for systems with $T_1 = 3.69$ μs or $T_1 = 1.85$ μs, respectively. The analytical results match very well with the simulation results of the MAI-free systems. When $U = 64$ and $T_1 = 3.69$ μs, the proposed CSDMA system operates in the presence of MAI, and it outperforms the MAI-free OFDMA system by 4.5 dB at BER = 5×10^{-3}. The performance improvement is mainly contributed by the multipath diversity enabled by the CSDMA system. In addition, the performance of the CSDMA system improves by reducing T_1, because a smaller T_1 means a larger channel length, thus a higher multipath diversity.

5.5 Conclusions

In this chapter, we presented the circular-shift division multiple access (CSDMA) system with MAI. When the number of users exceeds M/L the system will have MAI, where M is the number of repetitions in the frequency domain and L is the length of the equivalent discrete-time channel. Moreover, when the system is fully loaded, that is, the number of users equal to M, then there are at most L mutually interfering users at any given subcarrier. Both analytical and simulation results demonstrated that the proposed CSDMA system can achieve the full multipath diversity order regardless the MAI. Also, the performance of CSDMA systems with MAI is slightly worse than equivalent systems without MAI. Finally, the CSDMA system with MAI can achieve the same spectral efficiency as OFDMA systems, but with a much better energy efficiency performance due to the multipath diversity gains.

Chapter 6

CSDMA System with Time-Domain Oversampling

6.1 Introduction

Multiple access techniques are critical to the operations of wireless networks with multiple users transmitting to the same receiver, such as the uplinks of cellular systems, satellite systems, or wireless sensor networks. Most current and future broadband communication standards, including the fourth generation (4G) long term evolution advanced (LTE-A) and IEEE 802.11ad Wireless Gigabit Alliance (WiGig) systems, employ orthogonal frequency division multiple access (OFDMA) to support the simultaneous access of multiple users. However, OFDMA system cannot achieve multipath diversity inherent in frequency selective fading, because uncorrelated data streams are transmitted over orthogonal subcarriers.

Multi-carrier code division multiple access (MC-CDMA) system can achieve full multipath diversity by spreading one symbol across all the subcarriers with orthogonal or quasi-orthogonal spreading codes. The multipath diversity gains can be collected by using maximal ratio combining (MRC) [3, 5], equal gain combining (EGC) [25] or minimum mean squared error (MMSE) [27] receivers. MC-CDMA system can achieve the full multipath diversity gain while supporting the same number of simultaneous users as OFDMA systems. However, MC-CDMA suffers from multiple access interference (MAI), because the frequency selectivity of the fading channel will destroy the orthogonality among users. The negative impacts of MAI can be reduced by employing multi-user detection (MUD), the complexity of which grows significantly as the number of users increases [29]. MAI-free MC-CDMA system are proposed in [8]–[6] by employing a subset of Hadamard-Walsh codes. The

MAI-free operation is achieved at the cost of a lower spectral efficiency, because such systems can support no more than N/L simultaneous users, with N being the number of subcarriers and L the length of the discrete-time channel.

Multipath diversity gain in multi-carrier systems can also be collected by employing oversampling at the receiver [11], [33]. An oversampled OFDM (OOFDM) scheme is proposed in [11], where the receiver employs oversampling in the time domain and linear processing in the frequency domain without modifying the OFDM transmitter. OOFDM can achieve multipath diversity gain while preserving the same spectral efficiency as conventional OFDM. OOFDM is primarily designed for a single user system, and it is extended to a multi-user multi-carrier system in [33] by means of a frequency domain on-off accumulative transmission (FD-OOAT) scheme, where each data symbol is transmitted over a small subset of subcarriers to reduce MAI among users. It has been shown in [33] that oversampling in multi-carrier systems can not only enable multipath diversity, but also remove the negative impacts of asynchronous transmissions among the users.

In this chapter, we extend the circular-shift division multiple access (CSDMA) scheme for multi-carrier systems by employing the time-domain oversampling at the receiver side. In the extended CSDMA system, each modulated data symbol is spread over a subset of $M \leq N$ subcarriers through simple repetition codes. The obtained time domain signals are then circularly shifted by different number of samples at different users. The receiver observes the superposition of the circularly shifted time domain signals distorted by frequency selective fading and noise. The time domain circular shifting operation can remove or reduce MAI at the receiver. By choosing appropriate circular shifting values, there are at most L mutually interfering users at any given subcarrier for a system with at most N users, where L is the length of the equivalent discrete-time channel impulse response and N is the number of subcarriers. This is different from most existing MC multiple access schemes where the

number of interfering sources increases linearly with the number of users. Furthermore, if the number of users is no more than M/L, then MAI-free communication can be achieved.

At the receiver, oversampling is employed to ensure that the full multiplath diversity gain can be achieved by the CSDMA system. In addition, the oversampling operation can also remove the impact of the timing offset caused by the mismatch between the clocks at the transmitter and receiver. Based on the statistical properties of the oversampled channel coefficients and noise samples, optimum and sub-optimum receivers are proposed for systems without and with MAI, respectively. The exact symbol error rate (SER) expression of the MAI-free system is derived, and it can also serve as a lower bound for systems with MAI. Analytical and simulation results demonstrate that full multipath diversity gains can be achieved by the proposed CSDMA system regardless of the presence of MAI. The proposed CSDMA scheme can achieve the same spectral efficiency as OFDMA systems, but with a much better energy efficiency performance due to the multipath diversity gains.

The remainder of this chapter is organized as follows. The transmitter structure of the CSDMA system is presented in Section 6.2. The structure of the CSDMA receiver with oversampling is developed in Section 6.3. Optimum and sub-optimum receivers are designed in Section 6.4. The analytical SER expression of the CSDMA system with oversampling is derived in Section 6.5. Simulation results are presented in Section 6.6, and Section 6.7 concludes the chapter.

6.2 System Structure of CSDMA

Consider the uplink of a cellular system or a wireless network, where U users transmit to the same receiver simultaneously. Multi-carrier modulation is employed by the users, and each user uses N orthogonal subcarriers, indexed from 0 to $N-1$. The data stream at each user is divided into slots and each slot contains $K \leq N$ modulated symbols. Both K and N are assumed to be powers of two. Each data symbol is then spread onto a subset of $M = \frac{N}{K}$ orthogonal subcarriers using a repetition

code.

Denote $s_{uk} \in \mathcal{S}$ as the k-th modulated symbol of the u-th user, for $k = 0, \cdots, K-1$, where $\mathcal{S}$ is the modulation constellation set with cardinality S. Each symbol s_{uk} is spread onto a subset of M orthogonal subcarriers with indices $mK + k$, for $m = 0, \cdots, M-1$.

The frequency domain data vector to be transmitted by the u-th user can be represented by $\bar{\mathbf{s}}_u = \mathbf{1}_M \otimes \mathbf{s}_u \in \mathcal{S}^{N\times 1}$, where $\mathbf{s}_u = [s_{u0}, \cdots, s_{u(K-1)}]^T \in \mathcal{S}^{K\times 1}$ contains the K modulated symbols from user u. The frequency domain data vector is converted to the time domain by employing the inverse discrete Fourier transform (IDFT) as

$$\mathbf{x}_u = \mathbf{F}_N^H \bar{\mathbf{s}}_u, \tag{6.1}$$

where $\mathbf{F}_N$ is the normalized size-N discrete Fourier transform (DFT) matrix with the $(m+1, n+1)$-th element being $(\mathbf{F}_N)_{m+1,n+1} = \frac{1}{\sqrt{N}} \exp\left(-j\frac{2\pi mn}{N}\right)$. If the time duration of one OFDM symbol is T_0, then the time duration of one time domain sample will be $T_1 = \frac{T_0}{N}$.

At the u-th user, the time domain vector $\mathbf{x}_u$ is circularly shifted downwards by c_u samples, where c_u satisfies $\max\{c_u\} \leq M$. The circularly shifted data vector is denoted as $(\mathbf{x}_u)_{c_u}$. The circular shift operation in the time domain results in a signal structure that can avoid or reduce MAI. Details will be given in the next section. A cyclic prefix (CP) of length $L-1$ is then added to the circularly shifted time domain samples $(\mathbf{x}_u)_{c_u}$ to eliminate interference between OFDM symbols, where L is the length of the equivalent T_1-spaced discrete-time channel. The prefixed time domain samples are passed through a transmit filter $p_{_T}(t)$, and are then transmitted through the frequency selective fading channel.

The receiver observes the superposition of signals from all U users corrupted by an additive white Gaussian noise (AWGN). The received signal is passed through a receive filter, $p_{_R}(t)$. The output of

the receive filter is

$$r(t) = \sqrt{\frac{E_s}{M}} \sum_{u=0}^{U-1} \sum_{k=-\infty}^{\infty} x_u(k - c_u)_N h_u(t - kT_1) + w(t) \tag{6.2}$$

where E_s is the energy per symbol, $h_u(t) = p_{_T}(t) \odot g_u(t) \odot p_{_R}(t)$ is the composite impulse response (CIR) with $g_u(t)$ being the impulse response of the physical channel, and $p_{_T}(t)$ and $p_{_R}(t)$ are the transmit and receive filters, respectively.

The receiver samples the output of the receive filter with sampling period $T_2 = \frac{T_1}{\eta}$ with the oversampling factor, η, being an integer. Due to the clock mis-match between the transmitter and receiver, there might be a timing offset $\tau_0 \in \left[-\frac{T_2}{2}, \frac{T_2}{2}\right]$ at the receiver, such that the n-th sample is sampled at the time instant $nT_2 + \tau_0$. After the removal of the CP, the time domain samples at the output of the receive filter can be written as

$$r_n = \sqrt{\frac{E_s}{M}} \sum_{u=0}^{U-1} \sum_{l=0}^{\eta L-1} \tilde{x}_u(n - \eta c_u - l)_{\eta N} h_u(l) + w_n, \quad \text{for } n = 0, \cdots, \eta N - 1. \tag{6.3}$$

where $r_n = r(nT_2 + \tau_0)$ and $w_n = w(nT_2 + \tau_0)$ are the T_2-spaced samples of the received signal and the noise, respectively, $h_u(l) = h_u(lT_2 + \tau_0)$ is the equivalent discrete-time CIR of the u-th user, and $\tilde{x}_u(n)$ is the oversampled version of $x_u(n)$ defined as

$$\tilde{x}_u(n) = \begin{cases} x_u(n/\eta), & n/\eta \text{ is integer} \\ 0, & \text{otherwise.} \end{cases} \tag{6.4}$$

It should be noted that the channel length of the oversampled discrete-time CIR is assumed to be an integer multiple of the oversampling factor η, and this can always be achieved by padding zeros to the CIR.

The equivalent discrete-time CIR includes the effects of the transmit filter, the physical channel, the receive filter, and the timing offset. If the channel undergoes a wide sense stationary uncorrelated

scattering (WSSUS) frequency selective Rayleigh fading, then the discrete-time CIR, $h_u(l)$, is zero-mean complex Gaussian distributed with covariance $\rho_u(l_1, l_2) = \mathbb{E}\big[h_u(l_1)h_u^*(l_2)\big]$ given as [16].

$$\rho_u(l_1, l_2) = \int_{-\infty}^{\infty} R_{_{TR}}(l_1T_2 - \tau)R_{_{TR}}^*(l_2T_2 - \tau)G(\tau + \tau_0)d\tau, \tag{6.5}$$

where $G(\tau)$ is the normalized channel power delay profile (PDP) with $\int_{-\infty}^{\infty} G(\tau)d\tau = 1$, and $R_{_{TR}}(t)$ is the convolution of the transmit and receive filters. It should be noted that the effects of timing offset is incorporated in the channel covariance. It will be shown that the impacts of timing offset can be removed by using $\eta = 2$ for a system with at most 100% excessive bandwidth.

Eqn. (6.3) can be written in matrix format as

$$\mathbf{r} = \sqrt{\frac{E_s}{M}} \sum_{u=0}^{U-1} \tilde{\mathbf{H}}_u \cdot (\tilde{\mathbf{x}}_u)_{\eta c_u} + \mathbf{w}, \tag{6.6}$$

where $\mathbf{r} = [r(0), r(1), \cdots, r(\eta N - 1)]^T \in \mathcal{C}^{\eta N \times 1}$ and $\mathbf{w} = [w(0), w(1), \cdots, w(\eta N - 1)]^T \in \mathcal{C}^{\eta N \times 1}$ are the received signal vector and noise vector, respectively, $\tilde{\mathbf{x}}_u = [x_u(0), \mathbf{0}_{\eta-1}, x_u(1), \mathbf{0}_{\eta-1}, \cdots, \mathbf{0}_{\eta-1}, x_u(N-1)\mathbf{0}_{\eta-1}]^T \in \mathcal{C}^{\eta N \times 1}$ is the oversampled data vector in the time domain, and $\tilde{\mathbf{H}}_u \in \mathcal{C}^{\eta N \times \eta N}$ is a circulant matrix that contains the equivalent oversampled discrete-time (CIR) of the u-th user. The matrix $\tilde{\mathbf{H}}_u$ can be expressed as

$$\tilde{\mathbf{H}}_u = \big[\hat{\mathbf{h}}_u, (\hat{\mathbf{h}}_u)_1, (\hat{\mathbf{h}}_u)_2, \cdots, (\hat{\mathbf{h}}_u)_{\eta N-1}\big], \tag{6.7}$$

where $\hat{\mathbf{h}}_u = [h_u(0), h_u(1), \cdots, h_u(\eta L - 1), \mathbf{0}_{\eta(N-L)}]^T \in \mathcal{C}^{\eta N \times 1}$. In the proposed CSDMA scheme, the parameter M is chosen such that $M \geq L$.

The time domain systems equation in (6.6) can be alternatively written as

$$\begin{aligned} \mathbf{r} &= \sqrt{\frac{E_s}{M}} \sum_{u=0}^{U-1} \mathbf{H}_u \cdot (\mathbf{x}_u)_{c_u} + \mathbf{w}, \\ &= \sqrt{\frac{E_s}{M}} \sum_{u=0}^{U-1} (\mathbf{H}_u)_{-c_u} \cdot \mathbf{x}_u + \mathbf{w}, \end{aligned} \tag{6.8}$$

where $(\mathbf{x}_u)_{c_u}$ is a circularly shifted version of the time domain data vector, $\mathbf{x}_u = [x_u(0), x_u(1), \cdots, x_u(N-1)]^T \in \mathcal{C}^{N\times 1}$, $\mathbf{H}_u = \left[\hat{\mathbf{h}}_u, (\hat{\mathbf{h}}_u)_\eta, (\hat{\mathbf{h}}_u)_{2\eta}, \cdots, (\hat{\mathbf{h}}_u)_{(N-1)\eta}\right] \in \mathcal{C}^{\eta N\times N}$, and $(\mathbf{H}_u)_{-c_u} \in \mathcal{C}^{\eta N\times N}$ is obtained by circularly shifting the columns of $\mathbf{H}_u$ to the left by c_u positions as $(\mathbf{H}_u)_{-c_u} = \left[(\hat{\mathbf{h}}_u)_{\eta c_u}, \cdots, (\hat{\mathbf{h}}_u)_{\eta(N-1)}, \hat{\mathbf{h}}_u, \cdots, (\hat{\mathbf{h}}_u)_{\eta(c_u-1)}\right]$. Thus a downward circular shift of the transmitted signals results in an equivalent left circulant shift of the time domain channel matrix, $\mathbf{H}_u$.

Due to the effects of oversampling and the time span of the receive filter, the elements of the noise vector, $\mathbf{w}$, are mutually correlated. The noise vector $\mathbf{w}$ is zero-mean complex Gaussian distributed. The covariance matrix of $\mathbf{w}$ is $\mathbf{R}_w = \mathbb{E}[\mathbf{w}\mathbf{w}^H] = N_0\mathbf{R}_p$, and the (m,n)-th element of $\mathbf{R}_p$ is [16]

$$\mathbb{E}[w(m)w^*(n)] = \int_{-\infty}^{\infty} p_{_R}((m-n)T_2 + \tau)p_{_R}(\tau)d\tau. \tag{6.9}$$

6.3 Receiver Structure of CSDMA System with oversampling

The receiver structure of CSDMA system with oversampling is presented in this section.

At the receiver, the time domain signal is converted to the frequency domain by performing ηN-point DFT over $\mathbf{r}$ in (6.8) as $\mathbf{y} = \mathbf{F}_{\eta N}\mathbf{r}$, and the result is

$$\begin{aligned} \mathbf{y} &= \sqrt{\frac{E_s}{M}}\sum_{u=0}^{U-1}\mathbf{F}_{\eta N}(\mathbf{H}_u)_{-c_u}\mathbf{F}_N^H\bar{\mathbf{s}}_u + \mathbf{z}, \\ &= \sqrt{\frac{E_s}{M}}\sum_{u=0}^{U-1}\mathbf{G}_u\bar{\mathbf{s}}_u + \mathbf{z}, \end{aligned} \tag{6.10}$$

where $\mathbf{G}_u = \mathbf{F}_{\eta N}(\mathbf{H}_u)_{-c_u}\mathbf{F}_N^H \in \mathcal{C}^{\eta N\times N}$ is the frequency domain channel coefficient matrix, and $\mathbf{z} = \mathbf{F}_{\eta N}\mathbf{w} \in \mathcal{C}^{\eta N\times 1}$ is the frequency domain noise sample vector.

The frequency domain channel coefficient matrix, $\mathbf{G}_u$, can be partitioned into a stack of η sub-matrices as $\mathbf{G}_u = \left[\mathbf{G}_{u_0}^T, \cdots, \mathbf{G}_{u_{\eta-1}}^T\right]^T$, where $\mathbf{G}_{u_q} \in \mathcal{C}^{N\times N}$ is

$$\mathbf{G}_{u_q} = \mathbf{F}_{\eta N}(q)(\mathbf{H}_u)_{-c_u}\mathbf{F}_N^H, \text{ for } q = 0, \cdots, \eta-1, \tag{6.11}$$

with $\mathbf{F}_{\eta N}(q) \in \mathcal{C}^{N\times \eta N}$ being obtained by extracting the $qN+1$ to $(q+1)N$ rows of $\mathbf{F}_{\eta N}$.

Lemma 6.1: The matrix $\mathbf{G}_{u_q}$ is a diagonal matrix with the main diagonal being

$$\mathbf{d}_{u_q} = \sqrt{N}\mathbf{F}_{\eta N}(q)(\hat{\mathbf{h}}_u)_{\eta c_u}, \text{ for } q = 0, \cdots, \eta - 1, \tag{6.12}$$

Proof: To simplify the notation, define $\mathbf{g} = [g(0), \cdots, g(\eta N - 1)]^T = (\hat{\mathbf{h}}_u)_{\eta c_u}$. Based on the definition of $\mathbf{G}_{u_q}$ in (6.11), the $(m+1, n+1)$-th element of $\mathbf{G}_{u_q}$ is

$$\frac{1}{\sqrt{\eta}N} \sum_{l=0}^{N-1} e^{j2\pi \frac{ln}{N}} \sum_{k=0}^{uN-1} e^{-j2\pi \frac{(qN+m)k}{\eta N}} g(k - \eta l)_{\eta N} \tag{6.13}$$

Let $k = v\eta + i$, where $v = 0, \cdots, N-1$ and $i = 0, \cdots, \eta - 1$, then (6.13) can be written as

$$\frac{1}{\sqrt{\eta}N} \sum_{l_1=0}^{N-1} e^{j2\pi \frac{(v-l_1)n}{N}} \sum_{v=0}^{N-1} \sum_{i=0}^{\eta-1} e^{-j2\pi \frac{(qN+m)(v\eta+i)}{\eta N}} g(\eta l_1 + i) \tag{6.14}$$

where $l_1 = v - l$. Based on the identity $e^{j2\pi \frac{(v-l_1)n}{N}} = e^{j2\pi \frac{v(qN+n)}{N}} e^{-j2\pi \frac{\eta l_1 (qN+n)}{\eta N}}$, (6.14) can be expressed as

$$\begin{aligned} &\frac{1}{\sqrt{\eta}N} \sum_{l_1=0}^{N-1} \sum_{i=0}^{\eta-1} e^{-j2\pi \left[\frac{\eta l_1 (qN+n)}{\eta N} + \frac{i(qN+m)}{\eta N}\right]} g(\eta l_1 + i) \\ &\times \sum_{v=0}^{N-1} e^{j2\pi \frac{v(n-m)}{N}}, \end{aligned} \tag{6.15}$$

which is 0 if $n \neq m$. When $n = m$, the above expression can be written as

$$\frac{1}{\sqrt{\eta}} \sum_{l_1=0}^{N-1} \sum_{i=0}^{\eta-1} e^{-j2\pi \frac{(qN+m)(\eta l_1 + i)}{\eta N}} g(\eta l_1 + i) \tag{6.16}$$

This completes the proof. ■

If we stack the η vectors, $\mathbf{d}_{u_q}$, for $q = 0, \cdots, \eta - 1$, into a size ηN column vector, $\mathbf{g}_u$, then from Lemma 6.1, the k-th element of the vector is

$$g_u(k) = \frac{1}{\sqrt{\eta}} \sum_{n=0}^{\eta N-1} h_u(n - \eta c_u)_{\eta N} \exp\left(-j\frac{2\pi nk}{\eta N}\right). \tag{6.17}$$

In the frequency domain system given in (6.10), each user transmits K symbols, where each symbol is equivalently transmitted over ηM subcarriers. Define the set of subcarriers indices that are

bearing the same k-th modulated symbol as $\mathcal{I}_k = \{i_{km} | i_{km} = mK + k, m = 0, \cdots, \eta M - 1\}$, for $k = 0, \cdots, K-1$.

Define $\mathbf{y}_k = [y_k, \cdots, y_{(\eta M-1)K+k}]^T \in \mathcal{C}^{\eta M \times 1}$, which are the received frequency domain symbols contributed by $\{s_{uk}\}_{u=0}^{U-1}$, then from (6.10)

$$\mathbf{y}_k = \sqrt{\frac{E_s}{M}} \sum_{u=0}^{U-1} \mathbf{g}_{uk} s_{uk} + \mathbf{z}_k, k = 0, \cdots, K-1 \tag{6.18}$$

where $\mathbf{z}_k = [z_k, \cdots, z_{(\eta M-1)K+k}]^T \in \mathcal{C}^{\eta M \times 1}$ and $\mathbf{g}_{uk} = [g_u(k), \cdots, g_u((\eta M-1)K+k)]^T \in \mathcal{C}^{\eta M \times 1}$ are sub-vectors extracted from $\mathbf{z}$ and $\mathbf{g}_u$, respectively. The frequency domain channel coefficient vector $\mathbf{g}_{uk}$ can be expressed as

$$\mathbf{g}_{uk} = \sqrt{N} \tilde{\mathbf{F}}_k (\hat{\mathbf{h}}_u)_{\eta c_u}, k = 0, \cdots, K-1 \tag{6.19}$$

where $\tilde{\mathbf{F}}_k \in \mathcal{C}^{\eta M \times \eta N}$ is obtained by extracting a sub matrix of ηM rows with indices $\mathcal{I}_k$ from the DFT matrix $\mathbf{F}_{\eta N}$. Similarly, the frequency domain noise vector can be expressed as

$$\mathbf{z}_k = \tilde{\mathbf{F}}_k \mathbf{w} \tag{6.20}$$

where $\mathbf{w}$ is the time domain noise vector.

We have the following Proposition regarding the frequency domain channel coefficient vector $\mathbf{g}_{uk}$.

Proposition 6.1: The frequency domain channel coefficient vector $\mathbf{g}_{uk}$ can be expressed as

$$\mathbf{g}_{uk} = \sqrt{M} \cdot \mathbf{F}_{\eta M} \cdot \mathbf{\Lambda}_{k\eta c_u} \cdot (\mathbf{h}_u)_{\eta c_u}, \text{ for } u = 0, \cdots, U-1, \text{ and } k = 0, \cdots, K-1 \tag{6.21}$$

where $(\mathbf{h}_u)_{\eta c_u} \in \mathcal{C}^{\eta M \times 1}$ is obtained by shifting $\mathbf{h}_u = \left[h_u(0), \cdots, h_u(\eta L - 1), \mathbf{0}_{\eta(M-L)}\right]^T \in \mathcal{C}^{\eta M \times 1}$ downwards by ηc_u locations, and $\mathbf{\Lambda}_{k\eta c_u} = \text{diag}\left\{e^{-j\frac{2\pi \eta c_u k}{\eta N}} (\boldsymbol{\lambda}_k)_{\eta c_u}\right\}$, with $\boldsymbol{\lambda}_k = \left[e^{-j\frac{2\pi 0 k}{\eta N}}, \cdots, e^{-j\frac{2\pi(\eta M-1)k}{\eta N}}\right]^T \in \mathcal{C}^{\eta M \times 1}$.

Proof: If $K = 1$, $\mathbf{\Lambda}_{k\eta c_u}$ will be an identity matrix. Since $N = M$, (6.21) can be directly obtained from (6.19).

When $K > 1$, we will always have $h(-n) = 0$ for $n > 0$ in (6.17) because only the zero elements of $\hat{\mathbf{h}}_u$ will wrap around after shifting downwards by $\eta c_u \leq \eta M$ positions with $L \leq M$. The m-th element of $\mathbf{g}_{uk}$ is $g(mK + k)$, which can be calculated as

$$g(mK+k) = \frac{1}{\sqrt{\eta}} \sum_{n=\eta c_u}^{\eta c_u + \eta M - 1} h_u(n - \eta c_u)_{\eta N} \times \exp\left(-j\frac{2\pi n(mK+k)}{\eta N}\right). \tag{6.22}$$

The above equation can be alternatively expressed as

$$g(mK+k) = \frac{1}{\sqrt{\eta}} \Bigg\{ \sum_{n=\eta c_u}^{\eta M - 1} h_u(n - \eta c_u)_{\eta N} e^{-j\frac{2\pi nm}{\eta M}} e^{-j\frac{2\pi nk}{\eta N}} + \sum_{n=\eta M}^{\eta c_u + \eta M - 1} h_u(n - \eta c_u)_{\eta N} e^{-j\frac{2\pi nm}{\eta M}} e^{-j\frac{2\pi nk}{\eta N}} \Bigg\}. \tag{6.23}$$

The above equation can be further simplified to

$$g(mK+k) = \frac{1}{\sqrt{\eta}} \Bigg\{ \sum_{n=\eta c_u}^{\eta M - 1} h_u(n - \eta c_u)_{\eta N} e^{-j\frac{2\pi nk}{\eta N}} e^{-j\frac{2\pi nm}{\eta M}} + \sum_{n=0}^{\eta c_u - 1} h_u(n - \eta c_u + \eta M)_{\eta N} e^{-j\frac{2\pi (n+\eta M)k}{\eta N}} e^{-j\frac{2\pi (n+\eta M)m}{\eta M}} \Bigg\}. \tag{6.24}$$

We can write (6.24) in a matrix format as

$$g(mK+k) = \sqrt{M}\mathbf{f}_{\eta M}(m) \cdot \mathbf{\Lambda}_{k\eta c_u} \cdot (\mathbf{h}_u)_{\eta c_u}, \tag{6.25}$$

where $\mathbf{f}_{\eta M}(m) = \frac{1}{\sqrt{\eta M}}\left[e^{-j\frac{2\pi 0m}{\eta M}}, \cdots, e^{-j\frac{2\pi(\eta M-1)m}{\eta M}}\right]$ is the $(m+1)$-th row of $\mathbf{F}_{\eta M}$. Stacking $\{g(mK + k)\}_{m=0}^{\eta M-1}$ in (6.25) into a vector yields (6.21). ■

The result in Proposition 6.1 states that the frequency domain channel vector $\mathbf{g}_{uk}$ can be considered as the ηM-point DFT of $\mathbf{\Lambda}_{k\eta c_u} \cdot (\mathbf{h}_u)_{\eta c_u}$, which is a circularly shifted version of the time domain channel vector with some phase shifts.

Combining (6.18) and (6.21) yields a frequency domain systems equation

$$\mathbf{y}_k = \sqrt{E_s} \sum_{u=0}^{U-1} \mathbf{F}_{\eta M} \cdot \mathbf{\Lambda}_{k\eta c_u} \cdot (\mathbf{h}_u)_{\eta c_u} \cdot s_{uk} + \mathbf{z}_k. \tag{6.26}$$

Applying ηM-point IDFT to $\mathbf{y}_k$ as $\mathbf{r}_k = \mathbf{F}_{\eta M}^H \mathbf{y}_k$, then the time domain signal is obtained as

$$\mathbf{r}_k = \sqrt{E_s} \sum_{u=0}^{U-1} \mathbf{\Lambda}_{k\eta c_u} \cdot (\mathbf{h}_u)_{\eta c_u} \cdot s_{uk} + \mathbf{w}_k, \tag{6.27}$$

where $\mathbf{w}_k = \mathbf{F}_{\eta M}^H \mathbf{z}_k \in \mathcal{C}^{\eta M \times 1}$.

In (6.27), the CSDMA system is equivalently represented as the superposition of U single-input multiple-output (SIMO) systems, where each system contains ηM outputs.

Since $\mathbf{\Lambda}_{k\eta c_u}$ is a diagonal matrix, the product $\mathbf{\Lambda}_{k\eta c_u}(\mathbf{h}_u)_{\eta c_u} \in \mathcal{C}^{\eta M \times 1}$ is a vector with ηL non-zero elements. Furthermore, if the indices of the non-zero elements of $\mathbf{\Lambda}_{k\eta c_u}(\mathbf{h}_u)_{\eta c_u}$ and $\mathbf{\Lambda}_{k\eta c_v}(\mathbf{h}_v)_{\eta c_v}$ are not overlapping for $u \neq v$, then $\mathbf{\Lambda}_{k\eta c_u}(\mathbf{h}_u)_{\eta c_u}$ and $\mathbf{\Lambda}_{k\eta c_v}(\mathbf{h}_v)_{\eta c_v}$ are mutually orthogonal i.e. $(\mathbf{\Lambda}_{k\eta c_u}(\mathbf{h}_u)_{\eta c_u})^H \cdot \mathbf{\Lambda}_{k\eta c_v}(\mathbf{h}_v)_{\eta c_v} = 0$ for $u \neq v$. The existence of orthogonality among different users implies that the non-zero elements misalignment between the u-th user and other users leads to MAI-free signals superposition in (6.27). Therefore, we conclude that MAI among users can be avoided or reduced by carefully selecting the shifting values c_u and c_v. Next we will consider the receiver design of two cases: MAI-free systems and systems with MAI.

6.4 Optimum and Sub-Optimum Receivers of CSDMA Systems with Oversampling

6.4.1 MAI-free Systems

In (6.27), if $\mathbf{\Lambda}_{k\eta c_u}(\mathbf{h}_u)_{\eta c_u}$ and $\mathbf{\Lambda}_{k\eta c_v}(\mathbf{h}_v)_{\eta c_v}$ are mutually orthogonal, then there will be no mutual interference between users u and v. We have the following results regarding a set of users that are mutually orthogonal.

Proposition 6.2: Define a subset of $\lfloor \frac{M}{L} \rfloor$ users $\mathcal{U}_l$, such that if $u \in \mathcal{U}_l$, then the time shift employed

by the u-th user is $c_u = uL + l$, for $u = 0, \cdots, \lfloor \frac{M}{L} \rfloor - 1$, and l is an integer between 0 and $L-1$. The users belonging to the same subset $\mathcal{U}_l$ are mutually orthogonal.

Proof: We first consider the case $l = 0$. Since the maximum shift of the length ηM vector $\mathbf{h}_u$ is $(\lfloor \frac{M}{L} \rfloor - 1)\eta L \leq \eta M - \eta L$, there will be no wrapping around during the shifting operation, and all the shifts are linear shifts when $l = 0$. For the u-th user, the vector $(\mathbf{h}_u)_{\eta c_u}$ has ηL non-zero elements with indices $u\eta L, u\eta L + 1, \cdots, (u+1)\eta L - 1$, and all other elements are 0. It can be easily shown that $(\mathbf{h}_u)^H_{\eta c_u}(\mathbf{h}_v)_{\eta c_v} = 0$ for $u \neq v$ and $u, v \in \mathcal{U}_0$. Also, since $\mathbf{\Lambda}_{k\eta c_u}$ is diagonal, it can be easily proven that $(\mathbf{\Lambda}_{k\eta c_u} \cdot (\mathbf{h}_u)_{\eta c_u})^H \mathbf{\Lambda}_{k\eta c_v} \cdot (\mathbf{h}_v)_{\eta c_v} = 0$ for $u \neq v$ and $u, v \in \mathcal{U}_0$.

When $l > 1$, all the $\mathbf{h}_u$ vectors for users in $\mathcal{U}_l$ can be obtained by circularly shifting all the CIR vectors in $\mathcal{U}_0$ downwards by l locations, and the circular shifting operation does not affect the orthogonality among the channel vectors in the same subset. ■

The results in Lemma 6.2 state that $L\lfloor \frac{M}{L} \rfloor$ users can be divided into L subsets, with $\lfloor \frac{M}{L} \rfloor$ users in each subset. There is no mutual interference for users belonging to the same subset. For the special case $K = 1$, that is, one symbol is transmitted over all the subcarriers, the maximum number of orthogonal users is $\lfloor \frac{N}{L} \rfloor$. This is similar to the results in [8], which states that MAI-free communications can be achieved in a MC-CDMA system with at most $\lfloor \frac{N}{L} \rfloor$ users by using a subset of the Hadamard-Walsh codes.

MAI-free system can be used for cellular systems. Assume the cells are grouped into clusters with $R \geq L$ cells in each cluster. Users in the same cell belong to the same orthogonal subset, such that there is no MAI inside a cell. Users in different cells of the same cluster can use shifting patterns from the same or different orthogonal subsets based on the relative value between the cluster size R and the channel length L. Thus there might be co-channel interference (CCI) among neighboring cells. With such a structure, each cell can support up to $\lfloor \frac{M}{L} \rfloor$ simultaneous users. For a given channel

length, more simultaneous users can be supported in each cell by increasing M, at the cost of a wider bandwidth or a longer delay.

In an MAI-free system, during the detection of the u-th user, we can extract the ηL samples in $\mathbf{r}_k$ that are contributed exclusively by s_{uk} as

$$\mathbf{r}_k^{(u)} = \mathbf{\Gamma}_u \mathbf{r}_k = \sqrt{E_s}\mathbf{\Lambda}_{k\eta c_u}^{(u)} \cdot (\mathbf{h}_u)_{\eta c_u}^{(u)} \cdot s_{uk} + \mathbf{w}_k^{(u)}, \tag{6.28}$$

where $\mathbf{\Gamma}_u$ is a $\eta L \times \eta M$ sampling matrix that is obtained by circularly shifting the columns of $\mathbf{\Gamma} = \big[\mathbf{I}_{\eta L}, \mathbf{0}_{\eta L \times \eta(M-L)}\big]$ by c_u locations to the right, $\mathbf{\Lambda}_{k\eta c_u}^{(u)} = \mathbf{\Gamma}_u \mathbf{\Lambda}_{k\eta c_u} \mathbf{\Gamma}_u^T \in \mathcal{C}^{\eta L \times \eta L}$, $(\mathbf{h}_u)_{\eta c_u}^{(u)} = \mathbf{\Gamma}_u (\mathbf{h}_u)_{\eta c_u} \in \mathcal{C}^{\eta L \times 1}$, and $\mathbf{w}_k^{(u)} = \mathbf{\Gamma}_u \mathbf{w}_k \in \mathcal{C}^{\eta L \times 1}$.

Due to the time-span of the receive filter and the time domain oversampling, there is correlation among the noise samples. The noise vector $\mathbf{w}_k^{(u)}$ is a zero-mean colored Gaussian noise. Since $\mathbf{w}_k = \mathbf{F}_{\eta M}^H \mathbf{z}_k$, thus $\mathbf{w}_k^{(u)} = \mathbf{\Gamma}_u \mathbf{F}_{\eta M}^H \mathbf{z}_k$. From (6.9) and (6.20), the covariance matrix of $\mathbf{w}_k^{(u)}$ is

$$\mathbf{R}_w^{(u)} = \mathbf{\Gamma}_u \mathbb{E}\big[\mathbf{w}_k \mathbf{w}_k^H\big] \mathbf{\Gamma}_u^T = N_0 \mathbf{\Gamma}_u \mathbf{R}_{p_k} \mathbf{\Gamma}_u^T, \tag{6.29}$$

where

$$\mathbf{R}_{p_k} = \mathbf{F}_{\eta M}^H \tilde{\mathbf{F}}_k \mathbf{R}_p \tilde{\mathbf{F}}_k^H \mathbf{F}_{\eta M} \tag{6.30}$$

Since the noise samples are mutually correlated, the noise covariance matrix $\mathbf{R}_w^{(u)}$ could be rank deficient. If the rank of $\mathbf{R}_w^{(u)}$ is q_u, then define the pseudo-inverse of $\frac{1}{N_0}\mathbf{R}_w^{(u)}$ as

$$\mathbf{\Phi}_u = \boldsymbol{V}_u \mathbf{\Omega}_u^{-1} \boldsymbol{V}_u^H \in \mathcal{C}^{\eta L \times \eta L}, \tag{6.31}$$

where $\mathbf{\Omega}_u = \text{diag}\big[\omega_1, \omega_2, \cdots, \omega_{q_u}\big] \in \mathcal{C}^{q_u \times q_u}$ is a diagonal matrix with diagonal elements being the non-zero eigenvalues of $\frac{1}{N_0}\mathbf{R}_w^{(u)}$ in a decreasing order, and $\boldsymbol{V}_u = [\mathbf{v}_1, \mathbf{v}_2, \cdots, \mathbf{v}_{q_u}] \in \mathcal{C}^{\eta L \times q_u}$ is the matrix that contains the corresponding orthonormal eigenvectors.

Based on the pseudo-inverse definition in (6.31), the decision rule of the optimum diversity receiver for the equivalent SIMO system defined in (6.28) can be described in the following proposition.

Proposition 6.3: For the MAI-free SIMO system described in (6.28), if the transmitted symbols are equiprobable, then the optimum decision rule that minimizes the system error probability is

$$\hat{\boldsymbol{s}}_{uk} = \underset{s_{uk}\in\mathcal{S}}{\operatorname{argmin}} |\xi_{uk} - \sqrt{E_s}\beta_{uk}s_{uk}|^2, \tag{6.32}$$

where $\xi_{uk} = \left[\boldsymbol{\Lambda}^{(u)}_{k\eta c_u}(\mathbf{h}_u)^{(u)}_{\eta c_u}\right]^H \boldsymbol{\Phi}_u \mathbf{r}^{(u)}_k$, and $\beta_{uk} = \left[\boldsymbol{\Lambda}^{(u)}_{k\eta c_u}(\mathbf{h}_u)^{(u)}_{\eta c_u}\right]^H \boldsymbol{\Phi}_u \left[\boldsymbol{\Lambda}^{(u)}_{k\eta c_u}(\mathbf{h}_u)^{(u)}_{\eta c_u}\right]$.

Proof: Define the noise whitening matrix as $\mathbf{D}_u = \boldsymbol{\Omega}_u^{-\frac{1}{2}}\boldsymbol{V}_u^H \in \mathcal{C}^{q_u\times\eta L}$. Applying $\mathbf{D}_u$ to (6.28) yields

$$\bar{\mathbf{r}}^{(u)}_k = \sqrt{E_s}\mathbf{D}_u\boldsymbol{\Lambda}^{(u)}_{k\eta c_u}\cdot(\mathbf{h}_u)^{(u)}_{\eta c_u}\cdot s_{uk} + \bar{\mathbf{w}}^{(u)}_k, \tag{6.33}$$

where $\bar{\mathbf{r}}^{(u)}_k = \mathbf{D}_u\mathbf{r}^{(u)}_k \in \mathcal{C}^{q_u\times 1}$, and $\bar{\mathbf{w}}^{(u)}_k = \mathbf{D}_u\mathbf{w}^{(u)}_k \in \mathcal{C}^{q_u\times 1}$ is white noise with covariance matrix being $\bar{\mathbf{R}}^{(u)}_{\bar{w}} = N_0\mathbf{I}_{q_u}$. The optimum maximum likelihood decision rule of the system defined in (6.33) can be expressed as

$$\hat{\boldsymbol{s}}_{uk} = \underset{s_m\in\mathcal{S}}{\operatorname{argmin}} \left\|\bar{\mathbf{r}}^{(u)}_k - \sqrt{E_s}\mathbf{D}_u\boldsymbol{\Lambda}^{(u)}_{k\eta c_u}\cdot(\mathbf{h}_u)^{(u)}_{\eta c_u}s_m\right\|^2. \tag{6.34}$$

Simplifying the above equation yields

$$\hat{\boldsymbol{s}}_{uk} = \underset{s_m\in\mathcal{S}}{\operatorname{argmin}}\Big[E_s\beta_{uk}\cdot|s_m|^2 - 2E_s\Re(\xi_{uk}\cdot s^*_m)\Big], \tag{6.35}$$

which is equivalent to (6.32). ■

6.4.2 Systems with MAI

When there are more than $\lfloor\frac{M}{L}\rfloor$ users, there will be MAI in the system. From (6.27), the system equation in the presence of MAI can be alternatively expressed as

$$\mathbf{r}_k = \sqrt{E_s}\mathbf{Q}_k\boldsymbol{\theta}_k + \mathbf{w}_k, \tag{6.36}$$

where $\mathbf{Q}_k \in \mathcal{C}^{\eta M \times U}$ is the equivalent channel matrix with the u-th column being $\mathbf{\Lambda}_{k\eta c_u} \cdot (\mathbf{h}_u)_{\eta c_u}$, $\boldsymbol{\theta}_k = [s_{0k}, \cdots, s_{(U-1)k}]^T \in \mathcal{S}^{U\times 1}$, and $\mathbf{w}_k \in \mathcal{C}^{\eta M \times 1}$ is the noise samples vector. The MAI among the users is determined by the structure of $\mathbf{Q}_k$.

Since $(\mathbf{h}_u)_{\eta c_u}$ has at most ηL non-zero elements, there is at most ηL non-zero elements on each column of $\mathbf{Q}_k$. The interference between two users can be reduced by misaligning the non-zero elements in their respective channel vectors. We propose to circularly shift the time domain signals of the u-th user by

$$c_u = u\left\lfloor \frac{M}{U} \right\rfloor \tag{6.37}$$

where $U \leq M$ is the total number of users in the system. Such a shifting amount will create the maximum mis-alignment between the non-zero elements of any pair of discrete-time CIR vectors.

Proposition 6.4: Consider a system described in (6.36) with $U \leq M$ users. With the time domain circular shifting given in (6.37), there will be at most L interfering users on any subcarrier.

Proof: When there are $U = M$ users, we have $c_u = u$. In this case, each row of $\mathbf{Q}_k$ has at most L non-zero elements. This can be easily shown by considering the $(m+1)$-th row of $\mathbf{Q}_k$, which is $[\lambda_{k\eta c_0}(m)h_0(m)_{\eta M}, \lambda_{k\eta c_1}(m)h_1(m-\eta)_{\eta M}, \cdots, \lambda_{k\eta c_{M-1}}(m)h_{M-1}(m-(M-1)\eta)_{\eta M}]$, where $\lambda_{k\eta c_u}(m)$ is the $(m+1)$-th diagonal element of $\mathbf{\Lambda}_{k\eta c_u}$. Since $h_u(n) = 0$ for $n \geq \eta L$ and for all u, there are at most L non-zero elements on the m-th row of $\mathbf{Q}_k$. When there are $U < M$ users, $M - U$ columns of the $\mathbf{Q}_k$ matrix of a system with $U' = M$ users will be replaced with all-zero columns, thus the number of non-zero elements on each row is no more than L. ■

Based on the above analysis, each element of $\mathbf{r}_k$ is contributed by no more than L users. Consequently, there will be no more than L mutually interfering users at a given subcarrier. Thus the number of MAI sources is upper bounded by $L - 1$ on each subcarrier. In (6.36), the system is equivalently converted to a multiple-input multiple-output (MIMO) system. At any given subcarrier, there are at

most L simultaneous inputs, even though the length of the input vector $\boldsymbol{\theta}_k$ is U, which could be larger than L. Due to the special structure of $\mathbf{Q}_k$, the system can be considered as an L-input ηM-output system.

Similar to the MAI-free case, the time domain noise vector $\mathbf{w}_k$ is colored Gaussian noise with zero-mean and covariance matrix $\mathbf{R}_{wk} = \mathbb{E}(\mathbf{w}_k \mathbf{w}_k^H) = N_0 \mathbf{R}_{p_k}$, with $\mathbf{R}_{p_k}$ defined in (6.30). If the rank of $\mathbf{R}_{wk}$ is p_k, then we can define the pseudo-inverse of $\frac{1}{N_0}\mathbf{R}_{wk}$ as

$$\boldsymbol{\Psi}_k = \mathbf{U}_k \boldsymbol{\Upsilon}_k^{-1} \mathbf{U}_k^H \tag{6.38}$$

where $\boldsymbol{\Upsilon}_k = \text{diag}\big[\upsilon_1, \upsilon_2, \cdots, \upsilon_{p_k}\big] \in \mathcal{C}^{p_k \times p_k}$ is a diagonal matrix with diagonal elements being the non-zero eigenvalues of $\frac{1}{N_0}\mathbf{R}_{wk}$ in a decreasing order, and $\mathbf{U}_k \in \mathcal{C}^{\eta M \times p_k}$ is a matrix that contains the corresponding orthonormal eigenvectors. Define a noise whitening matrix as $\boldsymbol{\Delta}_k = \boldsymbol{\Upsilon}_k^{-\frac{1}{2}} \mathbf{U}_k^H \in \mathcal{C}^{p_k \times \eta M}$, then multiplying both sides of (6.36) by $\boldsymbol{\Delta}_k$ yields an equivalent systems with white noise

$$\bar{\mathbf{r}}_k = \sqrt{E_s}\bar{\mathbf{Q}}_k \boldsymbol{\theta}_k + \bar{\mathbf{w}}_k, \tag{6.39}$$

where $\bar{\mathbf{r}}_k = \boldsymbol{\Delta}_k \mathbf{r}_k \in \mathcal{C}^{p_k \times 1}$, $\bar{\mathbf{Q}}_k = \boldsymbol{\Delta}_k \mathbf{Q}_k \in \mathcal{C}^{p_k \times U}$, and $\bar{\mathbf{w}}_k = \boldsymbol{\Delta}_k \mathbf{w}_k \in \mathcal{C}^{p_k \times 1}$ is white noise with covariance matrix being $\mathbf{R}_{\bar{w}} = N_0 \mathbf{I}_{p_k}$.

The optimum detection of (6.39) requires the exhaustive search of $\boldsymbol{\theta}_k$, which might become prohibitively complex as L, S and U become large. We propose to solve the problem by using an iterative soft-input soft-output (SISO) block decision feedback equalization (BDFE) [12], which provides a balanced trade-off between performance and complexity.

Our simulation results indicate that the sub-optimum BDFE equalizer can achieve the performance that is very close to that of an MAI-free system, which means that the BDFE equalizer can effectively remove the MAI among the users.

The proposed CSDMA system includes other systems as special cases. When $\eta = 1$, $K = N$

and $M = 1$, the system degrades to a conventional OFDM system with no multipath diversity. When $\eta = 2$, $K = N$ and $M = 1$, the system represents an OOFDM system with multipath diversity [11]. When $\eta = 1$, $K = 1$ and $M = N$, the same symbol is transmitted over all N subcarriers, and this can be considered as a single carrier system.

When the CSDMA system is operating at its maximum capacity, that is, there are $U = M = \frac{N}{K}$ simultaneous users, then the spectral efficiency of the system is the same as OFDM or OFDMA, because the proposed system can simultaneously transmit $K \times U = N$ unique symbols over N subcarriers.

6.5 Performance Analysis

The theoretical error probability of the MAI-free CSDMA system with the optimum diversity receiver is derived in this section.

The decision variable in Proposition 6.3 can be alternatively represented by

$$\xi_{uk} = \sqrt{E_s}\beta_{uk} + (\mathbf{h}_u)_{\eta c_u}^{(u)H} \mathbf{\Lambda}_{k\eta c_u}^{(u)H} \mathbf{\Phi}_u \mathbf{w}_k^{(u)}. \tag{6.40}$$

Hence, the signal-to-noise ratio (SNR) of the MAI-free system can be written as

$$\gamma_{uk} = \gamma_0 (\mathbf{h}_u)_{\eta c_u}^{(u)H} \mathbf{\Phi}_u (\mathbf{h}_u)_{\eta c_u}^{(u)}, \tag{6.41}$$

where $\gamma_0 = \frac{E_s}{N_0}$ is the SNR without fading.

The scalar $\beta_{uk} = (\mathbf{h}_u)_{\eta c_u}^{(u)H} \mathbf{\Phi}_u (\mathbf{h}_u)_{\eta c_u}^{(u)}$ is a quadratic form of the complex Gaussian random vector (CGRV) $(\mathbf{h}_u)_{\eta c_u}^{(u)}$. The characteristic function (CHF) of $(\mathbf{h}_u)_{\eta c_u}^{(u)H} \mathbf{\Phi}_u (\mathbf{h}_u)_{\eta c_u}^{(u)}$ is [19]

$$\varphi_u(j\omega) = \left[\det\left(\mathbf{I}_{\eta L} - j\omega \mathbf{R}_{hu} \mathbf{\Phi}_u\right)\right]^{-1}, \tag{6.42}$$

where $\mathbf{R}_{hu} = \mathbb{E}\left[(\mathbf{h}_u)_{\eta c_u}^{(u)} (\mathbf{h}_u)_{\eta c_u}^{(u)H}\right]$ is the covariance matrix of $(\mathbf{h}_u)_{\eta c_u}^{(u)}$, with the elements given in (6.5).

Based on the CHF in (6.42), the SER for systems with M-ary phase shift keying (MPSK) or M-ary quadrature amplitude modulation (MQAM) can be written as [19]

$$\begin{aligned} P_u(E) &= \sum_{i=1}^{2} \frac{\sigma_i}{\pi} \int_0^{\theta_i} \left[\det \left(\mathbf{I}_{\eta L} + \frac{\zeta \gamma_0}{\sin^2 \theta} \mathbf{R}_{hu} \mathbf{\Phi}_u \right) \right]^{-1} d\theta, \\ &= \sum_{i=1}^{2} \frac{\sigma_i}{\pi} \int_0^{\theta_i} \left[\det \left(\mathbf{I}_{\eta L} + \frac{\zeta \gamma_0}{\sin^2 \theta} \mathbf{R}_{u} \right) \right]^{-1} d\theta, \end{aligned} \tag{6.43}$$

where the parameters σ_i, θ_i, and ζ are related to different modulation schemes as tabulated in [19, Table 1], $\mathbf{R}_u = \mathbf{\Phi}_u^{\frac{1}{2}} \mathbf{R}_{hu} (\mathbf{\Phi}_u^{\frac{1}{2}})^H$ with $\mathbf{\Phi}_u = (\mathbf{\Phi}_u^{\frac{1}{2}})^H \mathbf{\Phi}_u^{\frac{1}{2}}$, and the identity $\det(\mathbf{I} + \mathbf{XY}) = \det(\mathbf{I} + \mathbf{YX})$ is used to get the second equation in (6.43). Performing eigenvalue decomposition of $\mathbf{R}_u$ yields

$$P_u(E) = \sum_{i=1}^{2} \frac{\beta_i}{\pi} \int_0^{\theta_i} \prod_{l=1}^{\tilde{L}_u} \left[1 + \gamma_0 \cdot \frac{\zeta \lambda_{ul}}{\sin^2 \theta} \right]^{-1} d\theta. \tag{6.44}$$

where $\tilde{L}_u$ is the rank of $\mathbf{R}_u$, and λ_{ul} are the non-zero eigenvalues of $\mathbf{R}_u$. The average SER can then be evaluated as SER $= \frac{1}{U} \sum_{u=0}^{U-1} P_u(E)$. For modulations with Gray mapping, the bit error rate (BER) can be approximated by BER $\approx \frac{1}{\log_2(S)}$SER.

It should be noted that the error probability result is independent of N, M, K, or U, as long as the condition $U \leq M/L$ is satisfied.

6.6 Simulation Results

Simulation results are presented in this section to demonstrate the performance of the CSDMA system with oversampling receiver. In the simulations, the transmit and receive filters are root-raised cosine (RRC) filters with roll-off factor $\alpha = 1$. The sampling period at the input of the receive filter is assumed to be $T_1 = 3.69\mu$s, unless stated otherwise. Moreover, we use $\eta = 2$ for systems with oversampling, while $\eta = 1$ is used for systems without oversampling.

Fig. 6.1 compares the performance between systems with and without oversampling, for various modulation schemes. All systems are MAI-free with $M = 16$, $K = 4$ and $N = 64$. The power

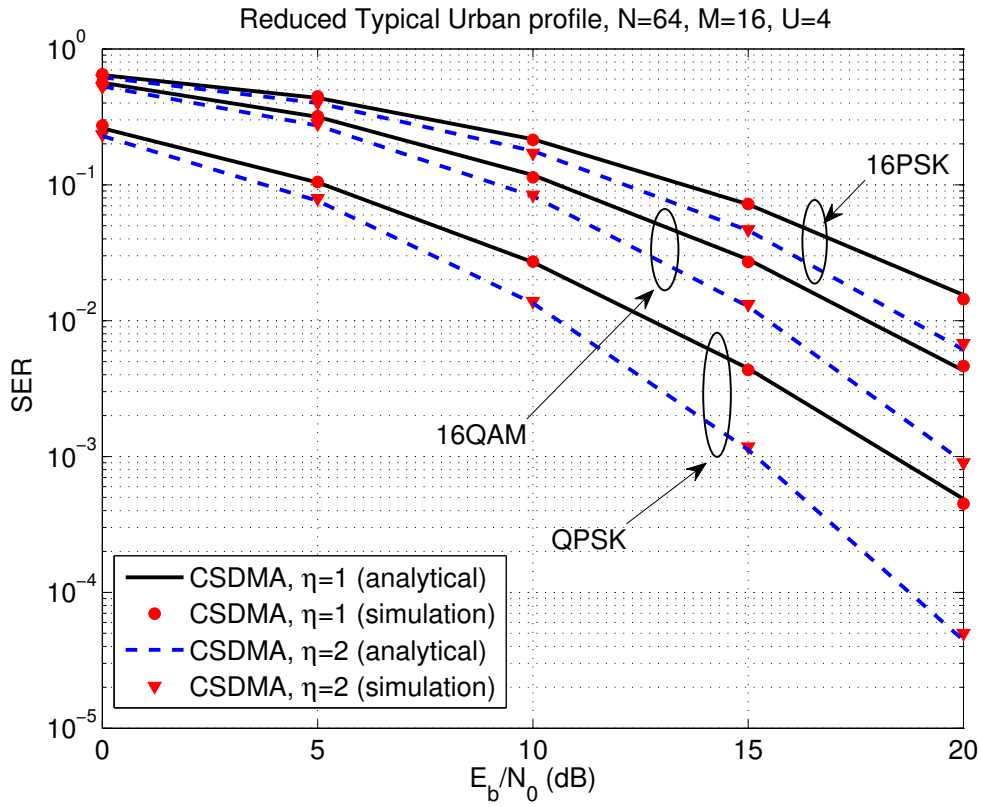

Figure 6.1: SER performance of systems in TU channel profile and various modulation schemes. $N = 64$, $M = 16$ and $U = 4$ are used in all systems. Results are obtained for both $\eta = 1$, and $\eta = 2$.

delay profile is the reduced typical urban (TU) profile. The number of users in each system satisfies the rule $U = \lfloor \frac{M}{L} \rfloor$ to achieve MAI-free communications. Again, excellent agreements are observed between the simulation and analytical results for all systems configurations. Systems with or without oversampling can support the same number of MAI-free users, yet oversampled systems consistently outperform those without oversampling for all modulation schemes. The performance improvement is contributed by the extra multipath diversity that is collected through time-domain oversampling.

Fig. 6.2 shows the SER performance of CSDMA with and without MAI for systems with QPSK modulation. There are $N = 64$ subcarriers at the transmitter for all systems. For system with $U = 64$ users, we have $M = 64$ and $K = 1$ given that U cannot be larger than M. For systems with $U = 1$ or $U = 4$, we have $M = 16$ and $K = 4$ to achieve MAI-free communications. When $U = 4$,

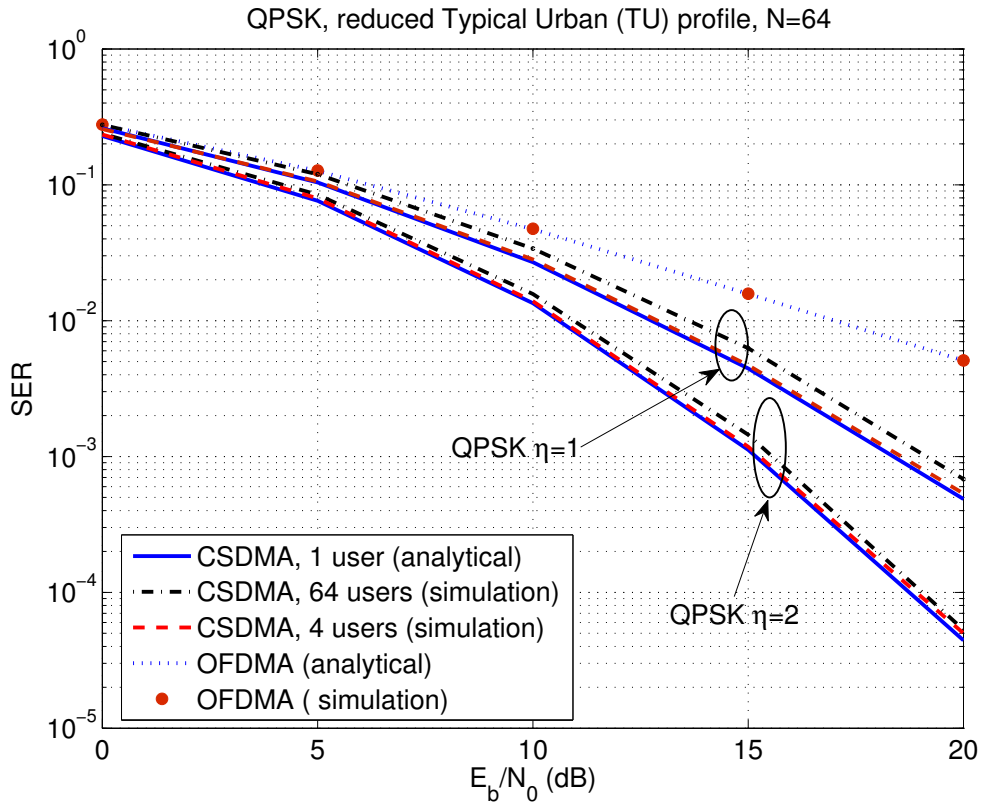

Figure 6.2: SER performance of systems with different number of users and with and without oversampling. QPSK modulation is used in all systems.

the simulated SER matches perfectly with the analytical one with $U = 1$ because there is no MAI. When $U = 64$, the simulation results are slightly worse than the $U = 4$ systems. At SER = 10^{-3} and $\eta = 1$, the performance of systems with $U = 64$ systems is 0.5 dB away from that with $U = 4$, and the performance difference drops to 0.2 dB at $\eta = 2$. The results indicate that the MAI does not significantly affect the system performance, in part because the number of interfering users are upper bounded by L. In addition, the sub-optimum BDFE receiver can effectively remove the effects of MAI.

The impacts of sampler timing offset τ_0 on the system SER performance for systems with and without oversampling are shown in Fig. 6.3. The simulation and analytical results are obtained for QPSK and 16QAM modulations. For all systems, we have $N = 64$, $M = 16$, and $U = 4$. For systems

without oversampling, the SER performance varies with the timing offset τ_0. The SER performance variations are due to the effect of spectrum aliasing of the received signals at the receiver. However, the spectrum aliasing of the received signals can be completely eliminated by using $\eta = 2$ for systems employing transmit and receive filters with a rollof factor $\alpha = 1$. Thus the performance of the oversampled system is independent of the timing offsets.

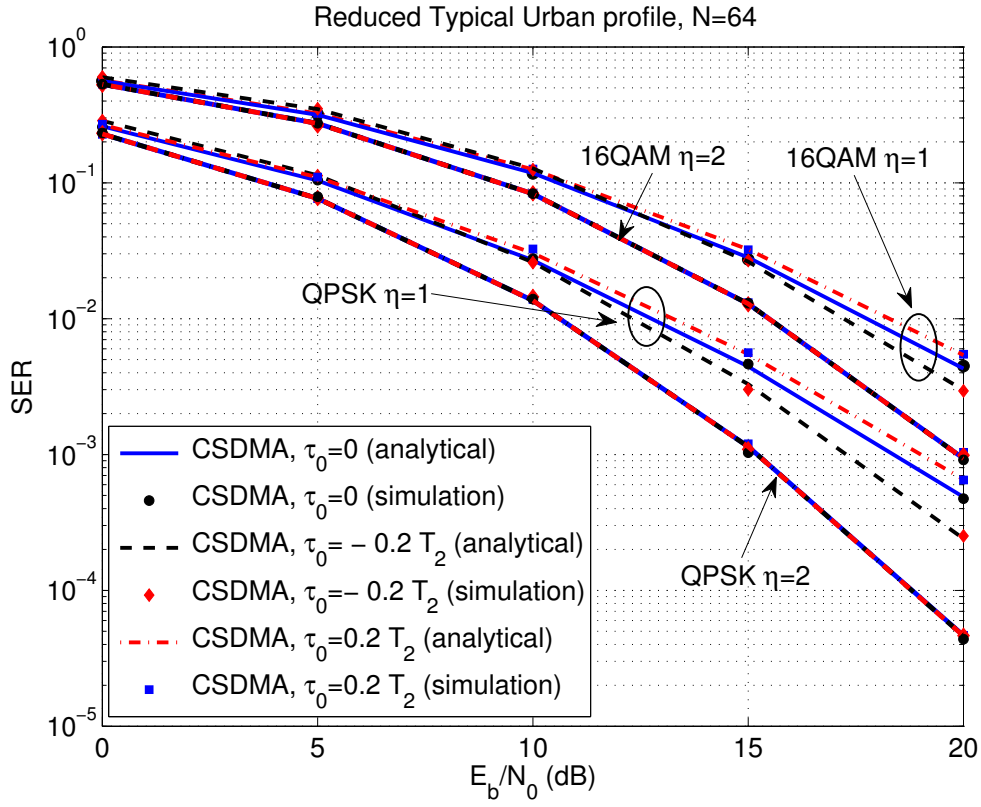

Figure 6.3: SER performance of systems in TU channel with and without oversampling and under the effect of sampler timing offset τ_0. $N = 64$, $M = 16$ and $U = 4$ are used for all systems.

In Fig. 6.4, the SER performance is plotted as a function of timing offset τ_0 for systems with and without oversampling. Both equal gain power delay profiles with $L = 3$ and reduced typical urban profiles are considered in this example. For all systems we have $\frac{E_b}{N_0} = 15$ dB, $N = 64$, $M = 16$ and $U = 4$. We have two observations. First, the effects of timing offset are completely removed by using oversampling. Second, for systems without oversampling, $\tau_0 = 0$ does not necessarily mean

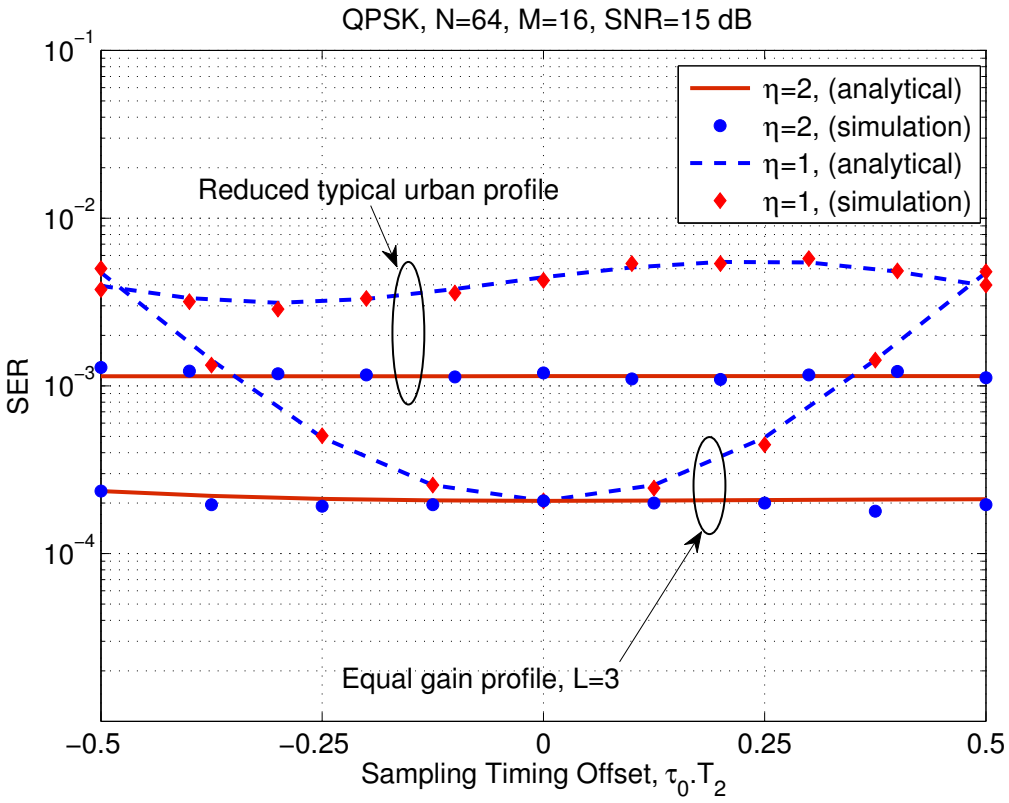

Figure 6.4: SER performance versus sampler offset τ_0 for systems with and without oversampling. Figures were obtained for both TU and EQ channel delay profiles, with $N = 64$, $M = 16$ and $U = 4$.

the best performance as evident for system with the TU power delay profile. This is due to the fact that τ_0 introduces a phase shift in the frequency domain, and different phase shifts might result in constructive or destructive combinations of the spectrum when $\eta = 1$.

In Fig. 6.5, we compared the performance of the proposed CSDMA system with both MC-CDMA [8] and OFDM-interleave division multiple access (OFDM-IDMA)[35] systems. The total number of subcarriers at the transmitter was set as $N = 64$ for all systems. In all systems, we set $M = 64$, $U = 64$, and $K = 1$. A typical urban (TU) power delay profiles, and binary phase shift Keying (BPSK) modulation were considered for all systems. In the MC-CDMA system, all users were assigned different spreading codes selected from a size N Hadamard-Walsh matrix, while the same spreading code was used for all users in OFDM-IDMA. The following observations can be made

from the figure: First, all systems have MAI when $N = U = 64$. Second, the CSDMA system with oversampling has the best performance among all systems, the performance improvement in CSDMA with oversampling was mainly due to multipath diversity. Third, the performance of OFDM-IDMA with six iterations is slightly better than CSDMA without oversampling, on the other hand, the performance of CSDMA without oversampling outperforms OFDM-IDMA with three iterations. However, the computational complexity of OFDM-IDMA with three or six iterations is higher than that of CSDMA. Finally, the MC-CDMA system has the worst performance among different systems.

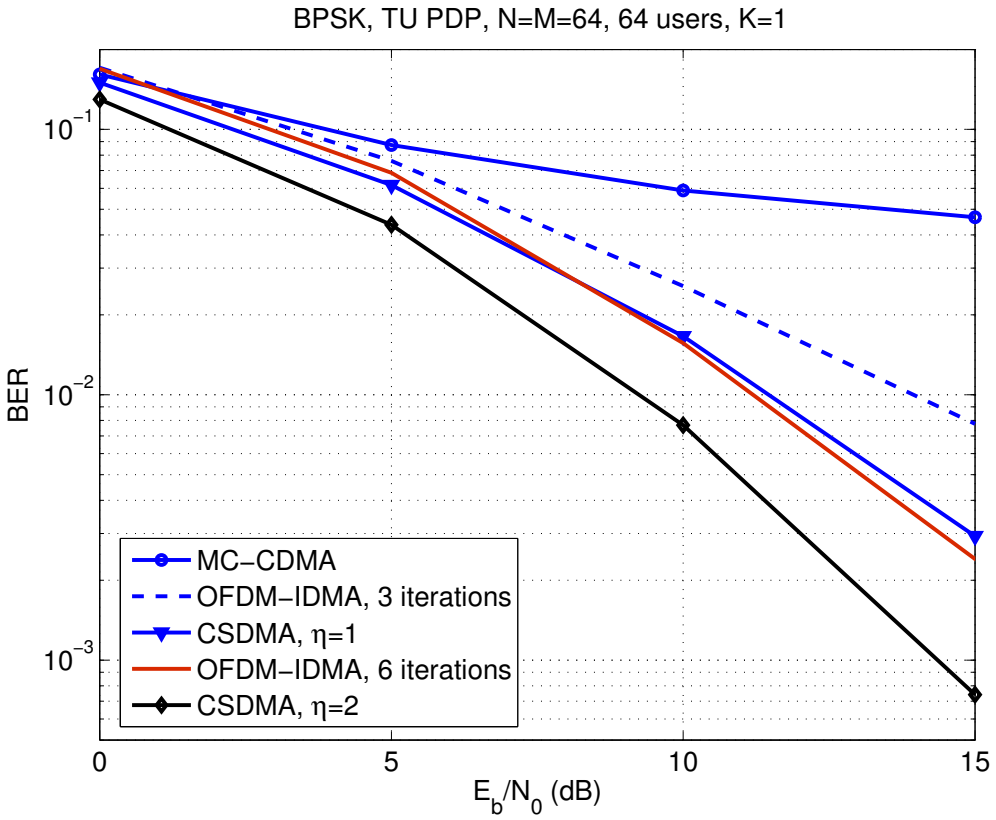

Figure 6.5: BER performance of different multi-carrier multi-user systems in reduced typical urban power delay profiles. BPSK modulations, $K = 1$, and $N = M = U = 64$ were used for all systems.

In Fig. 6.6, The performance of CSDMA, MC-CDMA, and OFDM-IDMA were plotted as a function of the number of users. The TU power delay profile was considered in all systems. The number of subcarriers at the transmitter was set as $N = 16$ for all systems. $K = 1$, and BPSK

modulation were assumed in all systems. In the MC-CDMA system we utilized the code selection priority proposed in [8]. The figure clarifies that the performance of our system with oversampling outperforms all other systems. Furthermore, the CSDMA system without oversampling has better performance than OFDM-IDMA with two or three iterations, consequently, the number of iterations plays a critical role in the performance of OFDM-IDMA, where higher number of iterations means larger computational complexity.

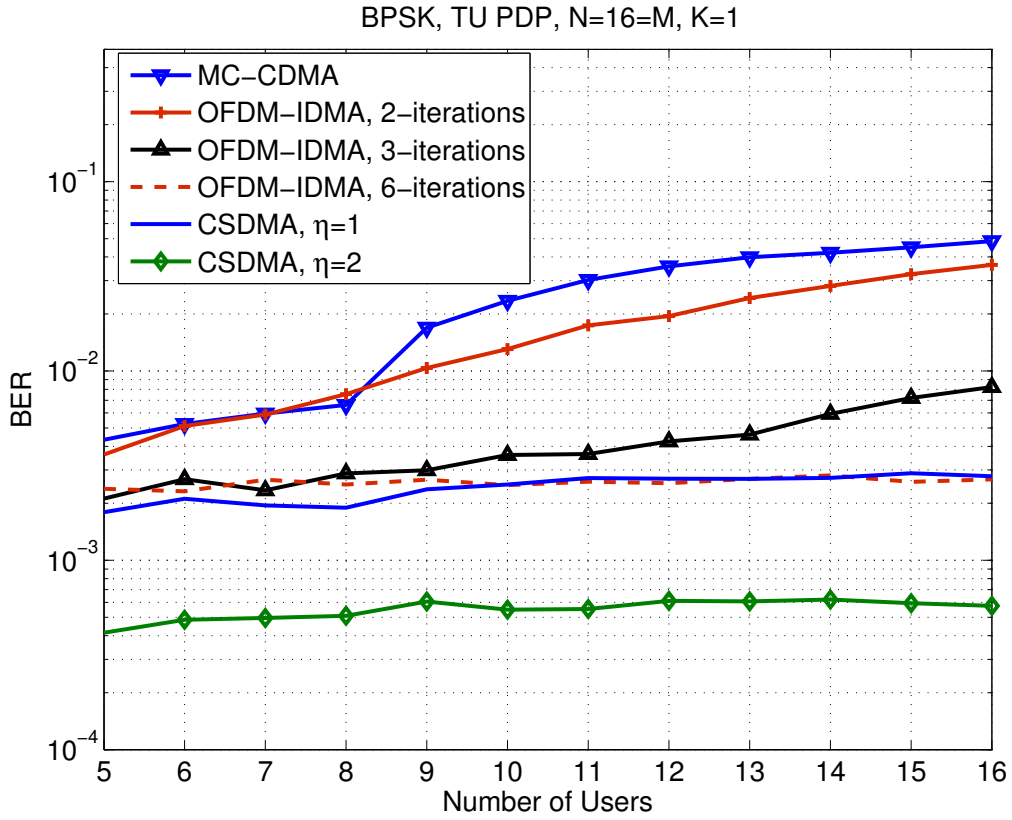

Figure 6.6: BER performance of various multi-carrier multi-user systems versus the number of transmitting users. TU PDP, BPSK modulations and $N = M = 16$ are used for all systems.

Fig. 6.7 shows the performance of the CSDMA system with oversampling, results were obtained for systems with and without MAI. The performance of the OFDM-IDMA system is also shown for comparison purposes. The number of subcarriers at the transmitter was $N = 64$ in all systems. The TU power delay profile was assumed in all systems. For CSDMA system with $U = 64$ users, we have

$M = 64$ and $K = 1$. while, for CSDMA system with $U = 1$ or $U = 4$ we have $M = 16$ and $K = 4$ to achieve MAI-free communications. In the simulations, we considered OFDM-IDMA with six iterations and four users, $U = 4$. Results in Fig. 6.7 indicates that the proposed CSDMA system with oversampling consistently outperforms the OFDM-IDMA system. The performance improvement of the CSDMA system with $\eta = 2$ is mainly contributed by the collected multipath diversity, where part of this diversity was provided through oversampling.

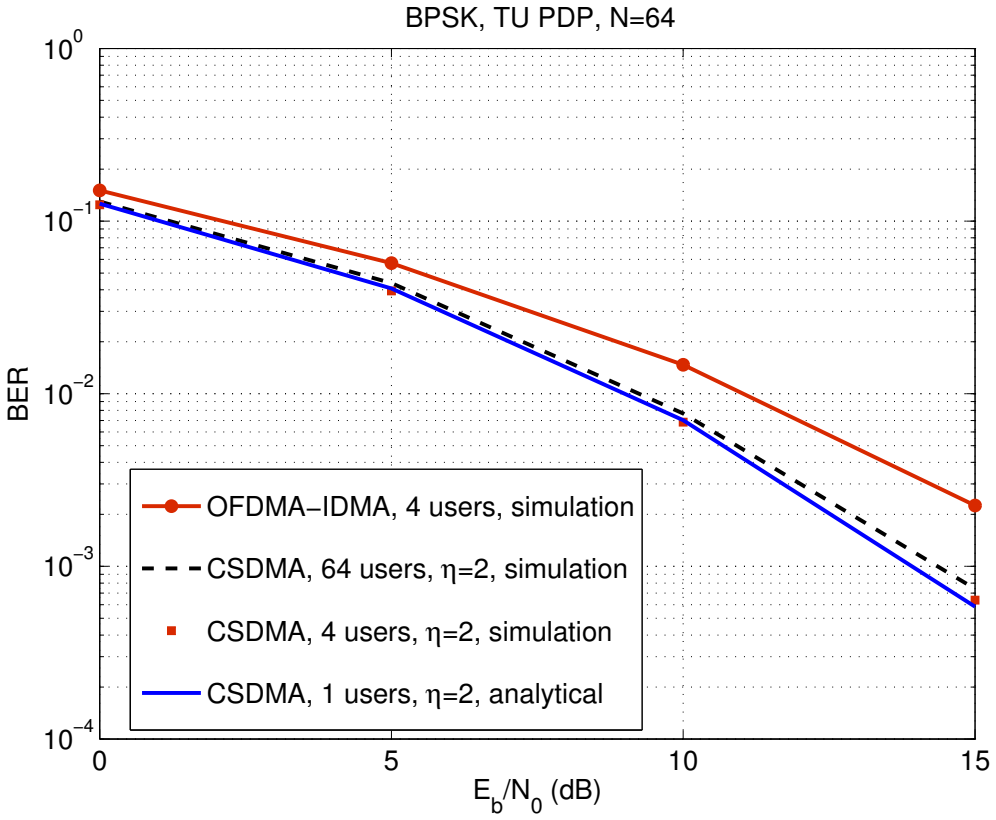

Figure 6.7: BER performance of CSDMA systems with oversampling receivers. Number of subcarriers at the transmitter was set as $N = 64$ for all systems.

6.7 Conclusions

A circular-shift division multiple access scheme with oversampling receivers has been proposed for multi-carrier wireless networks. The combination of circular shifting at the transmitter and oversampling at the receiver ensures full multipath diversity, and it renders a special signal structure that allows

the receiver to differentiate the signals from different users. When the number of users is no more than M/L, where L is the length of the equivalent discrete-time channel before oversampling, MAI-free communications can be achieved. When the system is fully loaded, that is, the number of users is no more than M, then there are at most L mutually interfering users at any given subcarrier. In addition, the oversampling operation removes the negative effects of timing offsets between clocks at transmitters and receiver. Both analytical and simulation results demonstrated that the proposed scheme is significantly outperforms OFDMA and OFDM-IDMA systems, and the oversampling operation leads to considerable performance gains over those without oversampling.

Chapter 7

Optimum Receiver Design with Channel Estimation Errors

7.1 Introduction

A major challenge of current and future mobile wireless communication systems is to provide reliable high-data rate communications for users in high mobility scenarios. Smartphones operated by individuals riding high-speed trains or airplanes are examples of wireless communications in a high mobility environment.

Accurate channel estimation plays a critical role in providing a dependable high mobility broadband wireless communications. High mobility introduces fast time channel variations, therefore, channel estimation becomes more difficult in high mobility wireless communications. The error performance of linearly modulated MPSK system with doubly selective (time selective and frequency selective) fading channel is presented in [28], a closed form for the error performance lower bounds have been derived for systems with and without time-domain oversampling. However, the channel state information (CSI) is assumed to be perfectly known at the receiver, which is not accurate assumption especially for high mobility wireless communication systems.

Many existing works focus on minimizing the mean squared error (MSE) between the true and the estimated channel coefficients [36]–[39]. In [36, 37], CSI estimation is obtained by employing the basis expansion model (BEM), where the time-varying channel impulse response is converted into a low dimensional transform domain leading to a reduction in the estimation computational complexity. CSI can also be attained through transmitting pilot patterns that are known at both the transmitter and receiver [38]–[43]. In [38], the least squares (LS) estimation is employed in the OFDM system

with a quasi-static channel where the sub-optimum pilot pattern for the estimator is obtained through numerical convex optimization techniques. In the LS estimation, the prior knowledge of channel statistics is not required, however, such information is needed in the minimum mean squared error (MMSE) estimation. In [39], the MSE of the MMSE channel estimation for the (OFDM) system is minimized by using identical equally-spaced frequency domain pilot clusters.

In the presence of channel estimation errors, the conventional maximum ratio combining (MRC) receiver is no longer optimum. In [40], the optimal decision rule that considers the impact of channel estimation errors is derived for receivers employing LS or MMSE channel estimations for M-ary phase shift keying (MPSK). When the optimum receiver is used, the SER of the MPSK system with MMSE CSI estimation is the same as the SER of the MPSK system with LS CSI estimation [40]. The exact error probability expressions for the optimal coherent diversity receivers are obtained in [40]. In [41], the optimum pilot design for high mobility wireless communication system with time-varying flat fading is studied; minimizing the SER of the system is considered as the pilot design optimization metric. According to results presented in [41], the SER is a decreasing function in pilot percentage, on the other hand, it is an increasing function in the Doppler spread. The optimum system design that can maximize the spectral efficiency of high mobility wireless communications under an imperfect CSI is discussed in [42]. The fast time-varying fading channel coefficients are estimated through the MMSE estimation; if the pilot samples the channel at rate greater or equal to the Nyquist rate of the time-varying channel, the MMSE channel estimation at pilots locations and the MMSE channel interpolation at data symbols locations have the same MSE. An expression for the relationship between the spectral efficiency and the pilot percentage is developed in [42], the expression quantifies the trade off between lower SER and excess pilot percentage [42].

The maximum Doppler diversity transmission with an imperfect CSI in high mobility system

is presented in [43]. It is shown in [43] that the SER is a quasi-convex in Doppler spread and a monotonically decreasing in terms of pilot percentage. However, the analysis in [41]-[43] are only applied to fast time-varying flat fading channels. The LS estimations of doubly selective channels are discussed in [44] for a multiple-input multiple-output (MIMO) OFDM system. To avoid matrix inversions during the LS channel estimation, the pilot matrix is designed as a unitary matrix, moreover, the pilot-tones represent orthogonal codes in space-frequency domain [44].

The impacts of pilot percentage on the MSE of the MMSE channel estimations with doubly-selective fading channel in high mobility wireless communication systems are studied in [45]. Channel correlations in both time and delay domains are employed to minimize the MSE of the MMSE channel estimator.

In this chapter, we study the impacts of the imperfect CSI on the performance of high mobility wireless communication systems with doubly-selective fading channels. We consider a system that employs pilot assisted MMSE channel estimation. The impacts of the energy allocation factor, pilot percentage and Doppler spread on both the MSE of the MMSE estimator and on the SER of a linearly modulated system are investigated. The conventional MRC receiver is not optimum in the presence of channel estimation errors, however, the optimal receiver can be obtained by considering the impact of channel estimation errors. The statistical properties of the estimated channel coefficients in both time and delay domains are obtained and then used to design the optimum receiver. The theoretical SER of the optimum receiver with an imperfect CSI is then derived for a linearly modulated systems; indeed, the obtained expressions quantify the effect of energy allocation factor, pilot percentage and Doppler spread on the system performance. Finally, the derived analytical results are supported by computer simulations.

The rest of this chapter is organized as follows. The system model is presented in Section 6.2.

Section 6.3 studies the pilot-assisted MMSE channel estimation. In Section 6.4, the optimum receiver and the error performance analysis are presented. Simulation results and conclusions are given in Section 6.5 and Section 6.6, respectively.

All over the chapter we use the following common notations: the superscripts $(\cdot)^T$ and $(\cdot)^H$ represent matrix transpose and Hermitian transpose, respectively; $\mathbb{E}(\cdot)$ is the mathematical expectation operator; $\mathcal{C}^{M\times N}$ denotes the $(M \times N)$-dimensional complex space; $\Re(a)$ is the real part operator; $\mathcal{C}^M$ is the space of M-dimensional complex column vectors; $\mathbf{I}_N$ is a size-N identity matrix; $\mathbf{0}_{M\times N}$ is $M \times N$ all-zero matrix; diag $\{\mathbf{a}\}$ is a diagonal matrix with the vector $\mathbf{a}$ on its main diagonal; $\mathcal{S}$ is the modulation constellation set, and $\odot$ is the time domain convolution operator.

7.2 System Model

Consider a wireless communication system where a pilot-assisted channel estimation is employed. Before transmission, data symbols are split into slots, where in each slot pilot patterns are inserted for channel estimation purposes. The pilot pattern has $2L-1$ pilot symbols, where L is the length of the equivalent discrete time channel. Each pilot pattern contains one active pilot symbol located at the middle of the pilot pattern and $L-1$ zeros, or silent pilot symbols, on the right and left sides of the active pilot symbol. The silent pilots are used in each pattern to obtain Inter-symbol-Interference (ISI)-free transmission of the active pilot symbol over doubly selective fading channels. Each transmitted slot contains N_p equally spaced pilot patterns and K data symbols occupy the space between each pair of adjacent pilot pattens, where K is a non-negative integer. Hence, the transmitted slot of length N is consisted of $N_s = N_pK$ data symbols, and $N_p(2L-1)$ pilot symbols, *i.e*, $N = N_pK + N_p(2L-1) = Np(K+2L-1)$.

Let $\mathbf{x} = [x_1, x_2, \cdots, x_N]^T$ denote the transmitted slot that contains both data and pilot symbols. Based on the slot structure, we denote the k-th active pilot symbol as $x_{i_k} = p_k$, where $i_k = K + L +$

$(k-1)M$, for $k = 1, \cdots, N_p$ and $M = K + 2L - 1$. Also, define $\mathcal{I}_s = \{n | n = n + (k-1)M, n = 1, \cdots, K, k = 1, \cdots, N_p\}$ as the set that contains the indices of the transmitted data symbols.

Also, denote the average transmission energy per active pilot symbol and per data symbol as E_p, and E_s, respectively. The average transmission energy per symbol is then $E_0 = E_p \frac{N_p}{N} + E_s \frac{N_s}{N}$. The active pilot symbols are known symbols at both the transmitter and the receiver, and they are inserted into each data slot to play a specific role different from that of data symbol, for that reason, we propose to allocate amount of energy to the pilot symbol different from that allocated to the data symbol. So, let $E_p = \alpha E_0 \frac{N}{N_p}$, and $E_s = (1-\alpha) E_0 \frac{N}{N_s}$, where $0 < \alpha < 1$ is the energy allocation factor, in addition, by changing α we can obtain a wide range of allocated energies for both pilot and data symbols. If we define the pilot percentage among the transmitted symbols, δ, as $\delta = \frac{(2L-1)N_p}{N}$, then in terms of δ and α, E_s and E_p can be represented as

$$E_s = E_0 \frac{(1-\alpha)}{(1-\delta)}, \tag{7.1a}$$

$$E_p = E_0 \frac{\alpha(2L-1)}{\delta}. \tag{7.1b}$$

Each slot with N elements is transmitted over a doubly selective fading channel where it is corrupted by an additive white Gaussian noise (AWGN) with variance N_0. Based on the above discussion, the observed signal at the receiver can be described by

$$\mathbf{y} = \mathbf{E}^{\frac{1}{2}} \mathbf{H} \cdot \mathbf{x} + \mathbf{z}, \tag{7.2}$$

where $\mathbf{y} = [y(1), y(2), \cdots, y(N)]^T \in \mathcal{C}^{N \times 1}$, $\mathbf{H} \in \mathcal{C}^{N \times N}$ is the time-domain channel matrix defined in (7.3) on the top of the next page, $\mathbf{z} = [z(1), z(2), \cdots, z(N)]^T \in \mathcal{C}^{N \times 1}$ is the noise vector with covariance matrix, $\mathbf{R}_z = N_0 \mathbf{I}_N$, and the matrix $\mathbf{E} = \text{diag}\{[E_1, \cdots, E_N]^T\}$ is a diagonal matrix with

E_n being the energy allocated to the n-th transmitted symbol.

$$\mathbf{H} = \begin{pmatrix} h(1,0) & 0 & \dots & h(1,L-1) & \dots & h(1,1) \\ h(2,1) & h(1,0) & \dots & 0 & h(2,L-1) & \dots \\ \vdots & \ddots & \ddots & \vdots & \vdots & \vdots \\ 0 & \dots & h(N,L-1) & \dots & \dots & h(N,0) \end{pmatrix} \in \mathcal{C}^{N\times N} \quad (7.3)$$

If the channel undergoes a wide sense stationary uncorrelated scattering (WSSUS) Rayleigh fading, then the time-domain correlation function $\rho(n_1 - n_2, l_1, l_2)$ of channel coefficients can be described by [31]

$$\rho(n_1 - n_2, l_1, l_2) = \mathbb{E}[h(n_1, l_1)h^*(n_2, l_2)] = J_0(2\pi f_{\text{D}}|n_1 - n_2|T_s) \cdot c(l_1, l_2), \quad (7.4)$$

where f_{D} is the maximum Doppler frequency of the fading channel, $J_0(\cdot)$ is the zero-order Bessel function of the first kind, T_s is the receiver sampling period, and $c(l_1, l_2)$ is the correlation between channel coefficients in the delay domain. Denote the transmit and the receive filters as $p_{_T}(t)$, $p_{_R}(t)$, respectively, $c(l_1, l_2)$ is then can be calculated as $c(l_1, l_2) = \int_{-\infty}^{\infty} R_{_{TR}}(l_1T_s - \nu)R^*_{_{TR}}(l_2T_s - \nu)G(\nu)d\nu$, where $G(\nu)$ is the normalized channel power delay profile (PDP) with $\int_{-\infty}^{\infty} G(\nu)d\nu = 1$, and $R_{_{TR}}(t) = p_{_T}(t) \odot p_{_R}(t)$ [31].

7.3 Channel Estimation

At the receiver, and before detection, an estimate of channel coefficients is obtained by utilizing the linear MMSE estimation. In this section, the MMSE channel estimation is presented, the impacts of the Doppler frequency f_{D}, pilot percentage δ, and energy allocation factor α on the estimation performance are studied.

For each transmitted pilot symbol there are L ISI-free observations at the receiver, these observations

can be presented as

$$\mathbf{y}_{p_k} = \sqrt{E_p}\mathbf{h}_{p_k}p_k + \mathbf{z}_{p_k}, \text{for } k = 1, \cdots, N_p, \tag{7.5}$$

where $\mathbf{y}_{p_k} = [y(i_k), \cdots, y(i_k+L-1)]^T \in \mathcal{C}^{L\times 1}$ is the received samples of the k-th transmitted active pilot, $p_k = x_{i_k}$ is the k-th transmitted active pilot symbol, $\mathbf{h}_{p_k} = [h(i_k, 0), \cdots, h(i_k + L - 1, L - 1)]^T \in \mathcal{C}^{L\times 1}$ is the equivalent discrete-time channel fading coefficient vector associated with the k-th transmitted active pilot symbol, and $\mathbf{z}_{p_k} = [z(i_k), z(i_k + 1), \cdots, z(i_k + L - 1)]^T \in \mathcal{C}^{L\times 1}$ is the noise samples vector corresponding to the k-th transmitted active pilot. Thus, for N_p transmitted pilot patterns over a channel of equivalent length L we have N_pL ISI-free observations at the receiver, these observations can be stacked into one column vector as [45]

$$\mathbf{y}_p = \sqrt{E_p} \cdot \mathbf{P} \cdot \mathbf{h}_p + \mathbf{z}_p, \tag{7.6}$$

where $\mathbf{y}_p = [\mathbf{y}_{p_1}^T, \cdots, \mathbf{y}_{p_{N_p}}^T]^T \in \mathcal{C}^{LN_p\times 1}$ is the received signals of all pilot symbols, $\mathbf{h}_p = [\mathbf{h}_{p_1}^T, \cdots, \mathbf{h}_{p_{N_p}}^T]^T \in \mathcal{C}^{LN_p\times 1}$ contains channel coefficients at pilot symbols locations, $\mathbf{z}_p = [\mathbf{z}_{p_1}^T, \cdots, \mathbf{z}_{p_{N_p}}^T]^T \in \mathcal{C}^{LN_p\times 1}$ is the noise samples at the received pilots positions, and the diagonal matrix $\mathbf{P} = \text{diag}\{[\mathbf{p}_1^T, \cdots, \mathbf{p}_{N_p}^T]^T\} \in \mathcal{C}^{LN_p\times LN_p}$ contains the transmitted pilot symbols, where $\mathbf{p}_k = [p_k, \cdots, p_k]^T \in \mathcal{S}^{L\times 1}$. Next, channel estimation at pilot symbols locations is presented and then followed by channel estimation at data symbols locations.

7.3.1 MMSE Channel Estimations at Pilot Locations

The first step in acquiring channel coefficients at data locations is to obtain an estimate of channel coefficients at pilot locations by minimizing the average MSE between the estimated channel coefficients and the true ones. The average MSE of channel estimation at pilot locations is defined as $\sigma^2_{p,LN_p} = \frac{1}{LN_p}\mathbb{E}(||\hat{\mathbf{h}}_p - \mathbf{h}_p||^2)$, where $||\mathbf{a}||$ is the L^2-norm of vector $\mathbf{a}$, and $\hat{\mathbf{h}}_p$ is the estimate of $\mathbf{h}_p$.

The linear MMSE estimation for channel coefficients at pilot positions can be written as

$$\hat{\mathbf{h}}_p = \mathbf{W}_p^H \mathbf{y}_p, \tag{7.7}$$

where $\mathbf{W}_p \in \mathcal{C}^{LN_p \times LN_p}$ is the MMSE estimation matrix. The MMSE estimation matrix $\mathbf{W}_p$ can be obtained by applying the orthogonal principal *i.e.*, $\mathbb{E}[\mathbf{e}_p \mathbf{y}_p^H] = 0$, where $\mathbf{e}_p = (\hat{\mathbf{h}}_p - \mathbf{h}_p)$ is the estimation error vector; the result can then be expressed as

$$\mathbf{W}_p = \sqrt{E_p}(E_p \mathbf{P}\mathbf{R}_{pp}\mathbf{P}^H + N_0 \mathrm{I}_{LN_p})^{-1}\mathbf{P}\mathbf{R}_{pp}, \tag{7.8}$$

where $\mathbf{R}_{pp} = \mathbb{E}[\mathbf{h}_p \mathbf{h}_p^H] \in \mathcal{R}^{LN_p \times LN_p}$ is the autocorrelation matrix of the pilot channel coefficients vector $\mathbf{h}_p$, the matrix $\mathbf{R}_{pp}$ is a block Toplitz matrix which can be written as [45]

$$\mathbf{R}_{pp} = \mathbf{R}_{pt} \otimes \mathbf{R}_{\tau}, \tag{7.9}$$

where $\mathbf{R}_{pt} \in \mathcal{R}^{N_p \times N_p}$ is correlation matrix in the time domain, and $\mathbf{R}_{\tau} \in \mathcal{R}^{L \times L}$ is the correlation matrix in the delay domain. The correlation matrix in the time domain, $\mathbf{R}_{pt}$, is a symmetric Toplitz matrix, the first column and the first row of $\mathbf{R}_{pt}$ can be written as $\mathbf{r}_t = [1, J_0(2\pi f_{\mathrm{D}} T_p), \cdots, J_o(2\pi f_{\mathrm{D}}(N_p - 1)T_p)]^T$, where $T_p = \frac{(2L-1)T_s}{\delta}$ is the time interval between two neighboring active pilot symbols. The delay correlation matrix, $\mathbf{R}_{\tau}$, can be represented as [28]

$$\mathbf{R}_{\tau} = \begin{bmatrix} c(0,0) & \cdots & c(0, L-1) \\ \vdots & \ddots & \vdots \\ c(L-1, 0) & \cdots & c(L-1, L-1) \end{bmatrix}. \tag{7.10}$$

By employing the orthogonal principal, the error correlation matrix $\mathbf{R}_{ee} = \mathbb{E}[\mathbf{e}_p \mathbf{e}_p^T] \in \mathcal{R}^{LN_p \times LN_p}$ is then obtained as

$$\mathbf{R}_{ee} = \mathbf{R}_{pp} - \mathbf{R}_{pp}\left[\mathbf{R}_{pp} + \frac{\delta}{\alpha(2L-1)\gamma_0}\mathrm{I}_{LN_p}\right]^{-1}\mathbf{R}_{pp}, \tag{7.11}$$

where $\gamma_0 = \frac{E_0}{N_0}$ is the average SNR. The average MSE can be calculated as $\sigma^2_{p,LN_p} = \frac{1}{LN_p}\text{trace}(\mathbf{R}_{ee})$. The calculation of the MSE, σ^2_{p,LN_p}, requires a matrix inversion followed by a trace operation, therefore, to simplify the calculations and to explicitly identify the impacts of design parameters on the MSE of the MMSE estimator, we utilize the asymptotic approach by assuming an infinite number of pilot patterns, *i.e.*, $N_p \to \infty$ while keeping a finite channel length L, pilot percentage δ, energy allocation factor α, and symbols period T_s. The obtained results can then be summarized in the following proposition [45].

Proposition 7.1: When the number of pilot patterns approaches infinity, *i.e.*, $N_p \to \infty$ while having a finite L, δ, α and T_s, the average asymptotic MSE, $\sigma^2_p = \lim_{N_p\to\infty}\sigma^2_{p,N_p}$, of the MMSE channel estimator at pilot locations can be described by

$$\sigma^2_p = \frac{1}{L}\sum_{i=0}^{L-1}\left[\lambda_i - \frac{8\alpha\gamma_0\lambda_i^2 \arctan\sqrt{\frac{2\alpha\gamma_0\lambda_i - w_d}{2\alpha\gamma_0\lambda_i + w_d}}}{\pi\sqrt{(2\alpha\gamma_0\lambda_i)^2 - (wd)^2}}\right] \text{ for } \delta \geq \frac{(2L\text{–}1)w_d}{\pi}, \quad (7.12)$$

where, $w_d = 2\pi f_{\text{D}} T_s$, and λ_i is the i-th eigenvalue of the delay domain correlation matrix $\mathbf{R}_\tau$.

Proof: The matrix, $\mathbf{R}_{pp}$, can be identified by the sequence $r_k^{u,v} = \{J_0(2\pi f_{\text{D}}|k|T_p)\cdot c(u,v)\}_{k,u,v}$, $k = -(N_p\text{–}1), ..., (N_p\text{–}1), u, v = 0, ..., L-1$. Applying the discrete-time Fourier transform (DTFT) on $r_k^{u,v}$ with respect to k results [45]

$$R^{u,v}(\Omega) = \sum_{k=-\infty}^{\infty} r_k^{u,v} e^{-jk\Omega} = c(u,v)\cdot\Lambda_t(\Omega), \quad (7.13)$$

where $\Lambda_t(\Omega) = \sum_{k=-\infty}^{\infty} J_0\left(2\pi f_{\text{D}}|k|T_p\right) e^{-jk\Omega}$ is the DTFT of the sequence $\{J_0\left(2\pi f_{\text{D}}|k|T_p\right)\}_k$.

Based on the result in [42], when $\delta \geq 2(2L\text{–}1) f_{\text{D}} T_s$, $\Lambda_t(\Omega)$ can be presented as [45]

$$\Lambda_t(\Omega) = \frac{2(\frac{\Omega}{2\beta})}{\sqrt{\beta^2 - \Omega^2}}, \quad -\pi \leq \Omega \leq \pi. \quad (7.14)$$

where $\beta = 2\pi f_{\text{D}} T_p$.

Let the DTFT of correlation matrix$\mathbf{R}_{pp}$ be written as [45],

$$\begin{aligned}\mathbf{\Lambda}(\Omega)=&\begin{bmatrix} R^{0,0}(\Omega) & R^{0,1}(\Omega) & \cdots & R^{0,L-1}(\Omega) \\ R^{1,0}(\Omega) & R^{1,1}(\Omega) & \cdots & R^{1,L-1}(\Omega) \\ \vdots & \vdots & \cdots & \vdots \\ R^{L-1,0}(\Omega) & R^{L-1,1}(\Omega) & \cdots & R^{L-1,L-1}(\Omega)) \end{bmatrix} \\ =&\mathbf{R}_{\tau}\cdot\Lambda_t(\Omega) \end{aligned} \tag{7.15}$$

where $R^{u,v}(\Omega)$ is given in (7.13).

Performing eigenvalue decomposition of $\mathbf{R}_{pp}$, the MSE in (7.12)as can be rewritten as

$$\begin{aligned}\sigma^2_{p,LN_p} &= \frac{1}{LN_p}\sum_{k=1}^{LN_p}\left[\lambda'_k-\left(\lambda'_k+\frac{\delta}{(2L-1)\alpha\gamma_0}\right)^{-1}\lambda_i'^2\right] \\ &= \frac{1}{LN_p}\sum_{k=1}^{LN_p}\left(\frac{\lambda'_k}{\lambda'_k(2L-1)\gamma_\alpha+1}\right), \end{aligned} \tag{7.16}$$

where $\gamma_\alpha=\frac{\alpha\gamma_0}{\delta},$ and λ'_k is the k-th eigenvalue of $\mathbf{R}_{pp}$.

According to [46, Theorem 3], when $N_p\to\infty$ (7.16) can be calculated as

$$\sigma_p^2=\frac{1}{2\pi L}\int_{-\pi}^{\pi}\sum_{i=0}^{L-1}\left[\frac{\lambda_i\Lambda_t(\Omega)}{\lambda_i\Lambda_t(\Omega)(2L-1)\gamma_\alpha+1}\right]d\Omega, \tag{7.17}$$

where $\lambda_i\Lambda_t(\Omega)$ is the i-th eigenvalue of the DTFT matrix defined in (7.15). Substituting (7.14) into (7.17) leads to,

$$\sigma_p^2=\frac{1}{2\pi L}\int_{-\beta}^{\beta}\sum_{i=0}^{L-1}\left[\frac{2\lambda_i}{2\lambda_i(2L-1)\gamma_\alpha+\sqrt{\beta^2-\Omega^2}}\right]d\Omega \tag{7.18}$$

It is worth mentioning that $\beta\le\pi$ when $\delta\ge 2(2L-1)f_{\text{D}}T_s$. Putting $\Omega=\beta\sin(x)$, the above integral can be simplified to the following integration as [45]

$$\int_{-\frac{\pi}{2}}^{\frac{\pi}{2}}\left[a+b\cos(x)\right]^{-1}dx=\frac{4\arctan\left(\sqrt{\frac{a-b}{a+b}}\right)}{\sqrt{a^2-b^2}}, \tag{7.19}$$

The last equation can be obtained by using equation (2.553.3) in [47] along with the identity $\arctan(jx)$ $= j(x)$ for $x \in \mathcal{R}$ and $j^2 = -1$. Employing (7.19) in (7.18) leads to equation (7.12) [45]. ■

7.3.2 MMSE Channel Estimations at Data Locations

The observed signals at pilot positions are used to obtain an estimate of channel coefficients at data symbols locations. Data symbols will be estimated in groups, therefore, before estimation data symbols with $N_s = KN_p$ elements are divided into K groups with N_p equally spaced data symbols in each group. Define the indices of the data symbols in the g-th group as $\{g_k = Mk+g, k = 0, \cdots, N_p - 1\}$, for $g = 1, \cdots, K$. Also, let the channel coefficients vector corresponding to the g-th data group be defined as $\mathbf{h}_g = [\mathbf{h}_{g_0}^T, \cdots, \mathbf{h}_{g_{(N_p-1)}}^T]^T \in \mathcal{C}^{LN_p \times 1}$, with $\mathbf{h}_{g_k} = [h(g_k, 0), \cdots, h(g_k+L-1, L-1)]^T \in \mathcal{C}^{L\times 1}$. The linear MMSE estimation of the channel coefficients at data locations can then be written as

$$\hat{\mathbf{h}}_g = \mathbf{W}_g^H \mathbf{y}_p, \tag{7.20}$$

where $\hat{\mathbf{h}}_g$ is the estimate of $\mathbf{h}_g$, and $\mathbf{W}_g^H$ is the MMSE estimation matrix, which can be calculated using the orthogonal principle, $\mathbb{E}[(\hat{\mathbf{h}}_g - \mathbf{h}_g)\mathbf{y}_p^H] = 0$, as

$$\mathbf{W}_g^H = \sqrt{E_p}\mathbf{R}_{gp}\mathbf{P}^H \left(E_p\mathbf{P}\mathbf{R}_{pp}\mathbf{P}^H + N_0\mathbf{I}_{LN_p}\right)^{-1}, \tag{7.21}$$

where $\mathbf{R}_{gp} = \mathbb{E}(\mathbf{h}_g\mathbf{h}_p^H) \in \mathcal{R}^{LN_p\times LN_p}$ is a block Toeplitz matrix, which can be found as [45]

$$\mathbf{R}_{gp} = \mathbf{R}_{gt} \otimes \mathbf{R}_\tau, \tag{7.22}$$

where $\mathbf{R}_{gt} \in \mathcal{R}^{N_p\times N_p}$ is a Toeplitz matrix.

The first row of $\mathbf{R}_{gt}$ is $[J_0(\omega_d|g'|), J_0(\omega_d|g' - M|), \cdots, J_0(\omega_d|g' - (N_p - 1)M|)]$, where $g' = g - (K + L - 1)$ and $\omega_d = 2\pi f_{\text{D}} T_s$. Also, the first column of the Toeplitz matrix $\mathbf{R}_{gt}$ can be identified as $[J_0(\omega_d|g'|), J_0(\omega_d|g' + M|), \cdots, J_0(\omega_d|g' + (N_p-1)M|)]^T$ [45].

Substitute (7.21) into (7.20) yields the estimate channel vector $\hat{\mathbf{h}}_g$ as

$$\hat{\mathbf{h}}_g = \sqrt{E_p}\mathbf{R}_{gp}\mathbf{P}^H \left(E_p\mathbf{P}\mathbf{R}_{pp}\mathbf{P}^H + N_0\mathbf{I}_{LN_p}\right)^{-1} \mathbf{y}_p. \tag{7.23}$$

The estimation error covariance matrix at data symbols positions, $\mathbf{\Psi}_{ee} \triangleq \mathbb{E}\left[(\hat{\mathbf{h}}_g - \mathbf{h}_g)(\hat{\mathbf{h}}_g - \mathbf{h}_g)^T\right]$, can then be calculated as

$$\mathbf{\Psi}_{ee}=\mathbf{R}_{pp}-\mathbf{R}_{gp}\left[\mathbf{R}_{pp} + \frac{1}{(2L-1)\gamma_\alpha}\mathbf{I}_{LN_p}\right]^{-1}\mathbf{R}_{gp}^H, \tag{7.24}$$

where $\gamma_\alpha = \frac{\alpha\gamma_0}{\delta}$, and $\mathbf{R}_{gg} = \mathbb{E}(\mathbf{h}_g\mathbf{h}_g^H) = \mathbf{R}_{pp}$ are used to obtain (7.24). The average MSE for channel estimation at data symbols locations is $\sigma^2_{e,LN_p} = \frac{1}{LN_p}\text{trace}\left(\mathbf{\Psi}_{ee}\right)$. The average MSE at data locations involves matrix inversion followed by trace operation, therefore, to clearly identify the effects of design parameters in the average MSE, we employ the asymptotic average MSE by letting $N_p \to \infty$ while keeping a finite channel length L, pilot percentage δ, energy allocation factor α, and symbols period T_s. The asymptotic average MSE for channel estimation at data symbols locations is given in the following proposition.

Proposition 7.2: When the number of pilot patterns approaches infinity, *i.e.*, $N_p \to \infty$ while maintaining finite values of α, L, δ, and T_s, if $\delta \geq \frac{(2L-1)w_d}{\pi}$, then channel estimations at data symbols locations through temporal interpolation results the same asymptotic MSE of channel estimations at pilot locations, i.e., $\sigma_e^2 = \lim_{N_p\to\infty}\sigma^2_{e,N_p} = \sigma_p^2$, with σ_p^2 defined in (7.12).

Proof: The proof is omitted here for brevity. ■

As a conclusion, if the number of the inserted pilot patterns is sufficient to sample the channel coefficients at a rate equal or greater than the Nyquist rate, *i.e.*, $\frac{1}{T_p} \geq 2f_{\text{D}}$, then the temporal interpolation will not degrade the performance of the MMSE estimator.

7.4 The Equivalent Optimum Receiver

This section presents the optimum diversity receiver with imperfect CSI, the theoretical error probability of systems employing the optimum diversity receiver is then derived.

7.4.1 Optimum Combining in the Presence of Imperfect CSI

In this subsection, we present the optimum receiver of a single user system in the presence of imperfect CSI, the statistical properties of the estimated channel coefficients will be employed to design the optimum diversity receiver.

Due to the special structure of pilot pattern, pilot symbols are observed at the receiver with ISI-free, while, data symbols are observed at the receiver with ISI. At the receiver, the observed signals of the g_k-th transmitted data symbol can be described by [28]

$$\mathbf{y}_{g_k} = \sqrt{E_s} \cdot [\mathbf{h}_{g_k} \cdot x_{g_k} + \check{\mathbf{H}}_{gk} \cdot \check{\mathbf{x}}_{g_k}] + \mathbf{z}_{g_k}, \tag{7.25}$$

where $g_k = Mk+g, k = 0, \cdots, N_p-1$,with $g = 1, \cdots, K$, $\mathbf{y}_{g_k} = [y(g_k), \cdots, y(g_k+L-1)]^T \in \mathcal{C}^{L\times 1}$ is the received samples vector, $\mathbf{h}_{g_k} = [h(g_k, 0), \cdots, h(g_k + L - 1, L - 1)]^T \in \mathcal{C}^{L\times 1}$ is the channel vector related to x_{g_k}, $\mathbf{z}_{g_k} = [z(g_k), \cdots, z(g_k+L-1)]^T \in \mathcal{C}^{L\times 1}$ is the noise vector, $\check{\mathbf{x}}_{g_k} = [x(g_k-L+1), \cdots, x(g_k-1), x(g_k+1), \cdots, x(g_k+L-1)]^T \in \mathcal{C}^{2(L-1)\times 1}$ is the interference vector associated with x_{g_k}, and $\check{\mathbf{H}}_{g_k} \in \mathcal{C}^{L\times 2(L-1)}$ is the corresponding interference channel matrix that can be defined as

$$\check{\mathbf{H}}_{g_k} = \begin{pmatrix} h(g_k, L-1) & \cdots & h(g_k, 1) & 0 & \cdots & 0 \\ 0 & h(g_k+1, L-1) & \cdots & h(g_k+1, 2) & h(1, L-1) & 0 \\ \vdots & \vdots & \vdots & \vdots & \vdots & \vdots \\ 0 & \cdots & 0 & h(g_k+L-1, L-2) & \cdots & h(g_k+L-1, 0) \end{pmatrix} \tag{7.26}$$

The interference components are minimized and can be neglected if MAP or MLSE equalization algorithms are employed in systems with long enough decoding length [28]. Based on the above discussion, the ISI-free input-output relation of the x_{g_k} can be represented as

$$\mathbf{y}_{g_k} = \sqrt{E_s} \cdot \mathbf{h}_{g_k} \cdot x_{g_k} + \mathbf{z}_{g_k}. \tag{7.27}$$

The system equation in (7.27) represents a single-input-multiple-output (SIMO) system in which a single data symbol x_{g_k} is transmitted over L mutually correlated flat fading channel, in other words, the transmission of x_{g_k} over a doubly selective fading channel of equivalent length L is identical to a transmission of the same symbol over mutually-correlated L parallel frequency flat fading channels.

If the channel experience a wide sense stationary uncorrelated scattering (WSSUS) frequency selective Rayleigh fading, then the channel vector $\mathbf{h}_{g_k}$ is zero mean complex Gaussian distributed with the covariance matrix $\mathbf{R}_h = \mathbb{E}[\mathbf{h}_{g_k}\mathbf{h}_{g_k}^H]$ given as [28]

$$\mathbf{R}_h = \begin{bmatrix} \rho(0;0,0) & \rho(1;0,1) & \cdots & \rho(L-1;0,L-1) \\ \rho(1;1,0) & \rho(0;1,1) & \cdots & \rho(L-2;1,L-1) \\ \vdots & \vdots & \cdots & \vdots \\ \rho(L–1;L–1,0) & \rho(L–2;L–1,1) & \cdots & \rho(0;L–1,L–1)) \end{bmatrix}, \tag{7.28}$$

Denote the estimate of $\mathbf{h}_{g_k} \in \mathcal{C}^{L\times 1}$ as $\hat{\mathbf{h}}_{g_k}$, then based on (7.23), $\hat{\mathbf{h}}_{g_k}$ can be obtained as

$$\hat{\mathbf{h}}_{g_k} = \sqrt{E_p}\mathbf{R}_{g_k p}\mathbf{P}^H \left(E_p \mathbf{P}\mathbf{R}_{pp}\mathbf{P}^H + N_0 \mathbf{I}_{LN_p}\right)^{-1} \mathbf{y}_p, \tag{7.29}$$

where $\mathbf{R}_{g_k p} = \mathbf{r}_{kt}^T \otimes \mathbf{R}_\tau \in \mathcal{C}^{L\times LN_p}$, with $\mathbf{r}_{kt}^T$ being the $(k+1)$-th row of matrix $\mathbf{R}_{gt}$.

At the receiver, the detection is performed based on the corrupted observed data symbols vector $\mathbf{y}_{g_k}$ and the estimated channel coefficients vector $\hat{\mathbf{h}}_{g_k}$. We have the following two lemmas about the statistical properties of the estimated CSI vector $\hat{\mathbf{h}}_{g_k}$, and the true vector ,$\hat{\mathbf{h}}_{g_k}$, conditioned on the estimated vector, *i.e* $\mathbf{h}_{g_k}|\hat{\mathbf{h}}_{g_k}$.

Lemma 7.1: For a system that experiences a WSSUS frequency selective Rayleigh fading, the estimated channel coefficients vector, $\hat{\mathbf{h}}_{g_k}$, is complex Gaussian distributed with zero mean and covariance $\hat{\mathbf{R}}_{g_k g_k} = \mathbf{R}_h - \mathbf{\Psi}_{ee}^{(k)}$, where $\mathbf{\Psi}_{ee}^{(k)} = E[(\hat{\mathbf{h}}_{g_k} - \mathbf{h}_{g_k})(\hat{\mathbf{h}}_{g_k} - \mathbf{h}_{g_k})^H] \in \mathcal{R}^{L\times L}$ is the autocorrelation of channel estimation error vector, $\mathbf{e}_{g_k} = \hat{\mathbf{h}}_{g_k} - \mathbf{h}_{g_k}$.

Proof: Since $\mathbf{h}_p$ and $\mathbf{z}_p$ in (7.6) are zero-mean complex Gaussian distributed, the observed pilot signals vector, $\mathbf{y}_p$, is also zero-mean complex Gaussian distributed with covariance matrix $\mathbb{E}\left[\mathbf{y}_p\mathbf{y}_p^H\right] = E_p\mathbf{P}\mathbf{R}_{pp}\mathbf{P}^H + N_0\mathbf{I}_{LN_p}$. The estimated channel coefficients vector $\hat{\mathbf{h}}_{g_k}$ is a linear transformation of $\mathbf{y}_p$ as illustrated in (7.29), accordingly, $\hat{\mathbf{h}}_{g_k}$ is zero mean complex Gaussian distributed with covariance $\hat{\mathbf{R}}_{g_kg_k} = \mathbf{R}_h - \mathbf{\Psi}_{ee}^{(k)}$. The matrix $\mathbf{\Psi}_{ee}^{(k)}$ can be obtained as $\mathbf{\Psi}_{ee}^{(k)} = \mathbf{\Gamma}_k\mathbf{\Psi}_{ee}\mathbf{\Gamma}_k^T \in \mathcal{C}^{L\times L}$ where $\mathbf{\Gamma}_k$ is a $L \times N_pL$ sampling matrix that is obtained by circularly shifting each row of $\mathbf{\Gamma} = \left[\mathbf{I}_L, \mathbf{0}_{L\times L(Np-1)}\right]$ by kL locations to the right. ■

Lemma 7.2: For the system that undergoes a WSSUS frequency selective Rayleigh fading, conditioned on the estimated channel coefficients vector, $\hat{\mathbf{h}}_{g_k}$, the actual channel coefficients vector $\mathbf{h}_{g_k}$ is complex Gaussian distributed with mean $\hat{\mathbf{h}}_{g_k}$ and covariance $\mathbf{\Psi}_{ee}^{(k)}$, *i.e.*, $\mathbf{h}_{g_k}|\hat{\mathbf{h}}_{g_k} \sim \mathcal{N}(\hat{\mathbf{h}}_{g_k}, \mathbf{\Psi}_{ee}^{(k)})$.

Proof: Since both $\hat{\mathbf{h}}_{g_k}$ and $\mathbf{h}_{g_k}$ are zero-mean Gaussian distributed, $\mathbf{e}_{g_k} = \hat{\mathbf{h}}_{g_k} - \mathbf{h}_{g_k}$ is also zero-mean Gaussian distributed. The cross-covariance matrix between $\mathbf{e}_{g_k}$ and $\hat{\mathbf{h}}_{g_k}$ is $\mathbb{E}(\mathbf{e}_{g_k}\hat{\mathbf{h}}_{g_k}^H) = 0$ by following the orthogonal principle. Therefore, $\mathbf{e}_{g_k}$ and $\hat{\mathbf{h}}_{g_k}$ are uncorrelated, the conditional mean can then be calculated as $\mathbf{u}_{\mathbf{h}_{g_k}|\hat{\mathbf{h}}_{g_k}} = \mathbb{E}(\mathbf{h}_{g_k}|\hat{\mathbf{h}}_{g_k}) = \hat{\mathbf{h}}_{g_k} - \mathbb{E}(\mathbf{e}_{g_k}|\hat{\mathbf{h}}_{g_k}) = \hat{\mathbf{h}}_{g_k}$. The covariance matrix is, $\mathbb{E}[(\mathbf{h}_{g_k} - \mathbf{u}_{\mathbf{h}_{g_k}|\hat{\mathbf{h}}_{g_k}})(\mathbf{h}_{g_k} - \mathbf{u}_{\mathbf{h}_{g_k}|\hat{\mathbf{h}}_{g_k}})^H] = \mathbb{E}[(\mathbf{h}_{g_k} - \hat{\mathbf{h}}_{g_k})(\mathbf{h}_{g_k} - \hat{\mathbf{h}}_{g_k})^H] = \mathbf{\Psi}_{ee}^{(k)}$. ■

To design the optimum receiver, we need to obtain the statistical properties of the observed samples vector $\mathbf{y}_{g_k}$. So let $x_m \in \mathcal{S}$ be the transmitted data symbol, then based on lemma 7.1 and lemma 7.2, the received samples vector $\mathbf{y}_{g_k}$ conditioned on the transmitted data symbol x_m and $\hat{\mathbf{h}}_{g_k}$ is complex Gaussian distributed, *i.e.*, $\mathbf{y}_{g_k}|(x_m, \hat{\mathbf{h}}_{g_k}) \sim \mathcal{N}(\mathbf{R}_{y_{g_k}|x_m,\hat{\mathbf{h}}_{g_k},\mathbf{u}_{y_{g_k}|x_m,\hat{\mathbf{h}}_{g_k}}})$, with the conditional mean matrix ,$\mathbf{u}_{y_{g_k}|(x_m,\hat{\mathbf{h}}_{g_k})}$, and conditional covariance matrix, $\mathbf{R}_{y_{g_k}|(x_m,\hat{\mathbf{h}}_{g_k})}$, given respectively as

$$\mathbf{u}_{y_{g_k}|(x_m,\hat{\mathbf{h}}_{g_k})} = \sqrt{E_s}\hat{\mathbf{h}}_{g_k}x_m \tag{7.30a}$$

$$\mathbf{R}_{y_{g_k}|(x_m,\hat{\mathbf{h}}_{g_k})} = E_s\mathbf{\Psi}_{ee}^{(k)} + N_0\mathbf{I}_L. \tag{7.30b}$$

Based on the statistical properties of $\mathbf{y}_{g_k}$ conditioned on the transmitted data symbol x_m and $\hat{\mathbf{h}}_{g_k}$, the decision rule of the optimum receiver with imperfect CSI is given in the following proposition.

Proposition 7.3: For the ISI-free SIMO system described in (7.27), if the transmitted symbols are equiprobable, then the optimum decision rule that minimize the system error probability is

$$\hat{x}_{g_k} = \underset{x_m \in S}{\text{argmin}} |\beta_{g_k} - x_m|^2, \tag{7.31}$$

where β_{g_k} is the decision variable and can be obtained as

$$\beta_{g_k} = \sqrt{E_s}\hat{\mathbf{h}}_{g_k}^H (\mathbf{\Psi}_{ee}^{(k)} + N_0 \mathrm{I}_L)^{-1} \mathbf{y}_{g_k}. \tag{7.32}$$

Proof: For the equiprobable transmitted data symbols the (pdf) function $p(\mathbf{y}_{g_k}|\hat{\mathbf{h}}_{g_k}, x_m)$ is

$$p(\mathbf{y}_{g_k}|\hat{\mathbf{h}}_{g_k}, x_m) = \frac{1}{\det(\pi \mathbf{R}_{y_{g_k}|(x_m, \hat{\mathbf{h}}_{g_k})})} \exp\left(\bar{\mathbf{y}}_{g_k}^H \mathbf{R}^{-1}_{y_{g_k}|(x_m, \hat{\mathbf{h}}_{g_k})} \bar{\mathbf{y}}_{g_k} \right), \tag{7.33}$$

where $\bar{\mathbf{y}}_{g_k} = \mathbf{y}_{g_k} - \mathbf{u}_{y_{g_k}|(x_m, \hat{\mathbf{h}}_{g_k})}$.

The error probability of the system can be minimized by maximizing the likelihood function, $p(\mathbf{y}_{g_k}|\hat{\mathbf{h}}_{g_k}, x_m)$, which is equivalent to minimize the cost function $C(x_m)$

$$C(x_m) = \bar{\mathbf{y}}_{g_k}^H \mathbf{R}^{-1}_{y_{g_k}|(x_m, \hat{\mathbf{h}}_{g_k})} \bar{\mathbf{y}}_{g_k}, \tag{7.34}$$

Thus, the optimum decision rule can be written as

$$\begin{aligned} \hat{x}_{g_k} &= \underset{x_m \in S}{\text{argmin}} \{C(x_m)\} \\ &= \underset{x_m \in S}{\text{argmin}} \{-2\Re(\beta_{g_k} \cdot x_m)\} \\ &= \underset{x_m \in S}{\text{argmin}} |\beta_{g_k} - x_m|^2, \end{aligned} \tag{7.35}$$

■

For systems with perfectly known CSI *i.e.*, $\hat{\mathbf{h}}_{g_k} = \mathbf{h}_{g_k}$, the decision variable in (7.32) is reduced to $\beta_{g_k} = \frac{\sqrt{E_s}}{N_0} \mathbf{h}_{g_k}^H \mathbf{y}_{g_k}$ since $\mathbf{\Psi}_{ee}^{(k)} = 0$, and the optimum receiver is reduced to a conventional MRC receiver.

7.4.2 Error Performance Analysis

The symbol error rate (SER) performance of system employing the optimum diversity receiver with an imperfect CSI is derived in this subsection. The obtained analytical results reflect the impacts of mobility on the system performance and quantify the effect of design parameters δ, and α on the acquired analytical SER.

The conditional error probability $P_{g_k}(E|\hat{\mathbf{h}}_{g_k}, x_m)$ is first derive, which is then used to obtain the unconditional error probability $P_{g_k}(E)$ of the optimum diversity receiver with imperfect CSI.

The received vector $\mathbf{y}_{g_k}$ conditioned on $\hat{\mathbf{h}}_{g_k}$ and x_m is zero-mean Gaussian distributed, thus, the decision variable β_{g_k}, which is conditioned on $\hat{\mathbf{h}}_{g_k}$ is also Gaussian distributed *i.e.*, $\beta_{g_k}|(x_m, \hat{\mathbf{h}}_{g_k}) \sim \mathcal{N}(\sigma^2_{\beta_{g_k}|x_m,\hat{\mathbf{h}}_{g_k}}, u_{\beta_k|x_m,\hat{\mathbf{h}}_{g_k}})$ with mean and variance given respectively as

$$u_{\beta_{g_k}|x_m,\hat{\mathbf{h}}_{g_k}} = ||d_{g_k}||^2 x_m, \tag{7.36a}$$

$$\sigma^2_{\beta_{g_k}|x_m,\hat{\mathbf{h}}_{g_k}} = ||d_{g_k}||^2, \tag{7.36b}$$

where $||d_{g_k}||^2 = \hat{\mathbf{h}}^H_{g_k}\left(\mathbf{\Psi}^{(k)}_{ee} + \frac{1}{\gamma_s}\mathbf{I}_L\right)^{-1}\hat{\mathbf{h}}_{g_k}$, and $\gamma_s = \frac{E_s}{N_0}$ is the SNR of the transmitted data symbol. The conditional probability density function (pdf) of β_{g_k} is given by

$$p(\beta_{g_k}, \theta|\hat{\mathbf{h}}_{g_k}, x_m) = \frac{1}{\pi\sigma^2_{\beta_{g_k}|x_m,\hat{\mathbf{h}}_{g_k}}}\exp\left(\frac{|-\beta_{g_k} - u_{\beta_{g_k}|x_m,\hat{\mathbf{h}}_{g_k}}|^2}{\sigma^2_{\beta_{g_k}|x_m,\hat{\mathbf{h}}_{g_k}}}\right) \tag{7.37}$$

To simplify derivations, we represent the pdf of the decision variable β_{g_k} in a polar coordinate system with the origin located at $u_{\beta_{g_k}|x_m,\hat{\mathbf{h}}_{g_k}}$ as shown in 7.1, in this case, the pdf of β_{g_k} is represented as

$$p(r, \theta|\hat{\mathbf{h}}_{g_k}, x_m) = \frac{r}{\pi\sigma^2_{\beta_k|x_m,\hat{\mathbf{h}}_{g_k}}}\exp\left(-\frac{r^2}{\sigma^2_{\beta_{g_k}|x_m,\hat{\mathbf{h}}_{g_k}}}\right), \tag{7.38}$$

where $\beta_{g_k} = r\mathrm{e}^{j\theta}$. Based on the above decision rule, the probability of having an error is equivalent to the probability of having β_{g_k} outside the decision region. For a wireless communication system with

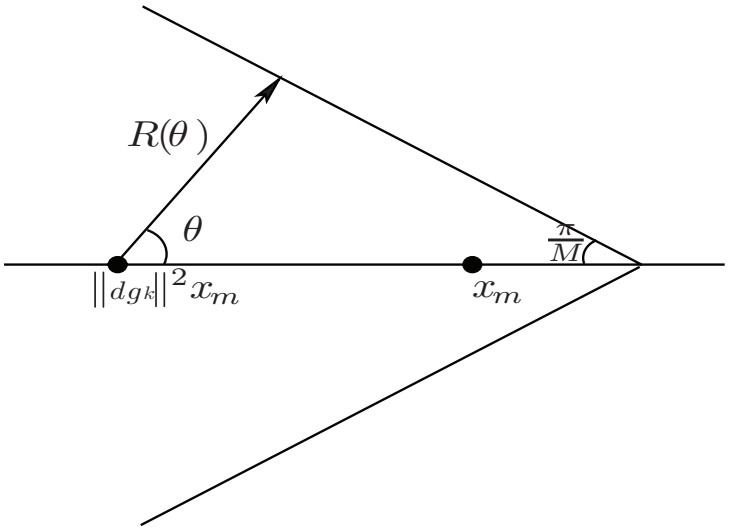

Figure 7.1: The decision region for M-ary PSK (MPSK) modulation

M-ary phase shift keying (MPSK) modulation, the decision region is shown in Fig. 7.1. The detection region of β_k is the $\frac{2\pi}{M}$ angle sector centered around the symbol x_m. Using the polar coordinate system in (7.38) along with Fig. 7.1, the conditional error probability can be obtained as

$$\begin{aligned} P_{g_k}(E|\hat{\mathbf{h}}_{g_k}) =& 2\sum_{1}^{M} P(x_m) \int_0^{\pi-\frac{\pi}{M}} \int_{R(\theta)}^{\infty} p(r,\theta|\hat{\mathbf{h}}_{g_k}, x_m) dr d\theta \\ =& \frac{1}{\pi} \int_0^{\pi-\frac{\pi}{M}} p(r,\theta|\hat{\mathbf{h}}_{g_k}, x_m) dr d\theta \\ =& \frac{1}{\pi} \int^{\pi-\frac{\pi}{M}} \exp\left[-\hat{\mathbf{h}}_{g_k}^H \boldsymbol{\Upsilon}_k \hat{\mathbf{h}}_{g_k} \frac{\sin^2(\frac{\pi}{M})}{\sin^2(\phi)}\right] d\phi, \end{aligned} \tag{7.39}$$

where M is the modulation level, $\boldsymbol{\Upsilon}_k = (\boldsymbol{\Psi}_{ee}^{(k)} + \frac{1}{\gamma_s}\mathbf{I}_L)^{-1}$,

$R(\theta) = \frac{\sin^2(\pi/M)}{\sin^2(\theta)} \left| \hat{\mathbf{h}}_{g_k}^H \left(\boldsymbol{\Psi}_{ee}^{(k)} + \frac{1}{\gamma_s}\mathbf{I}_L \right)^{-1} \hat{\mathbf{h}}_{g_k} x_m \right|$, and $P(x_m) = \frac{1}{M}$ for equiprobable transmitted MPSK symbols. The final result in (7.39) can be obtained by replacing the integration variable with $\phi = \pi - (\theta + \frac{\pi}{M})$.

The unconditional error probability $P_{g_k}(E)$ of a system with MPSK modulation can be computed based on the conditional error probability derived in (7.39). In order to evaluate the impacts of imperfect CSI, we derive the unconditional error probability of the system with MPSK modulation by employing the statistical properties of the estimated channel vector $\hat{\mathbf{h}}_{g_k}$. The quantity $\eta_{g_k} = \hat{\mathbf{h}}_{g_k}^H \boldsymbol{\Upsilon}_k \hat{\mathbf{h}}_{g_k}$

in (7.39) reflects the dependency of the conditional error probability on the estimated CSI. The vector $\hat{\mathbf{h}}_{g_k}$ is zero-mean Gaussian distributed with covariance matrix $\hat{\mathbf{R}}_{g_k g_k} = \mathbf{R}_h - \mathbf{\Psi}_{ee}^{(k)}$, hence, the quantity η_{g_k} is a quadratic form of complex Gaussian random vector. The moment generating function (MGF) of η_{g_k} is [43]

$$\begin{aligned}\Psi_{\eta_{g_k}}(t) =& (e^{t\eta_{g_k}}) \\ &= \left[\det\left(\mathbf{I}_L - t\cdot\hat{\mathbf{R}}_{g_k g_k}\mathbf{\Upsilon}_k\right)\right]^{-1},\end{aligned} \tag{7.40}$$

With (7.40) the unconditional SER, $P_{g_k}(E)$ can then be computed as

$$\begin{aligned}P_{g_k}(E) &= \frac{1}{\pi}\int^{\pi-\frac{\pi}{M}}\left[\det\left(\mathbf{I}_L + \frac{\sin^2(\frac{\pi}{M})}{\sin^2(\phi)}\hat{\mathbf{R}}_{g_k g_k}\mathbf{\Upsilon}_k\right)\right]^{-1}d\phi, \\ &= \frac{1}{\pi}\int^{\pi-\frac{\pi}{M}}\left[\det\left(\mathbf{I}_L + \frac{\sin^2(\frac{\pi}{M})}{\sin^2(\phi)}\bar{\mathbf{R}}_{g_k}\right)\right]^{-1}d\phi,\end{aligned} \tag{7.41}$$

where the matrix $\bar{\mathbf{R}}_{g_k} = \mathbf{\Upsilon}_k^{\frac{1}{2}}\hat{\mathbf{R}}_{g_k g_k}(\mathbf{\Upsilon}_k^{\frac{1}{2}})^H$ with $\mathbf{\Upsilon}_k^{\frac{1}{2}}$ being the square root of the matrix $\mathbf{\Upsilon}_k$ that meets the condition $\mathbf{\Upsilon}_k = (\mathbf{\Upsilon}_k^{\frac{1}{2}})^H(\mathbf{\Upsilon}_k^{\frac{1}{2}})$, and the identity $\det(\mathbf{I}+\mathbf{AB}) = \det(\mathbf{I}+\mathbf{BA})$ is used to obtain (7.41). Perform eigenvalue decomposition of the product matrix $\bar{\mathbf{R}}_{g_k} = \mathbf{\Upsilon}_k^{\frac{1}{2}}\hat{\mathbf{R}}_{g_k g_k}(\mathbf{\Upsilon}_k^{\frac{1}{2}})^H$ we get

$$\bar{\mathbf{R}}_{g_k} = \mathbf{V}_k\mathbf{\Lambda}_k\mathbf{V}_k^H \in \mathcal{C}^{L\times L}, \tag{7.42}$$

where $\mathbf{\Lambda}_k = \text{diag}[\lambda_{k_1}, \cdots, \lambda_{k_L}] \in \mathcal{C}^{\bar{L}\times\bar{L}}$ is a diagonal matrix with the diagonal elements being the non-zero eigenvalues of $\bar{\mathbf{R}}_{g_k}$ in a decreasing order with $\bar{L}$ being the number of non-zero eigenvalues, and the matrix $\mathbf{V}_k \in \mathcal{C}^{L\times\bar{L}}$ contains the corresponding eigenvectors. With (7.42), the unconditional SER, $P_{g_k}(E)$ can then be simplified to

$$P_{g_k}(E) = \frac{1}{\pi}\int^{\pi-\frac{\pi}{M}}\prod_{l=1}^{\bar{L}}\left[1 + \frac{\lambda_{k_l}\sin^2(\frac{\pi}{M})}{\sin^2(\phi)}\right]^{-1}d\phi, \tag{7.43}$$

When the power delay profile is the T_s-spaced equal gain profile, *i.e.*, $G(\tau) = \sum_{l=0}^{L-1}\frac{1}{L}\delta(\tau - lT_s)$

we can use the approximation $\mathbf{\Psi}_{ee}^{(k)} \approx \sigma_e^2 \mathbf{I}_L$, where $\sigma_e^2 = \frac{1}{LN_p}\text{trace}\left(\mathbf{\Psi}_{ee}\right)$. Employing the aforementioned approximation the MGF, $\Psi_{\eta_{g_k}}(t)$, can be written as

$$\begin{aligned}\Psi_{\eta_{g_k}}(t) &= \left[\det\left(\mathbf{I}_L - t\cdot\left(\mathbf{R}_h - \mathbf{\Psi}_{ee}^{(k)}\right)\left(\mathbf{\Psi}_{ee}^{(k)} + \frac{1}{\gamma_s}\mathbf{I}_L\right)^{-1}\right)\right]^{-1} \\ &\approx \left[\det\left(\mathbf{I}_L - t\cdot\left(\mathbf{R}_h - \sigma_e^2\mathbf{I}_L\right)\left(\sigma_e^2\mathbf{I}_L + \frac{1}{\gamma_s}\mathbf{I}_L\right)^{-1}\right)\right]^{-1} \end{aligned} \tag{7.44}$$

The MGF in (7.44) can then be simplified as

$$\Psi_{\eta_{g_k}}(t) = \prod_{l=1}^{\tilde{L}}\left[1 - t\cdot\frac{d_l - \sigma_e^2}{\sigma_e^2 + \frac{1}{\gamma_s}}\right]^{-1}, \tag{7.45}$$

where $\tilde{L}$ is the number of non-zero eigenvalues of $\mathbf{R}_h$, and d_l is a non-zero eigenvalues of $\mathbf{R}_h$. The SER of systems with MPSK modulations and equal gain profile is then expressed as

$$\tilde{P}_{g_k}(E) = \frac{1}{\pi}\int^{\pi-\frac{\pi}{M}}\prod_{l=1}^{\tilde{L}}\left[1 + \frac{\sin^2(\frac{\pi}{M})}{\sin^2(\theta)}\frac{d_l - \sigma_e^2}{\sigma_e^2 + \frac{1}{\gamma_s}}\right]^{-1} d\theta. \tag{7.46}$$

Next simulation results are presented.

7.5 Simulation Results

In this section, we present numerical and simulation results to investigate the impacts of system design parameters such as, the pilot percentage, the normalized Doppler spread and the energy allocation factor on the average MSE. The bit error rate (BER) performance of a binary phase-shift keying (BPSK) modulated wireless communication system under imperfect CSI is also presented. In simulations, $T_s = 3.69\mu s$, and a typical urban (TU) power delay profile is employed to model the frequency-selective Rayleigh fading channel. Also, a root-raised cosine (RRC) filter with 100% excessive bandwidth is used as transmit and receive filters. The Maximum-Likelihood Sequence Estimation (MLSE) Viterbi equalizer is employed at the receiver.

In Fig. 7.2, the average MSE is plotted as a function of the energy allocation factor, α, for systems with different values of slot length, N. The pilot percentage is set as $\delta = 0.2$, the normalized Doppler

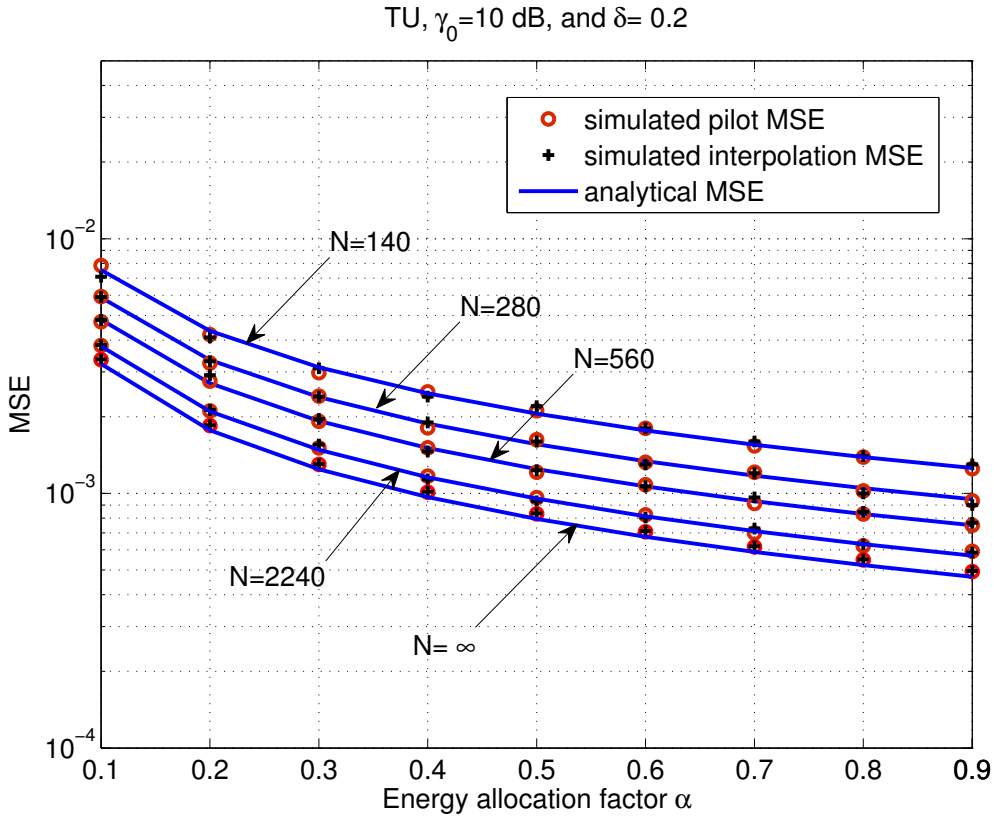

Figure 7.2: The average MSE as a function of energy allocation factor, α, for variable slot length, N. Pilot percentage is $\delta = 0.2$, and $\gamma_0 = 10$ dB.

spread is $f_{\text{D}}T_s = 0.003$, and the average SNR is $\gamma_0 = 10$ dB. The slot length is set as $N = 15400$ to represent the infinity slot length. Three observations can be made about Fig. 7.2. First, the simulated average MSE at pilot locations is the same as the simulated average MSE at data symbols locations, which means that the interpolation does not degrade the channel estimator performance. Second, excellent agreements between simulation and analytical results are observed. Third, the average MSE is a decreasing function in both the slot length N and the energy allocation factor, α, because the energy allocated to pilot symbols and the number of pilot symbols increases linearly with α and N, respectively.

In Fig. 7.3, the average asymptotic MSE is plotted as a function of the energy allocation factor, α, for systems with different values of normalized Doppler spread, $f_{\text{D}}T_s$. The pilot percentage is set

as $\delta = 0.25$, the average SNR $\gamma_0 = 10$ dB, and the slot length is set as $N = 15400$. The figure

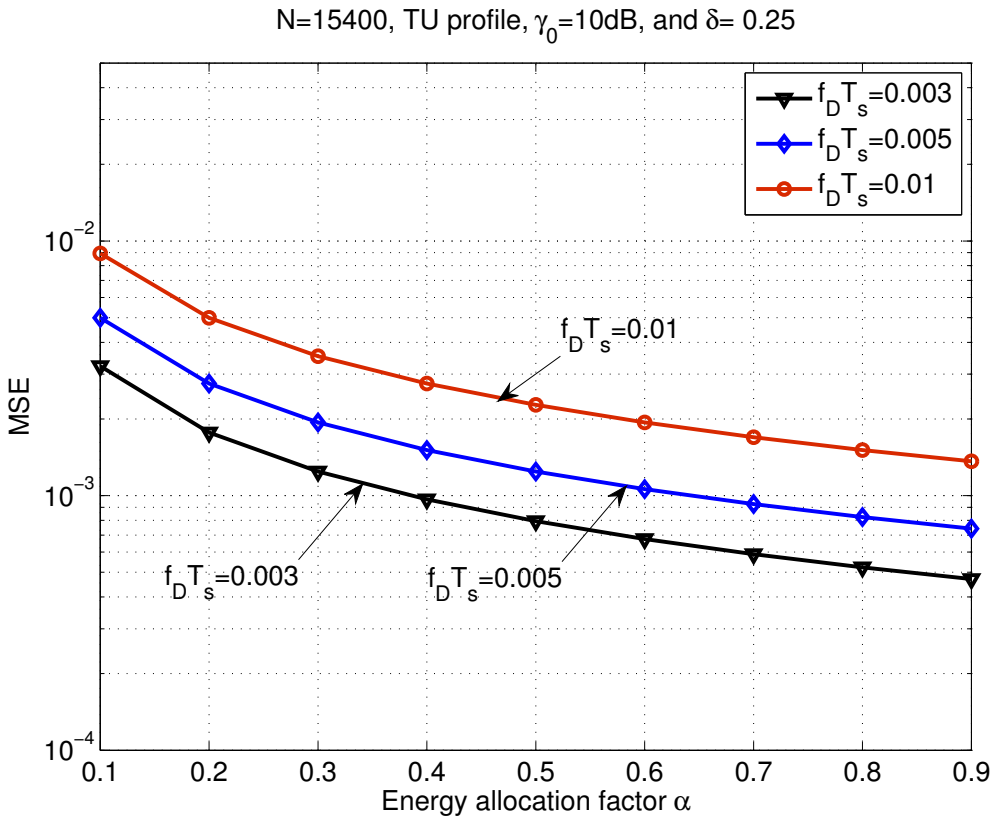

Figure 7.3: The average asymptotic MSE as a function of the energy allocation factor α with various normalized Doppler spread $f_{\text{D}}T_s$.

shows that the average MSE is an increasing function in the normalized Doppler spread, $f_{\text{D}}T_s$. On the other hand, it is a decreasing function in the energy allocation factor, α. At large normalized Doppler spread, $f_{\text{D}}T_s$, the estimation process encounters more errors, because at large Doppler spread values, the channel experiences fast time-variations. Furthermore, the average MSE decreases as the energy allocation factor, α, increases due to the increase of the energy allocated to each transmitted pilot symbol. Thus, the MSE is a monotonically decreasing function in energy allocation factor, α.

Fig. 7.4 shows a plot of the average MSE as a function of the energy allocation factor, α, under different values of SNR, γ_0. The pilot percentage is set as $\delta = 0.2$, the normalized Doppler spread, $f_{\text{D}}T = 0.005$, and the slot length $N = 280$. As expected the average MSE is improved as the SNR

rises due to the increase in the energy allocated to each transmitted pilot symbol. As a result, the MSE is a monotonically decreasing function in SNR.

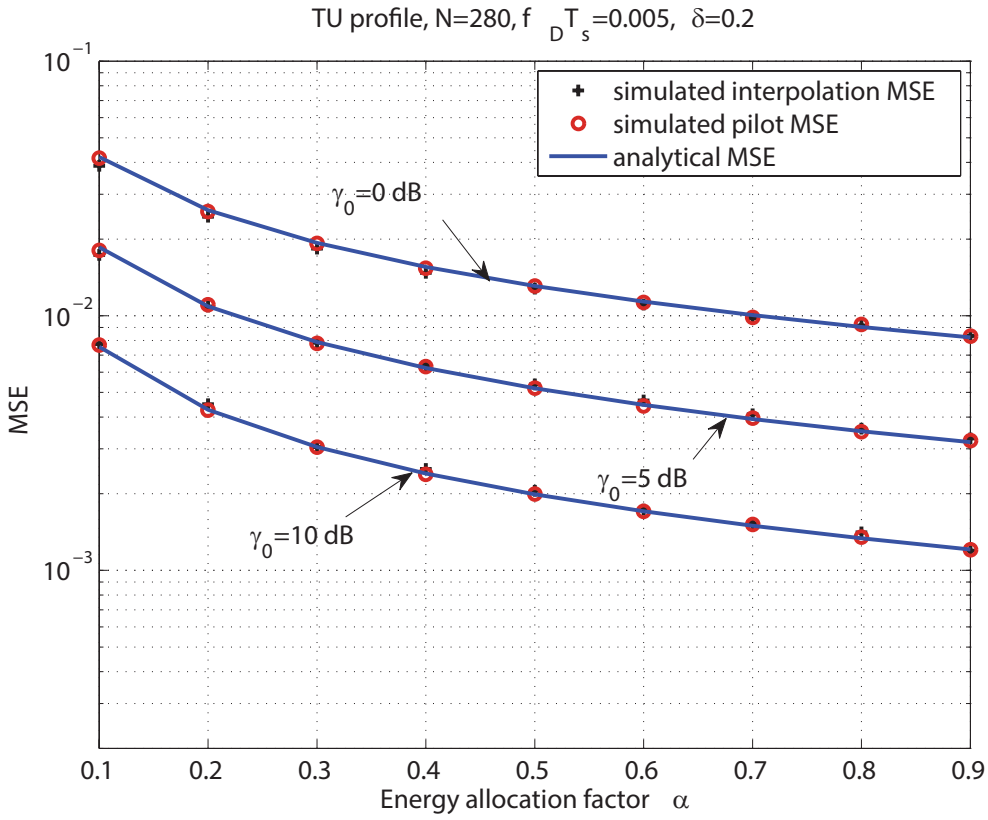

Figure 7.4: The average MSE as a function of the energy allocation factor α for systems with different values of SNR, γ_0.

In Fig. 7.5, we plot the BER performance of the BPSK system under different values of the energy allocation factor, α. The pilot percentage is set as $\delta = 0.2$, the slot length is $N = 140$, and the normalized Doppler spread is $f_{\text{D}}T_s = 0.01$. Two observations can be made from the figure: First, the error performance improves with the γ_0 increase due to the increase of allocated energy to both pilot and data symbols. Second, the error performance reaches its minimum at a specific energy allocation factor, α, value. Increasing the energy allocation factor above that value leads to performance degradation, because increasing the energy allocation factor, α, above that value increases the energy

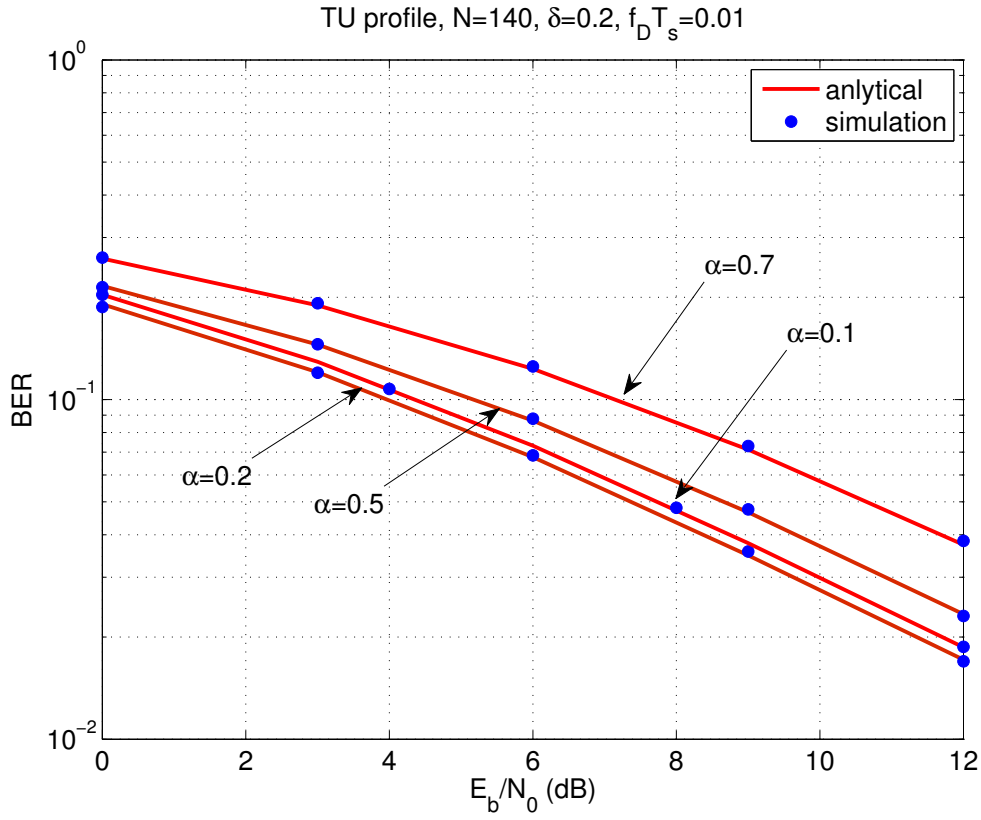

Figure 7.5: The BER of systems with BPSK modulation and different values of energy allocation factor.

allocated to pilot symbols and decreases the energy allocated to data symbols leading to performance degradation. Thus, there is a certain energy allocation factor, α, value that results an improvement in CSI estimation without sacrificing the system error performance. The BER has the minimum value at $\alpha = 0.2$, however, the BER becomes gradually worse as α takes values 0.1, 0.5, and 0.7, respectively.

Fig. 7.6 shows the BER performance of systems with BPSK modulations and different values of γ_0. As shown in Fig. 7.6, the BER improves as γ_0 increases, because the energy per data symbol increases linearly with γ_0 leading to BER improvement. Furthermore, $\alpha = 0.2$ is the energy allocation value where the system can have small estimation errors without scarifying the BER performance. The figure shows that the BER performance is a quasi-convex in energy allocation factor

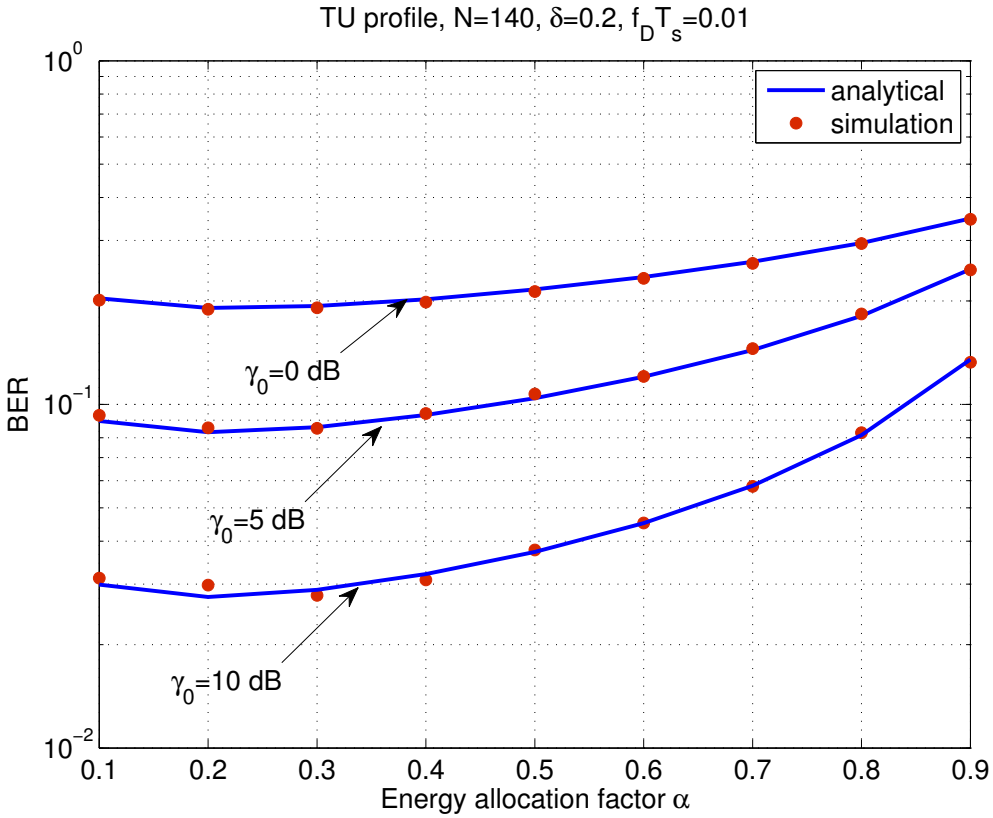

Figure 7.6: The BER performance of the BPSK modulated system as a function of the energy allocation factor for systems with different values of SNR.

Finally, in Fig. 7.7, the BER performance versus the energy allocation factor, α, is plotted for systems with $f_{\text{D}}T_s = 0.005$, and $f_{\text{D}}T_s = 0.01$. The slot length is set as $N = 140$, and the pilot percentage is selected as $\delta = 0.2$. It is apparent from the figure that the system with largest $f_{\text{D}}T_s$ has the worst BER performance, because at higher Doppler spread, f_{D}, the estimation process encounters more errors due to fast channel time-variations, estimation errors result BER degradation.

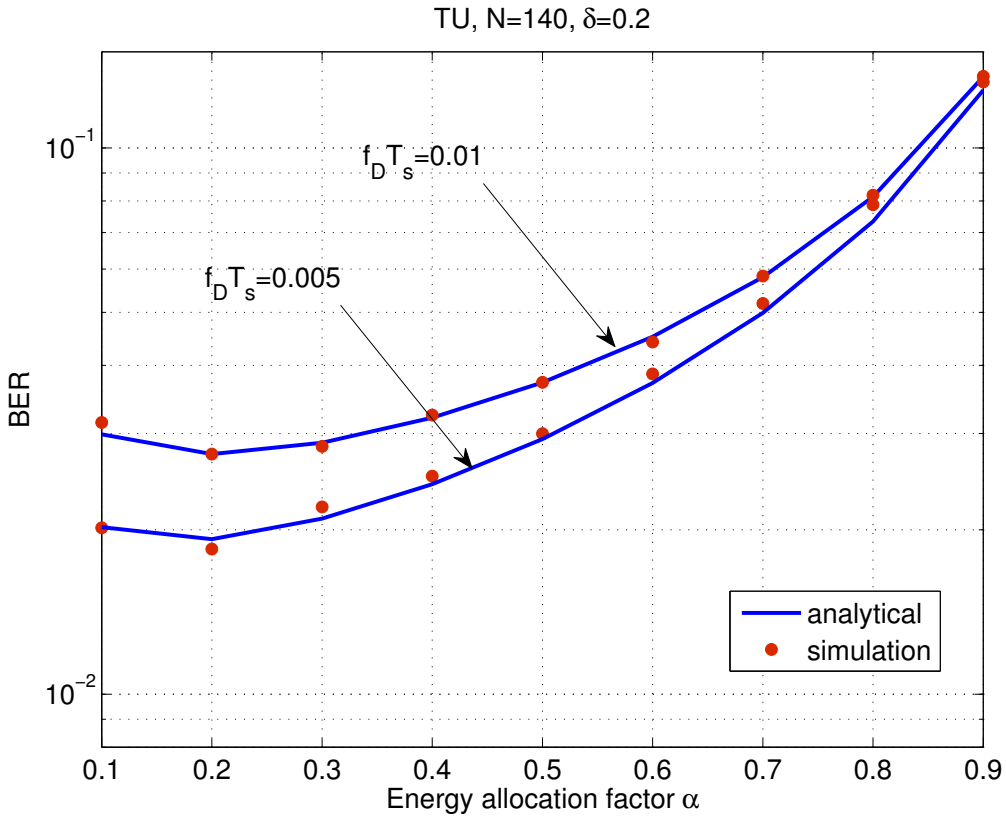

Figure 7.7: The BER of BPSK modulated system as a function of energy allocation factor α for systems with $f_{\text{D}}T_s = 0.01$ and $f_{\text{D}}T_s = 0.005$.

7.6 Conclusions

In this chapter, we investigated the impacts of different design parameters such as, the pilot percentage δ, the normalized Doppler spread $f_{\text{D}}T_s$, and the energy allocation factor α on both the average MSE of the MMSE estimator and on the error performance of high mobility wireless systems. We found that the error performance of a linearly modulated system is a quasi-convex in energy allocation factor α and monotonically decreasing in terms of γ_0. Furthermore, the MSE is a monotonically decreasing in both γ_0 and the energy allocation factor α. Consequently, a trade-off between the average MSE and the error performance should be considered when selecting the energy allocation factor α.

Chapter 8

Conclusions

In this chapter, we summarize the main contributions of this dissertation, also we list outlines for future works that might enrich the work done in this dissertation and lead to new discoveries and research achievements.

8.1 Contributions

Throughout this dissertation, we presented multiple access interference (MAI) reduction techniques for multi-user multiple access wireless systems. Also, we derived lower bounds for linearly modulated systems employing different MAI reduction techniques. The statistical properties of the discrete-time system model for systems employing various MAI reduction techniques were given, and based on these properties we designed optimum and sub-optimum receivers for these systems. All presented multi-user systems were investigated under various system configurations. The main contributions of this dissertation can be listed in the following aspects.

In this dissertation, we first employed the MAI-reduction technique proposed in [6] along with the time-domain oversampling at the receiver side to improve the performance of the MC-CDMA system in the uplink direction. Theoretical analysis and simulation results were given for the over-sampled MC-CDMA system. Results showed that the performance of the MC-CDMA system with oversampling outperforms the equivalent system without oversampling. Furthermore, performance fluctuations due to the timing offset induced by mismatching between transmitter and receiver sampler clocks were avoided by using the time-domain oversampling. Both systems with and without oversampling can support the same number of users.

Second, based on an appropriate code selection technique MAI-free MC-CDMA system was presented in [8] for the uplink direction. In this dissertation, we extended the system in [8] by introducing the time-domain oversampling at the receiver side. For TU PDP, the performance of the system with oversampling was much better than the equivalent system without oversampling. A significant enhancement in multipath diversity was observed for system with oversampling. Moreover, the impacts of time synchronization between transmitter and receiver clocks on the system performance were eliminated by using the time-domain oversampling.

Third, we proposed a circular-shift division multiple access (CSDMA) MAI reduction scheme for multi-user wireless networks. The proposed scheme can be employed in uplink-wireless systems, such as cellular systems, satellite systems, or wireless sensor networks. In the CSDMA scheme, each modulated symbol is spread over multiple sub-carriers; then, the obtained time-domain signals are circularly shifted by different number of locations at different users before transmitting over frequency selective fading and noise. The time-domain circular shifting operations at the transmitter allow the receiver to observe signals from all users without MAI or with small MAI depending on the number of users. Furthermore, the number of interfering sources in the CSDMA scheme was upper bounded by the channel length, while in most existing multi-carrier multi-user systems the number of interfering sources is proportional with the number of users. In addition, using the SISO-BDFE receiver, the performance of system with MAI was slightly worse than MAI-free one. The proposed CSDMA scheme achieved the same spectral efficiency as the OFDMA system, but with a much better energy efficiency performance due to the multipath diversity gains.

Fourth, we performed comparisons between the CSDMA system and various multi-carrier multi-user systems under same conditions and systems configurations. Computer simulations and analytical results showed that the performance of CSDMA with oversampling outperforms OFDMA,

MC-CDMA, and OFDM-IDMA systems.

Finally, impacts of imperfect CSI on the performance of high mobility wireless communication systems with doubly-selective fading channels was studied. Furthermore, we investigated the influence of design parameters, such as the energy allocation factor, pilot percentage and Doppler spread on both the mean squared error (MSE) of the MMSE channel estimator and on the error probability of a linearly modulated system. Expressions that quantify the effect of energy allocation factor, pilot percentage and Doppler spread on the system performance were derived.

8.2 Future Works

Inspired by theoretical and simulation results obtained so far in this dissertation we now present some outlines for future research that might add to this dissertation to accomplish considerable research achievements and discoveries in multi-user multiple access wireless systems.

First, the MAI-free CSDMA system can be investigated under high mobility conditions, where channels experience fast-time variations. Channel estimations error will play a critical role in CSDMA system performance. Indeed, optimum receiver for CSDMA can be developed in the presence of channel estimation errors.

Second, channel estimation for CSDMA system with MAI and under high mobility conditions can be considered for future work.

Third, The effect of carrier phase offset (CPO) on both the error performance and on the MAI of the CSDMA system can be inspected as apart of a future works. Finally, we proposed the CSDMA system in the uplink direction, therefore, investigate the CSDMA system in the downlink direction can enrich the research conducted in this dissertation.

Bibliography

[1] J.A.C. Bingham. "Multicarrier Modulation for Data Transmission: An Idea Whose Time Has Come." *IEEE Commun. Mag.*, pp. 514,May 1990.

[2] Y. Nathan, J. M. Linnartz and G. Fettweis, "Multi-carrier CDMA in indoor wireless radio networks," *Proc. PIMRC,* 1993.

[3] S. Hara and R. Prasad, "Overview of multicarrier CDMA," *IEEE Commun. Mag.*, vol. 35, pp. 126-133, 1997.

[4] S. Verdu, "Multiuser Detection. Cambridge," U.K.: Cambridge Univ. Press, 1998.

[5] Z. Li and M. Latva-Aho, "Analysis of MRC receivers for asynchronous MC-CDMA with channel estimation errors,"in *Proc. IEEE Intern. Symp. Spread Spectrum Techniques and Applications*, pp. 343-347, 2002.

[6] S. Tsai, Y. Lin and C. Kuo, "A repetitively coded multicarrier CDMA (RCMC-CDMA) transceiver for multiuser communications," in *Proc. IEEE Wireless Commun. Network. Conf. WCNC'04*, pp. 959-964, 2004.

[7] S. Tsai , Y. Lin and C. J. Kuo, "Performance evaluation of approximately MAI-free multiaccess OFDM transceiver", *Proc. IEEE 60th Veh. Technol. Conf.*, vol. 1, pp.588 -592 2004.

[8] S. Tsai, Y. Lin and C. Kuo, "MAI-free MC-CDMA systems based on HadamardWalsh codes," *IEEE Trans. Sig. Processing*, vol. 54, pp. 3166-3179, 2006.

[9] L. Tadjpour, S. Tsai and C.J. Kuo, "Orthogonal codes for MAI-free MC-CDMA with carrier frequency offsets (CFO)," *Proc. IEEE Globecom Conf.*, 2006.

[10] L. Sanguinetti, L. Taponecco and M. Morelli, "Interference-free code design for MC-CDMA uplink transmissions," *IEEE Trans. Wireless Commun.*, vol. 8, pp. 5461-5465, 2009.

[11] J. Wu and Y. R. Zheng, "Oversampled orthogonal frequency division multiplexing in doubly selective fading channels", *IEEE Trans. Commun.*, vol. 59, pp. 815 -822, 2011.

[12] J. Wu and Y. R. Zheng, "Low complexity soft-input soft-output block decision feedback equalization," *IEEE J. Selected Areas Commun.*, vol. 26, pp. 281-289, 2008.

[13] S. Q. Lee, N. Park, C. Cho, H. Lee, and S. Ryu, "The wireless broadband (wibro) system for broadband wireless internet services," *IEEE Trans. Commun. Mag.*, vol. 44, no. 7, pp. 106-112, Jul. 2006.

[14] A. Chouly, A. Brajal and S. Jourdan, "Orthogonal multicarrier techniques applied to direct sequence spreading spectrum CDMA systems," *IEEE Globecom Conf.*, 1993.

[15] S. Kondo and B. Milstein, "Performance of multicarrier DS CDMA systems," *IEICE Trans. Commun.*, vol. 44, pp. 238-246, 1996.

[16] C. Xiao, J. Wu, S.-Y. Leong, Y. R. Zheng, and K. B. Letaief, "A discrete-time model for spatio-temporally correlated mimo wssus multipath channels," *Proc. IEEE Wireless Comm. and Networking Conf.*, vol. 1, pp.354-358, 2003.

[17] J. Wu, Y.R. Zheng, K.B. Letaief and C. Xiao, "On the error performance of wireless systems with frequency selective fading and receiver timing phase offset," *IEEE Trans. Wireless Commun.*, vol. 6, pp. 720-729, 2007.

[18] M. K. Simon and M. Alouini, Digital Communication Over Fading Channels. Wiley-IEEE Press, 2004.

[19] J. Wu and C. Xiao, "Performance analysis of wireless systems with doubly selective Rayleigh fading," *IEEE Trans. Veh. Technol.*, vol. 56, pp. 721-730, Mar. 2007.

[20] B. M. Masini, "The impact of combined equalization on the performance of MC-CDMA systems," *J. Commun.*, vol. 3, pp. 31-39, 2008.

[21] S. Siwamogsatham, M. P. Fitz, and J. H. Grimm, "A new view of performance analysis of transmit diversity schemes in correlated fading," *IEEE Trans. Inf. Theory*, vol. 48, no. 4, pp. 950956, Apr. 2002.

[22] Z. Li and M. Latva-aho, "Simple analysis of MRC receivers for MC-CDMA systems in fading channels,"in *International Conferences on Info-Tech & Info-Net (ICII)*, October 2001.

[23] S. Kaiser, "On the performance of different detection techniques for OFDM-CDMA in fading channels," *IEEE Globecom Conf.*, pp. 2059-2063. 1995

[24] Z. Wu, X. Zhang and X. Xie, "Combining techniques for MC-CDMA,"in *IEEE Signals, Systems and Computers, 2004. Conference Record of the Thirty-Seventh Asilomar Conference on*, vol. 1, pp. 480-484, 2003.

[25] A. Shah and A. Haimovich, "Performance analysis of maximal ratio combining and comparison with optimum combining for mobile radio communications with cochannel interference," in *IEEE Trans. Veh. Technol.*, vol. 49, pp. 1454-1463, 2000.

[26] Q. Shi, Y. Guan, Y. Gong and C. Law, "Receiver design for multicarrier CDMA using frequency-domain oversampling," *IEEE Trans Wireless Commun.*, vol. 8, pp. 2236-2241, 2009.

[27] K. Zhang, Y. L. Guan and Q. Shi, "Complexity reduction for MC-CDMA with MMSEC," in *IEEE Trans. Veh. Technol.*, vol. 57, pp. 1989-1993, 2008.

[28] J. Wu and C. Xiao, "On the error performance of linearly modulated systems with doubly selective Rayleigh fading channels," in *Proc. IEEE Global Telecommun. Conf. GLOBECOM04*, vol.1, pp.308-312, Dec. 2004.

[29] U. Tureli, D. Kivanc and H. Liu, "Channel estimation for multicarrier CDMA," in *Proc. IEEE Intern. Conf. Acoustics, Speech, Sig. Proc. ICSSP'00*, pp. 2909-2912, 2000.

[30] J. Wu, A. Alqatawneh, and H. Lin, "Multi-carrier circular-shift division multiple access for multi-user wireless systems," *IEEE Globecom Conf.*, 2014.

[31] C. Xiao, J. Wu, S. Leong, Y.R. Zheng and K.B. Letaief, "A discrete-time model for triply selective MIMO Rayleigh fading channels," *IEEE Wireless Commun.*, vol. 3, pp. 1678-1688, Sept. 2004.

[32] J. Wu and G. Y. Li, "Collision-tolerant media access control with on-off accumulative transmission," *IEEE Trans. Wireless Commun.*, vol. 12, pp. 50-59, Jan. 2013.

[33] G. Wang, J. Wu, G. Zhou, and G. Y. Li, "Collision-tolerant media access control for asynchronous users over frequency-selective channels," *IEEE Trans. Wireless Commun.*, vol. 12, pp. 5162-5171, Oct. 2013.

[34] A. Stamoulis, G. B. Giannakis, and A. Scaglione, "Block FIR decisionfeedback equalizers for filterbank precoded transmissions with blind channel estimation capabilities," *IEEE Trans. Wireless Commun.*, vol. 49, pp. 69- 83, Jan. 2001.

[35] L. Ping, Q. Guo, and J. Tong, "The OFDM-IDMA approach to wireless communication systems," *IEEE Trans. Wireless Commun.*, vol. 14, no. 3,pp. 1824, June 2007.

[36] T. Whitworth, M. Ghogho and D. McLernon, "Optimized training and basis expansion model parameters for doubly-selective channel estimation," *IEEE Trans. Wireless Commun.*, vol. 8, pp. 1490-1498, Mar. 2009.

[37] F. Qu and L. Yang, "On the estimation of doubly-selective fading channels," *IEEE Trans. Wireless Commun.*, vol. 9, pp. 1261-1265, Apr. 2010.

[38] R.J. Baxley, J.E. Kleider and G.T. Zhou, "Pilot design for OFDM with null edge subcarriers," *IEEE Trans. Wireless Commun.*, vol. 8, pp. 396-405, Jan. 2009.

[39] K.Z. Islam, T.Y. Al-Naffouri and N. Al-Dhahir, "On optimum pilot design for comb-type OFDM transmission over doubly-selective channels," *IEEE Trans. Commun.*, vol. 59, pp. 930-935, Apr. 2011.

[40] J. Wu and C. Xiao, "Optimal diversity combining based on linear estimation of Rician fading channels," *IEEE Trans. Commun.*, vol. 56, pp. 1612-1615, Oct. 2008.

[41] N. Sun and J. Wu, "Minimum Error Transmissions with Imperfect Channel Information in High Mobility Systems," in *Proc. IEEE Military Commun. Conf.*, vol. 1, pp. 922-927, Nov. 2013.

[42] N. Sun and J. Wu, "Maximizing Spectral Efficiency for High Mobility Systems with Imperfect Channel State Information," *IEEE Trans. Wireless Commun.*, vol. 13, pp. 1462-1470, Mar. 2014.

[43] W. Zhou, J. Wu, and P. Fan, "Maximum Doppler diversity transmissions for high mobility systems with imperfect channel state information," in *IEEE Intern. Commun. Conf. ICC'14*, June 2014.

[44] Z. Wu, J. He, and G. Gu, "Design of optimal pilot-tones for channel estimation in MIMO-OFDM systems," *Proc. IEEE Wireless Commun. and Network. Conf.*, vol. 1, pp. 12-17, Mar. 2005.

[45] N. Sun and J. Wu, "On the performance of doubly-selective fading estimations in high mobility systems," in *IEEE Veh. Technol. Conf. VTC'14 Spring*, May 2014.

[46] H. Gazzah, P.A. Regalia and J. Delmas, "Asymptotic eigenvalue distribution of block Toeplitz matrices and application to blind SIMO channel identification," *IEEE Trans. Inform. Theory*, vol.47, pp. 1243-1251, Mar. 2001.

[47] I. S. Gradshteyn, and I. M. Ryzhik, *Table of Integrals, Series, and Products*, 6nd ed. Academic Press, July 2000.